New advanced methods for the spectral analysis of time-varying waveforms in power systems

A Dissertation by

Luisa Alfieri

Submitted in Partial Fulfilment of the Requirements for the Degree of Doctorate of Philosophy

in

Electrical Engineering

Supervisors:

Prof. Guido Carpinelli

Dr. Antonio Bracale

Coordinator:

Prof. Claudio Serpico

Department of Electrical Engineering and Information Technology
University of Naples Federico II

April - 2017

Therefore do not worry about tomorrow,
for tomorrow will worry about itself.
Matthew 6:34

Felicità
C'è un'ape che se posa
su un bottone de rosa:
lo succhia e se ne va...
Tutto sommato, la felicità
è una piccola cosa.
Trilussa

Contents

List of figures

List of tables

List of abbreviations

ASD	Adjustable Speed Drive
CWT	Continuous Wavelet Transform
CZT	Chirp-z transform
DFT	Discrete Fourier Transform
DWT	Discrete Wavelet Transform
EDAEM	ESPRIT-DFT-Analytical-ESPRIT Method
EDAPM	ESPRIT-DFT-Analytical-Prony Method
EMC	ElectroMagnetic Compatibility
EMD	Empirical Mode Decomposition
ESPRIT	Estimation of Signal Parameters by Rotational Invariance Technique
HHT	Hilbert-Huang Transform
HT	Hilbert Transform
IEC	International Electrotechnical Commission
IMF	Intrinsic Mode Function
JEDM	Joint ESPRIT-DFT Method
JPDM	Joint Prony-DFT Method
MDL	Minimum Description Length criterion
MEA	Modified ESPRIT Algorithm
MEM	Modified ESPRIT Method
MUSIC	MUltiple SIgnal Classification
PCC	Point of Common Coupoling
PDAEM	Prony-DFT-Analytical-ESPRIT Method
PDAPM	Prony-DFT-Analytical-Prony Method
PQ	Power Quality
STDFT	Short Time Discrete Fourier Transform
STFT	Short Time Fourier Transform
STFTM	Short Time Fourier Transform Method
SWWMEM	Sliding-Window Wavelet-Modified ESPRIT Method
TEA	Traditional ESPRIT Algorithm
TEM	Traditional ESPRIT Method
THD	Total Harmonic Distortion
TPM	Traditional Prony's Method
TSM	Three Step Method
WPT	Wavelet Packet Transform
WT	Wavelet Transform

List of the main symbols

$\left(\hat{f}_{h,dc}^{os}\right)^{LPF_1}$	$f_{h,dc}^{os}$ estimated in the range [0÷200]Hz
$\left(\hat{f}_{ih,ss}\right)^{LPF_1}$	$f_{ih,ss}$ estimated in the range [0÷200]Hz
a	Wavelet scale parameter
b	Wavelet translation parameter
$c_i(t)$	i-th IMF
$d_i(t)$	HT of the i-th IMF
e_n	Estimation error of the n-th sample of the waveform
f^{os}	Fundamental frequency of the voltage on the ASD converter output-side
f_{bs}	bands' separation frequency in SWWMEM
$\hat{f}_{f.s.}$	Frequencies estimated in the first step of EDAEM, EDAPM, PDAEM and PDAPM
$f_{h,dc}^{os}$	Harmonic frequencies introduced by the inverter of an ASD
$f_{h,ss}$	ASD converter supply-side harmonic frequencies
$f_{ih,ss}$	ASD converter supply-side interharmonic frequencies
f_k	Frequency of the k-th spectral component
$\hat{f}_k^{BW}$	Frequency of the k-th spectral component evaluated in a basis window
f_{max}	Maximum frequency of interest
f_s	Sampling frequency
f_{ss}	Fundamental frequency of the supply system of an ASD
h_k	Time-independent term of the k-th spectral component in the parametric method model
k_f	Number of analysis windows between two successive basis windows
$r(n)$	n-th sample of the additive white noise
$\boldsymbol{v}(n)$	Vector of the measurement with noise in Kalman Filter
$\boldsymbol{w}(n)$	Vector of the model with noise in Kalman Filter
$x(n)$	n-th point of the sampled waveform
$\boldsymbol{x}(n)$	Measurement vector in Kalman Filter
$\hat{x}(n)$	Estimation of the n-th point of the sampled waveform
$x_1(n)$	n-th point of the sampled waveform to be analysed in the second step of JPDM, EDAEM, EDAPM, PDAEM and PDAPM
$x_2(n)$	n-th point of the sampled waveform to be analysed in the last step of JPDM, EDAEM, EDAPM, PDAEM and PDAPM
$\hat{x}_{f.s.}(n)$	n-th point of the estimated sampled waveform obtained in the first step of JPDM, EDAEM, EDAPM, PDAEM and PDAPM
$x_h(n)$	n-th point of the high-frequency waveform in SWWMEM
$\hat{x}_{harm}(n)$	n-th point of the estimated sampled waveform obtained in the second step of JPDM, EDAEM, EDAPM, PDAEM and PDAPM
$x_l(n)$	n-th point of the low-frequency waveform in SWWMEM
$x_{LPF}(n)$	n-th point of the filtered sampled waveform in JPDM
$x_{LPF1}(n)$	n-th point of the [0÷200]Hz filtered sampled waveform in EDAEM, EDAPM, PDAEM and PDAPM
$x_{LPF2}(n)$	n-th point of the [0÷5000]Hz filtered sampled waveform in

	EDAEM, EDAPM, PDAEM and PDAPM
$\boldsymbol{y}(n)$	State vector in Kalman Filter
z_k	Time-dependent term of the k-th spectral component in the parametric method model
$A_i(t)$	Instantaneous amplitude
$A_j\,(k)$	Approximate DWT coefficient
A_k	Amplitude of the k-th spectral component
A_k^{BW}	Amplitude of the k-th spectral component in a basis window
$D_j\,(k)$	Detailed DWT coefficient
$D_{2j}^m(k)$	WPT coefficient
$\mathbf{E}$	Error subspace matrix
$F_0(\zeta)$	Low-pass filter of a two-channel synthesis filter bank
$F_1(\zeta)$	High-pass filter of a two-channel synthesis filter bank
$\mathrm{H}(\cdot)$	HT of a function
$H_0(\zeta)$	Low-pass filter of a two-channel analysis filter bank
$H_1(\zeta)$	High-pass filter of a two-channel analysis filter bank
$\mathbf{H}_{\boldsymbol{KF}}(n)$	Kalman Filter measurement matrix
$Im(\cdot)$	Imaginary part of a complex number
$\mathbf{K}_{\boldsymbol{KF}}(n)$	Kalman gain
L	Length of the finite sampled waveform
L^*	Length of the finite sampled waveform in the first step of JPDM
L^{**}	Length of the finite sampled waveform in the last step of JPDM
L_1	Order of the auto-correlation matrix
L_{max}	Number of decomposition levels in the first step of SWWMEM
M	Number of spectral components
M^*	Number of spectral components in the first step of JPDM
M^{**}	Number of spectral components in the last step of JPDM
$\boldsymbol{P}_{\boldsymbol{KF}}(\boldsymbol{n})$	Update of the covariance error matrix in Kalman Filter
$\boldsymbol{P}_{\boldsymbol{KF}}^{-}(\boldsymbol{n})$	Prediction of the covariance error matrix in Kalman Filter
$\mathbf{R}$	Auto-correlation matrix
$\widehat{\mathbf{R}}$	Estimation of the auto-correlation matrix
$Re(\cdot)$	Real part of a complex number
$\mathbf{S}$	Signal subspace matrix
$\hat{T}_{fund}$	Estimated period of the fundamental component
T_s	Sampling time interval
T_w	L-point sequence time duration
$\boldsymbol{V}_{\boldsymbol{KF}}(n)$	Measurement noise covariance matrix in Kalman Filter
$\boldsymbol{W}_{\boldsymbol{KF}}(n)$	Process noise covariance matrix in Kalman Filter
$X_{CZ}(\zeta_k)$	CZT of a z-plane point
α_k	Damping factor of the k-th spectral component
$\hat{\alpha}_k^{BW}$	Damping factor of the k-th spectral component evaluated in a basis window
ε_{j-curr}^2	Mean square relative reconstruction error in the j-th time window
ε_{th}	Reconstruction error threshold
ε_{thr}^2	Threshold value of the mean square relative reconstruction error
ζ_k	Variable in the z-plane
$\theta_i(t)$	Instantaneous phase
λ_k	Time-independent term of the k-th spectral component in the

	parametric method model
$\hat{\lambda}_k^{BW}$	Time-independent term of the k-th spectral component evaluated in a basis window
$\psi_{a,b}(t)$	Mother wavelet function
$\psi_{j,k}(t)$	Mother wavelet function with discrete scale and time parameters
$\varphi(t)$	Wavelet scaling function
ϕ_k	Initial phase of the k-th spectral component
ϕ_k^{BW}	Initial phase of the k-th spectral component in a basis window
ω_k	Angular velocity of the k-th spectral component
Δf	Frequency resolution
$\mathbf{\Phi}$	Rotation matrix
$\mathbf{\Phi_{KF}}(n)$	Kalman Filter transition matrix
$\widehat{\mathbf{\Phi}}$	Estimation of the rotation matrix

Acknowledgment

The reached milestones have a greater value when they are shared with someone, and, fortunately, during these years many people always surrounded me. I would like to thank all of them. First, I would like to thank Prof. Guido Carpinelli, that steadily gave me valuable guidance, advices and opportunities, and Dr. Antonio Bracale that taught me to give and learn more and more every day. Their enthusiasm toward their work led me to conduct and love scientific research. I am extremely grateful also to Prof. Pierluigi Caramia for his continuous support and for the trust he had in me. I thank also my Ph.D coordinator, Prof. Claudio Serpico, for his willingness during these years.

I would like to express my gratitude also to all of the other professors and colleagues of my research group, in particular Prof. Mario Pagano, Prof. Davide Lauria, Prof. Elio Chiodo, Prof. Pietro Varilone, Dr. Daniela Proto, Dr. Fabio Mottola, Dr. Luigi Pio Di Noia. My experience would not have been the same without any of them.

I was joyful also to work with the students that cooperated with me during their thesis projects. They contribute to lighten many days up.

Furthermore, I would like to thank my family, especially my mother, my father and my brother, for their invaluable support in any my choice. Their endorsement was, is and will be an important gift in all of the main steps of my life.

Finally, I would like to thank my Love. His central rule and his simultaneous and constant presence in my life as partner, friend, colleague and accomplice gives me the happiness, the certainty and the cheerfulness that anyone wishes to have.

This thesis is dedicated to my family and to my Love.

Introduction

Substantial modifications are currently occurring in electrical distribution systems as they move toward the smart grid concept. In the context of a widespread use of distributed generation, controllable loads and storage systems, the main objectives of smart grids are the efficient use of energy, the reduction of losses in the system, and the power quality improvement. In particular, the increasing diffusion of controllable and non-linear loads and the new needs of liberalized markets impose new requirements in term of both continuity and quality of electrical energy, in order to avoid dangerous effects to the devices.

Continuity usually refers to the uninterrupted electricity supply, while quality refers to a variety of disturbances that can occur in power systems and that can influence the characteristics of current and voltage waveforms. Among these disturbances, distortions of voltage and current waveforms have been extensively discussed in relevant literature, since they are gaining great interest as a consequence of several factors, such as:

- the sensitivity of customers to distortions. Waveform distortions can determine considerable problems to many types of devices, such as overheating, aging effects, sub-synchronous oscillations and voltage fluctuations;
- the growing penetration of electrical devices that significantly contribute to waveform distortions. For example, static converters that are used to supply loads and to connect distributed generation units or electrical storage systems to the grid are among the main sources of waveform distortions in modern power systems.

Several international Standards and Recommendations have been developed and updated to characterize this type of disturbances, mainly dealing with time-varying waveforms. However, the majority of Standards are based on the application of the Short Time Fourier Transform. As all of the non-parametric methods, Short Time Fourier Transform is suitable to globally quantify the waveform distortions, but it does not allow the accurate individuation of detailed information on single spectral components. Alternatively, many papers have presented different parametric methods that were able to accurately analyse both stationary and non-stationary waveforms, allowing the identification of each spectral component with a very high resolution. Despite this, parametric methods are usually characterized by a heavier computational effort than Standard methods; for this reason, recent studies have been addressed to develop new methods able to provide an accurate estimation of spectral components parameters, while keeping a relatively low computational effort.

This thesis focuses indeed on this research activity, presenting new advanced methods for the spectral analysis of time-varying waveforms in power systems. First, the main non-parametric, parametric and hybrid methods are presented in details under an analytical review

of the state of the art, stressing both their advantages and their weaknesses. Then, a new advanced modified parametric method and three new advanced hybrid methods are presented in this thesis. All of the proposed methods guarantee an accuracy typical of the parametric methods, though with a significantly lower computational efforts.

The proposed modified parametric method is the *sliding-window modified ESPRIT method.* It is based on a variation of the traditional ESPRIT algorithm from which it descends. The aim of this variation is the decreasing of the computational burden required for the spectral analysis of time-varying waveforms; this is reached by reducing the number of equation systems to be solved in each analysis window that slides over time. Specifically, observing that in most cases the frequencies are much less variable versus time than amplitudes, this advanced modified parametric method evaluates the frequencies and the damping factors of the exponentials included in the ESPRIT model only once or, at most, only a few times. Therefore, only one equation system must be solved to evaluate amplitudes and initial phases of the exponentials in each time window, with great benefits in terms of computational burden.

The proposed hybrid methods are based on the joint of parametric and non-parametric methods. Each of these three methods is characterized by the ability of combining the advantages of both parametric and non-parametric techniques, while significantly curtailing their main shortcomings. In particular, the first method is the *sliding-window Prony-DFT-Prony method*, a three-step method that combines the Prony's method with the discrete Fourier transform. The second method is the *sliding-window Parametric-DFT-analytical-parametric method* and it is a four-step method, specifically addressed for an accurate and fast assessment of current waveform distortions caused by adjustable speed drives. Eventually, the third method is the *sliding-window Wavelet-modified ESPRIT method*, based on the use of a discrete Wavelet transform and on the successive application of the modified ESPRIT method. Differently to the previous ones, this last method is expressly designed to meet the modern requirements in terms of spectral analysis of waveforms with spectral content from 0 to 150 kHz.

With reference to the proposed modified parametric method, the main innovative contributions are:

(i) the use of a model (ESPRIT) that takes into account the white noise;

(ii) the possibility of dramatically reducing the computational burden required by the analysis, without the need of prior assumptions of the frequencies of all of the spectral components to be known and of the damping factors to be zero;

(iii) the ability to perform a check on the reliability of the results in time during the analysis; if the check fails, there is the possibility to evaluate again all of the fixed parameters, in order to always provide high accuracy.

With reference to the proposed hybrid methods, the main original contributions are:

(i) for the *sliding-window Prony-DFT-Prony method*, the improvement in the estimation of the spectral component amplitudes in respect to similar methods based on different parametric methods, although preserving a similar computational effort;

(ii) for the *sliding-window Parametric-DFT-analytical-parametric method*, the significant reduction of the computational effort required for the analysis of the

current waveform distortions caused by adjustable speed drives, in respect to the parametric method and to the other hybrid methods specifically addressed to the analysis of the same waveform typology, although providing very accurate results;

(iii) for the *sliding-window Wavelet-modified ESPRIT method*, the ability to perform a detailed estimation in time of each low-frequency and high-frequency spectral component, using an optimal time and frequency resolution in each band, in order to obtain an accurate time-frequency representation.

The thesis is organized in three chapters. The first chapter provides an overview of the state of the art and it includes the main methods available in relevant literature for the spectral analysis of time-varying waveforms in power systems. The new advanced modified parametric method is presented in the second chapter, while the third chapter deals with the new advanced hybrid methods. The conclusions are in the last part of the thesis.

Chapter 1.
Methods for the spectral analysis of time-varying waveforms in power systems: state of art

1.1 Introduction

In ideal operating conditions of electrical systems, voltage and current waveforms are sinusoidal waves characterized by proper, fixed values of amplitude and frequency. The deviations of voltage, as well as the deviations of current, from the ideal waveform are defined "Power Quality (PQ) disturbances" [1]. PQ disturbances can be classified as variations and events; the formers are quasi-steady-state disturbances, while the latters are sudden disturbances with well-defined beginning and ending times [2]. The waveform distortions of currents and voltages are variations that greatly hold researchers' interest, due to the wide use of static converters in modern power systems and due to the harmful effects on power system operations and on power system components.

The waveform distortions consist in voltage and current signals that differ from single-frequency sinusoidal waves, since harmonic and interharmonic components are added to the fundamental component at the power system frequency[1]. The International Electrotechnical Commission (IEC) Standards define harmonic and interharmonic components as sinusoidal waves characterized by frequencies that are integer multiple and not-integer multiple of the fundamental frequency, respectively. The spectral content of both voltage and current waveforms can be detected by performing a spectral analysis, and the evaluation of proper indices, e.g., relative individual spectral components or total harmonic distortion (THD), allows to estimate the level of distortion.

Waveforms can be classified also as stationary (if they are statistically time invariant) and non-stationary (if they are statistically variable in time). Strictly stationary waveforms rarely occur in real power systems; nevertheless, in presence of sufficiently small variations it is still possible to assume the waveforms to be stationary. Anyway, the spectral analysis of both stationary and non-stationary waveforms can suffer from problems when the underlying assumptions of the applied methods is not fulfilled; in these conditions, non-negligible inaccuracies in the detection of spectral components and, consequently, in the evaluation of the PQ indices can often arise. For example, when a Fourier analysis of a stationary waveform is performed, spectral leakage problems can occur in presence of deviations from the

[1] In this thesis, the term "power system frequency" indicates the nominal frequency of the electrical power system (50 or 60 Hz in western countries). As well known, some deviations of the actual frequency from the nominal value can occur in normal operating conditions of the electrical power system, e.g., due to the instantaneous unbalance between power generation and load demand. For sake of clarity, in the following, the term "fundamental frequency" is used to indicate the actual frequency of the electrical power system.

fundamental frequency; on the other hand, the additional problem of the location in time of the spectral components occurs in the analysis of a non-stationary waveform.
Different advanced methods for the spectral analysis and time-frequency distribution have been proposed in the relevant literature in order to overcome the involved inaccuracies [1-28]. The aim of this Chapter is to provide an overview of the most important methods for the spectral analysis of time-varying waveforms in power systems. In particular, the following Sections of this Chapter deal with non-parametric methods, parametric methods, hybrid methods and filter-bank based techniques, respectively; the main methods per category are deepened in the corresponding Section. Finally, by underlining the pros and cons of each considered category, a brief theoretical comparison among the methods is provided in the last Section.

1.2 Non-Parametric Methods

Non-parametric methods estimate the distribution of the waveform power content over the different frequencies through proper transformations [1,3-5,7-10,29]. Specifically, their approach consists in estimating the waveform spectrum through the evaluation of some coefficients (e.g., the amplitudes) of known functions (also called basis functions) that are used for the transformation. Fourier Transform, Wavelet Transform, Hilbert-Huang Transform and Chirp z-Transform are among the main techniques applied to power system waveform analysis that belong to this category of spectral analysis methods.
The aforesaid techniques, together with their discrete and advanced versions, are presented in the following, with a particular focus on their characteristic features and on the issues related to the analysis of time-varying waveforms.

1.2.1 Fourier Transform

Fourier Transform is one of the most effective and widely used tools to perform the transformation of a generic waveform from the time domain to the frequency domain, by means of the representation of the original waveform through complex exponentials.
The Fourier Transform $X(f)$ of the generic continuous-time waveform $x(t)$, with $t \in]-\infty; +\infty[$, is defined as [3-5]:

$$X(f) = \int_{-\infty}^{+\infty} x(t) e^{-j2\pi ft} dt \tag{1.1}$$

with $f \in]-\infty; +\infty[$. The inverse transformation is a dual expression provided by:

$$x(t) = \int_{-\infty}^{+\infty} X(f) e^{j2\pi ft} df. \tag{1.2}$$

The complex function $X(f)$ is the spectrum of $x(t)$ in the frequency domain.
By sampling the continuous waveform $x(t)$, a discrete-time waveform is obtained as sequence of samples $x(n)$; in this case the Eq. (1.1) can be rewritten as follows:

$$X(f) = \sum_{n=-\infty}^{+\infty} x(n)\, e^{-j2\pi f n T_s} \tag{1.3}$$

where $f \in]-\infty; +\infty[$ and T_s is the sampling time interval[2]. Note that each sample of the waveform should be properly indicated as $x(nT_s)$, but assuming T_s to be constant, it is possible to use the compact notation $x(n)$.

Generally, in practical applications, the available sampled waveforms are sequences with a finite number L of samples, so the L-points Discrete Fourier Transform (DFT) $X(k)$ can be defined:

$$X(k) = \sum_{n=0}^{L-1} x(n)\, e^{-j2\pi \frac{k}{L} n} \tag{1.4}$$

with $k = 0,1,\dots,L-1$. Also in the Eq. (1.4) the proper notation $X\left(\frac{k}{LT_s}\right)$ of the DFT is substituted by the compact notation $X(k)$.

A comparison between Eqs. (1.3) and (1.4) shows that the L-point DFT is equal to the Fourier Transform of the discrete-time waveform at discrete frequencies $f = \frac{k}{LT_s}$, with $k = 0,1,\dots,L-1$. So the L-point DFT can be obtained by uniformly sampling the Fourier Transform of the discrete-time waveform in the frequency domain, with the distance between subsequent samples equal to $\Delta f = \frac{1}{LT_s}$; Δf is defined as the frequency resolution, and $LT_s = T_w$ is the L-point sequence time duration.

The evaluation of the L-point DFT through the Eq. (1.4) requires $O(L^2)$ operations; however, the Fast Fourier Transform (FFT) is usually preferred in order to reduce the computational burden. The FFT is a very efficient algorithm in terms of computational efforts, as it requires only $O(L \log L)$ operations; this algorithm appears to be particularly suitable when the length L of the sequence is an integer power of 2 [1,30].

Given a discrete-time waveform, the L-point finite sequence of samples can be obtained by multiplying the sampled waveform by a proper discrete function that is different from zero only in a finite-length window (windowing process). Different window functions can be used for the windowing process; this is shown with more details afterwards. However, for sake of conciseness, the definitions given hereafter assume the use of a rectangular window, since it is typically used in the windowing process.

Windowing process can cause different problems, since:

- the spectrum of the windowed signal is obtained by the convolution of signal DFT and the selected window DFT;
- the spectrum obtained by the DFT is constituted by components at integer multiples of the frequency resolution. Therefore, the "picket fence" effect can affect the spectrum, as the exact behaviour is observable only at discrete points. The properties of the original signal are joint to the properties of the selected window, hence a further interpretation of the results is required;

[2] The sampling frequency $f_s = 1/T_s$ should be greater than the double of the maximum frequency present in the waveform spectrum, according to the Nyquist-Shannon sampling theorem.

- the duration of the time window T_w should be an integer multiple of the Fourier fundamental period in order to guarantee the synchronization condition and to elude spectral leakage problems. The Fourier fundamental period is the reciprocal of the Fourier fundamental frequency, defined as the greatest common divisor of each frequency contained in the waveform [4,31]. In particular, the Fourier fundamental frequency is selected as submultiple of the power system frequency with an adequate compromise in terms of both frequency and time resolution. In fact, if the Fourier fundamental frequency is too small (high frequency resolution), T_w might become too large (low time resolution), thus preventing the detection of some variations in the amplitudes, frequencies and initial phases of harmonics and interharmonics.

In order to better explain the spectral leakage problem, let $s_w(n)$ be a sampled, windowed single spectral component, given by:

$$s_w(n) = x(n) \cdot w(n) = A \cdot \sin(2\pi f_a n T_s + \varphi) \cdot w(n) \tag{1.5}$$

where $n = 0,1,\dots,L-1$, $w(n)$ is a rectangular time window sampled at f_s with unitary amplitude, while A, f_a and φ are the amplitude, the frequency and the initial phase of the considered spectral component, respectively.

Considering that the multiplication in the continuous time domain corresponds to a convolution in the frequency domain, the spectrum of s_w can be calculated as the convolution of the Fourier Transform of the waveform $x(n)$ with the $sinc$ function[3] (i.e., the Fourier Transform of the rectangular window, whose absolute value is shown in Fig. 1.1).

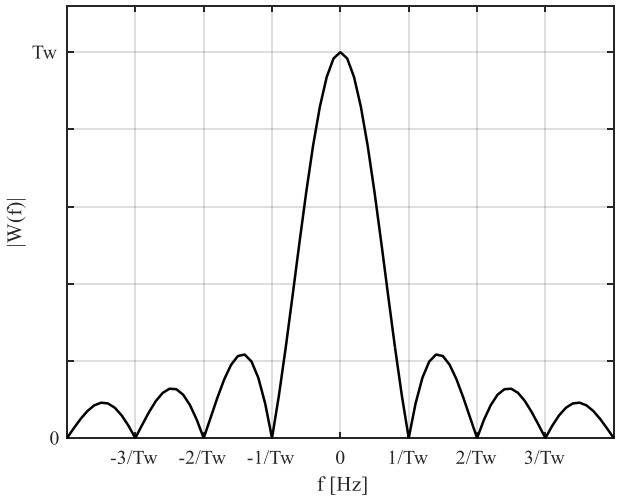

Figure 1.1 *- Absolute value of the spectrum of a rectangular window of unitary amplitude in the interval* $[-\boldsymbol{T_w/2}, \boldsymbol{T_w/2}]$

Then, the unilateral spectrum corresponding to the (1.5) can be expressed by discretizing as:

$$S_w(k) = \frac{A}{2j} \cdot e^{j\varphi} \cdot W\left(\frac{k}{LT_s} - f_a\right) = \frac{A}{2j} \cdot e^{j\varphi} \cdot W(k\Delta f - f_a) \tag{1.6}$$

[3] The *sinc* function assumes zero amplitudes at frequencies multiple of $1/T_w$, except for the frequency of the central lobe.

where W is the spectrum of the rectangular window.
The amplitude of the spectrum is obtained as:

$$|S_w(k)| = \frac{A}{2} \cdot |W(k\Delta f - f_a)| \tag{1.7}$$

where $k = 0,1, \dots, \frac{L}{2} - 1$.
Eq. (1.7) clearly shows that the amplitude of the spectrum depends on the $L/2$ samples of the absolute value of $sinc$ function centred at $f = f_a$, where each sample is taken in correspondence of a multiple of the frequency resolution $\Delta f = \frac{1}{LT_s} = \frac{1}{T_w}$. This leads to two different scenarios:

1. the frequency f_a is an integer multiple of Δf, i.e., $f_a = r \cdot \Delta f$, with r positive integer number;
2. the frequency f_a is not an integer multiple of Δf, i.e. $f_a = r \cdot \Delta f + \delta$, with $\delta < \Delta f$ positive real number.

For the scenario 1), the Eq. (1.7) becomes:

$$|S_w(k)| = \frac{A}{2} \cdot \left|W\big((k-r) \cdot \Delta f\big)\right| = \frac{A}{2} \cdot \left|W\left(\frac{k-r}{T_w}\right)\right| \tag{1.8}$$

with $k = 0,1, \dots, \frac{L}{2} - 1$. Samples of the amplitude of the spectrum are taken in correspondence of frequencies that are integer multiples of $1/T_w$; in particular, if $k \neq r$, the sample is located in correspondence of a zero of the absolute value of the $sinc$ function, otherwise, if $k = r$, the sample is located at the peak of the absolute value of the $sinc$ function (the centre of the main lobe). In this circumstance, even neglecting the negative frequencies, each component of the original spectrum in the frequency domain is correctly reproduced (Fig. 1.2.a).
On the other hand, for the scenario 2), the Eq. (1.7) becomes:

$$|S_w(k)| = \frac{A}{2} \cdot \left|W\big((k-r) \cdot \Delta f - \delta\big)\right| = \frac{A}{2} \cdot \left|W\left(\frac{k-r}{T_w} - \delta\right)\right| \tag{1.9}$$

with $k = 0,1, \dots, \frac{L}{2} - 1$. Samples of the amplitude of the spectrum are taken in correspondence of frequencies that are not integer multiples of $1/T_w$, due to the δ contribution. In this case, for each value of k, the samples are always taken in correspondence of non-zero values of the absolute value of the $sinc$ function (Fig. 1.2.b); therefore, neglecting the negative frequencies leads to the incorrect reconstruction of the original single spectral components of the waveform in the frequency domain.
For this reason, it is important to always verify the condition $f_a = r \cdot \Delta f$, with r positive integer number, in order to obtain correct information on the spectrum. This condition in the time domain becomes:

$$T_w = \frac{1}{\Delta f} = \frac{r}{f_a} = r \cdot T_a \tag{1.10}$$

that defines the synchronization condition: the time window duration T_w must be an integer multiple of the spectral component period T_a.
If the synchronization condition is not satisfied, the spectral leakage phenomenon occurs and additive, non-zero components appear in the spectrum, providing inaccurate information.

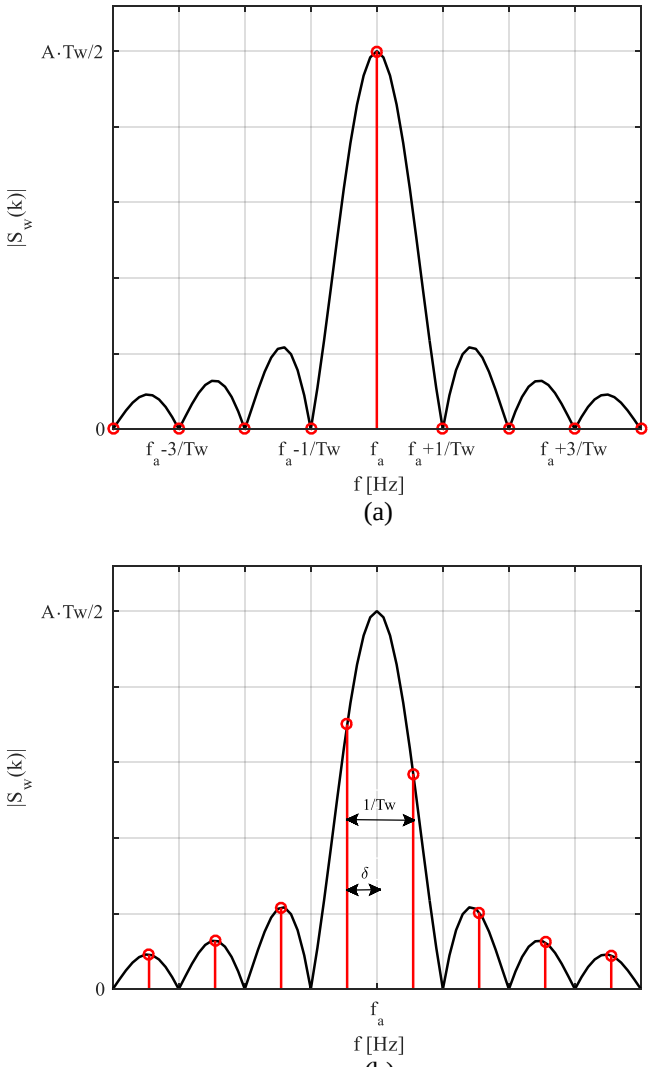

Figure 1.2 *- Example of synchronized spectrum (a) and non-synchronized spectrum (b) for the waveform in Eq.(1.5)*

Note that the DFT is a linear transform, so, if a waveform is constituted by several components, the waveform spectrum can be obtained as the sum of the spectra of each component, and the synchronization condition should to be verified for each component in order to prevent the spectral leakage phenomenon. Specifically, if the Eq. (1.10) is not verified for each component, also "interferences" among neighbor tones can occur due to the spectral leakage effect.
The duration of the time window T_w is generally chosen as an integer multiple of the fundamental period of the waveform to prevent spectral leakage, but this rule requires the

prior knowledge of the signal characteristics; anyway, it becomes ineffective in presence of non-synchronized interharmonics.
Hence, the main causes of spectral leakage problems in power systems are due to [32]:
(i) the deviations of the actual fundamental frequency from the expected fundamental frequency, leading to errors in the synchronization between fundamental and harmonics; and
(ii) the presence of non-synchronized interharmonics.
Several solutions have been proposed in relevant literature to improve the Fourier Transform tools for the estimation of power system waveform spectra [33-37]. For example, interpolation and synchronization techniques have been proposed in order to overcome the problems related to the selected duration of the analysis window and to the correspondent number of waveform samples [1,35].
Other solutions to overcome the spectral leakage deal with the use of windows different from the rectangular one [31-32,38-39]. Basically, the aim was to reduce the discontinuity at the boundaries of an observation with duration not adequate to the natural period of the waveform. This objective could be reached by setting to zero (or near zero) as many orders of derivative of the weighted sequence as possible [31,39]. Also, the window spectrum has to be characterized by a narrow main lobe and by low amplitude in correspondence on the other lobes, decreasing as the frequency increases. The effect of this approach is the minimization of the spread of each harmonic component.
Some of the most commonly used windows in power systems are the Hanning window, the Hamming window and the Gaussian window.

a) Hanning Window
The Hanning window is one of the most useful time windows proposed as alternative to the rectangular window [1,31-32]. The Hanning window is characterized in the frequency domain by an amplitude spectrum with side lobes very small and quickly decaying, as shown in Fig. 1.3a. This feature allows to contain the interference conditions that can occur among neighbor tones, due to the spectral leakage.
However, compared to the rectangular window, the Hanning window is less suitable to guarantee the best resolution among tones that are close in frequency, since the main lobe of the amplitude spectrum of the Hanning window is double than the main lobe of the rectangular window. Nevertheless, an acceptable resolution is still provided also by the Hanning window.

b) Hamming Window
The Hamming window is another useful window that is often used as an alternative to the rectangular window [31]. The Hamming window can be considered as a modified version of the Hanning window, characterized, in the frequency domain, by a deep attenuation at the absent side lobe positions and by lower side lobes near to the main lobe, as shown in Fig. 1.3b. Fig. 1.3b shows also that the side lobes of the Hamming window decay slower than the side lobes of the Hanning window, while the main lobe is still double than the main lobe of the rectangular window.
Note also that the Hamming window differs in the time domain from the Hanning window, since its edge values are not very close to zero.

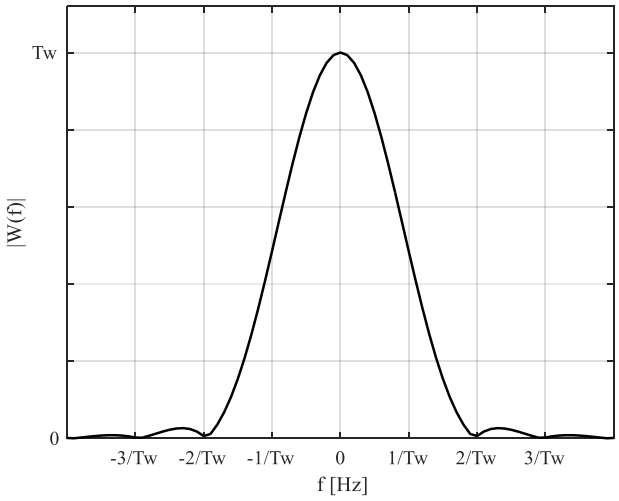

(a)

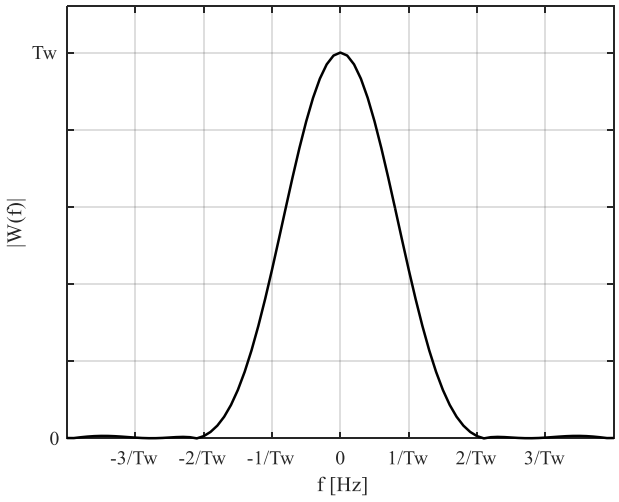

(b)

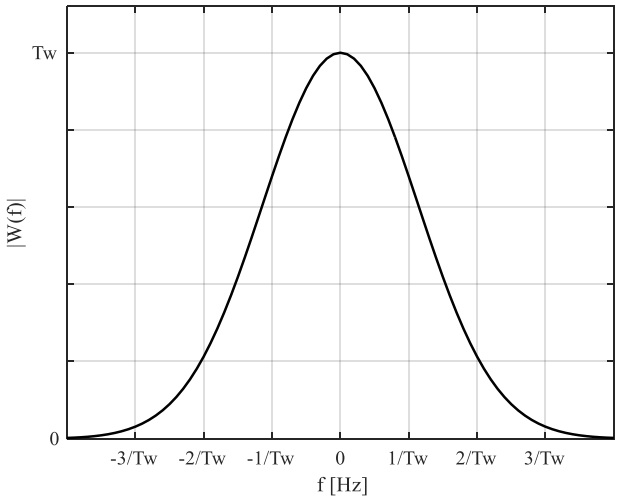

(c)

Figure 1.3 – *Absolute value of amplitude spectrum of: (a) Hanning Window; (b) Hamming Window; (c) Gaussian Window*

c) Gaussian Window

In order to maximise the performance of the DFT, the time window in Eq. (1.5) should to be a smooth positive function, and its Fourier Transform should have a tall, thin feature. Unfortunately, it is impossible to simultaneously reach high levels of ideality both in time and in frequency domain for a generic window. Nevertheless, the Gaussian pulse is a good window function candidate since the product between its mean square values of time duration and of bandwidth is minimum [31].

Actually, tails should be truncated in order to use the Gaussian pulse as window function; in this case the time-bandwidth product for this window is no longer the minimum. However, setting the truncation in correspondence to three time as much as the standard deviation, the error appears negligible and the aforesaid property still can be considered valid [31].

A parameterized window is therefore obtained; the parameter is the reciprocal of the standard deviation. When this parameter increases, the width of the time window decreases and the edge discontinuities of the window in the time domain become smoother. This means that the absolute value of the amplitude spectrum of Gaussian window is characterized by very wide main lobe and reduced side lobes that rapidly decay, as shown in Fig. 1.3c, where the reciprocal of the standard deviation is 3.5.

Anyway, although the leakage effects of a rectangular window are significant in non-synchronized conditions, the International Electrotechnical Commission (IEC) standard recommends the use of a rectangular window, since it assures the best frequency resolution [40].

The improvement of the Fourier Transform performances in presence of non-stationary waveforms was also investigated in relevant literature, in order to detect the variations in the time domain of waveform spectrum in terms of both amplitudes and frequencies. This objective was achieved through the Short Time Fourier Transform (STFT) [1].

The STFT is an extension of the Fourier Transform, based on the use of a time window that slides in the time over the waveform, with or without overlap. The idea is to break the waveform in small segments, that are separately analysed by the Fourier Transform in order to detect the variation of the spectrum of a non-stationary waveform during time. In this way, associating each spectrum to the centre of the time window, a three-dimensional representation (amplitudes and frequencies at each time) of the spectrum can be obtained, in order to detect the spectral components included in a waveform at a specific time interval (time-frequency representation).

Specifically, let $x(t)$, with $t \in]-\infty; +\infty[$, be the generic continuous-time waveform; its STFT is defined as [1]:

$$STFT(f,\tau) = \int_{-\infty}^{+\infty} x(t)w(t-\tau)e^{-j2\pi ft}dt \qquad (1.11)$$

where w is the sliding time window of duration T_w and τ is the time shift of the same window. Eq. (1.11) can be rewritten by discretizing the time domain as:

$$STDFT(f,\tau) = \sum_{n=0}^{L-1} x(n)\, w(n-m) e^{-j2\pi \frac{k}{L} n} \tag{1.12}$$

with $k = 0,1,\dots,L-1$. Note that $x(n)$ and $w(n)$ are the generic samples of the waveform and sliding-window respectively, and that L is the finite number of samples for each window, while m is related to the shift of the sliding-window in the discrete time domain.

Once again the duration $T_w = LT_s$ of the sliding time window fixes the frequency resolution Δf of the DFT spectrum. Moreover, since the frequency resolution is the reciprocal of the sliding-window duration, a detailed time resolution is obtained by choosing a short time window, but the frequency resolution gets worse, and vice versa.

The shape of the time window can lead to false information about the spectral component values. The IEC standard suggests the application of the STFT with rectangular time windows of duration equal to 10 or 12 cycles of the fundamental period for 50-Hz or 60-Hz systems, respectively [40]. Anyway, in relevant literature, also other differently-shaped windows have been alternatively used for the STFT, following the same previous motivations.

Eventually, the DFT is still the most widely used method for a fast spectral analysis, although all of the limits highlighted in this Section. In particular, many works in relevant literature are specifically addressed to the application of DFT-based methods for the waveform distortion detection in power system. A detailed literature overview in this field is in [32,34-37,39,41-48].

1.2.2 Wavelet Transform

The Wavelet Transform (WT) performs a simultaneous analysis of waveforms in both time and frequency domains and it is extensively used as a time-frequency technique for signal processing. The main differences with the STFT are: i) the possibility of performing multi-resolution time-frequency analyses, and (ii) the use, in the mathematical definition, of wavelets ("small waves"). These are functions with limited energy and zero mean, and their role is the same of the sine and cosine functions in Fourier analysis [1].

Different wavelet functions are available for the transformation, so the need to choose a specific wavelet (mother wavelet) to be used for each application. The mother wavelet depends on two parameters that determine how the mother wavelet has to be dilated (stretched) and translated (shifted in time), respectively. Let $a \in \mathbb{R}^+$ be the scale parameter and $b \in \mathbb{R}$ be the translation parameter; the mother wavelet is defined as [1,8]:

$$\psi_{a,b}(t) = \frac{1}{\sqrt{a}} \psi\left(\frac{t-b}{a}\right). \tag{1.13}$$

The Eq. (1.13) shows that a stretched basis function is obtained if the scale parameter $a > 1$, while a compressed basis function is available if $a < 1$. Examples of the wavelet for two different values of the scale parameter a are in Fig. 1.4. Note also that the wavelet function slowly varies when $a > 1$, and therefore it is possible to take into account the lower frequencies of the signal through its use; for $a < 1$ the wavelet function varies instead more rapidly, so its use allows to take into account the higher frequencies. The translation

parameter b in Eq. (1.13) is linked to shift of the wavelet that can be moved along the waveform in time. The term $1/\sqrt{a}$ is a weight related to energy conservation.

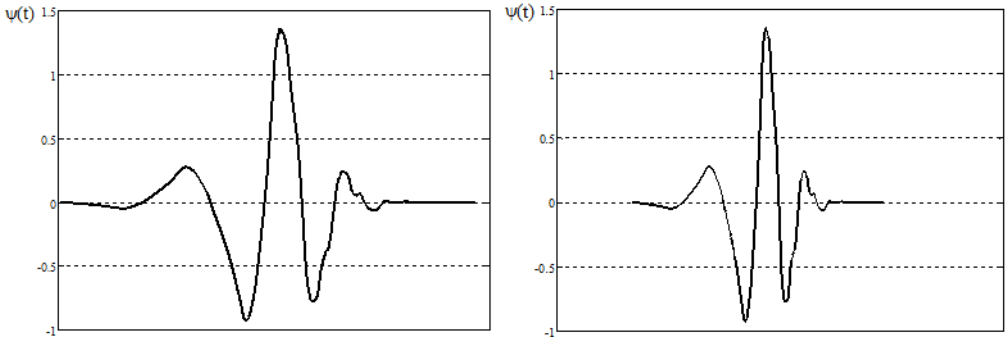

(a) (b)

Figure 1.4 *– Wavelet examples: a) a > 1 ; b) a < 1*

As previously observed, selecting $a < 1$ or $a > 1$, wavelet functions in (1.13) can be used to get information at higher and lower frequencies of the waveform, respectively. Therefore, a scaling function $\varphi(t)$ can be introduced to obtain information at low frequencies of the signal. This scaling function can be defined as an aggregation of the wavelets with scale parameters $a > 1$. Also the scaling function can be scaled and translated.

If the mother wavelet $\psi_{a,b}(t)$ is a complex signal, the Continuous Wavelet Transform (CWT) of a given waveform $x(t)$ is the following dot product [1]:

$$CWT(a,b) = \langle x, \psi_{a,b} \rangle = \int_{-\infty}^{+\infty} x(t) \frac{1}{\sqrt{a}} \check{\psi}\left(\frac{t-b}{a}\right) dt \qquad (1.14)$$

where the symbol ˇ represents the complex conjugate and the symbol $\langle , \rangle$ represents the inner product.

For an assigned pair of parameters a and b, the coefficient obtained by the Eq. (1.14) characterizes the link between the waveform $x(t)$ and the scaled, translated mother wavelet. Therefore, varying the a and b values for a chosen mother wavelet, the wavelet representation of the waveform $x(t)$ can be reached in time (through the translation parameter b) and in frequency (through the scale parameter a) domains.

However, CWT is a redundant and heavily-implementable transform, since the mother wavelet is continuously translated and scaled. This redundancy can be overcome by recurring to a Discrete Wavelet Transform (DWT) that refers to a discrete number of expansions (a values) and translations (b values). Due to its reduced computational effort, the DWT, rather than CWT, is preferably used for PQ disturbance assessment.

Scaling and translation parameters can be discretized, i.e., as $a = a_0^j$ and $b = kb_0a_0^j$, where k and j are integers and $a_0^j > 1$, $b_0 > 0$ are fixed values. Substituting in (1.13), the following expression results [1]:

$$\psi_{j,k}(t) = \frac{1}{\sqrt{a_0^j}} \psi\left(\frac{t - kb_0a_0^j}{a_0^j}\right). \qquad (1.15)$$

Similar replacements stand also for the scaling function $\varphi(t)$, as for all next relations.
Using the Eq. (1.15) in the definition (1.14), the following coefficients for the wavelet transform of a continuous signal $x(t)$ with discrete scale and time parameters are obtained [1]:

$$CWT(j,k) = \langle x, \psi_{j,k} \rangle = \frac{1}{\sqrt{a_0^j}} \int_{-\infty}^{+\infty} x(t) \breve{\psi} \left(\frac{t - k b_0 a_0^j}{a_0^j} \right) dt. \tag{1.16}$$

The original waveform can be reconstructed by using the inverse wavelet transform, defined as:

$$x(t) = \sum_{j=-\infty}^{+\infty} \sum_{k=-\infty}^{+\infty} \langle x, \psi_{j,k} \rangle \, \psi_{j,k}(t). \tag{1.17}$$

If only a finite sequence $x(n)$ of L samples of the waveform is considered, the L-point DWT with discrete scale and time parameters can be defined as [1]:

$$DWT(j,k) = \frac{1}{\sqrt{a_0^j}} \sum_{n=0}^{L-1} x(n) \breve{\psi} \left(\frac{n - k b_0 a_0^j}{a_0^j} \right). \tag{1.18}$$

The choice of proper values for a_0^j and b_0 is based on the selected wavelet; the dyadic expansion is often used. This expansion is characterized by the scale parameter value $a_0 = 2$ and so $a_0^j = 2^j, \ \forall j = 1,2, ...$, while the translation parameter is $b_0 = 1$.
The DWT is a non-uniform representation of the waveform both in time and in frequency, since the time and frequency spreads vary with the scale parameter a, although in an opposite manner: the former is proportional to a, while the latter is proportional to $1/a$. The scaling used in Eq. (1.18) gives a logarithmic frequency coverage to the DWT, in opposition to the uniform frequency coverage of STDFT, as shown in Fig. 1.5 [8].

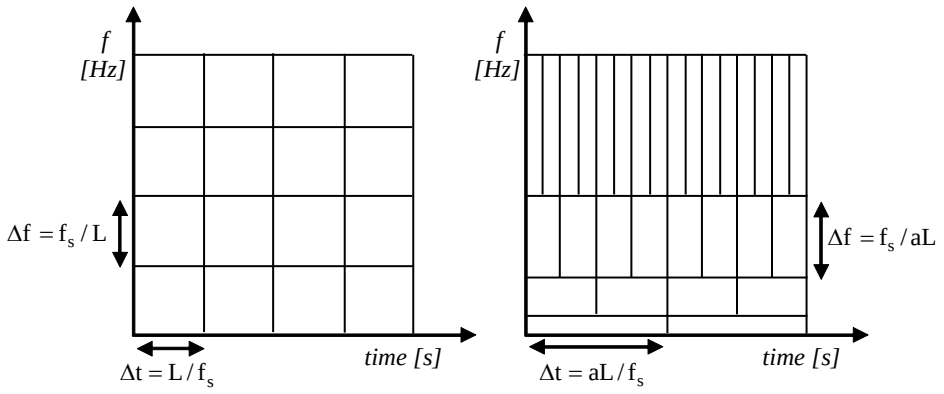

***Figure 1.5** – Comparison of time-frequency resolution between (a) STDFT and (b) DWT with dyadic expansion*

Coherently to the theoretical aspects in Section 1.2.1, Fig. 1.5.a shows the constant time and frequency resolutions (Δt and Δf) of the STDFT (fixed square boxes). Conversely, the DWT

resolution, shown in Fig. 1.5.b, varies across the plane. Specifically, at low frequency, the DWT time resolution is coarse, while the DWT frequency resolution is fine, cause of a dilated version of the mother wavelet, related to high value of scale parameter a. DWT resolutions are exactly inverse for the high frequency range, due to the contracted version of the mother wavelet (low value of scale parameter a) that provides a fine time resolution and a coarse frequency resolution. This behavior allows a multi-resolution analysis of waveforms.
The DWT can be implemented as multi-stage filter, constituted by high-pass and low-pass filters with down-sampling in cascade, as shown in Fig. 1.6. The high-pass and low-pass filters are related to the selected wavelet and scaling functions. As shown in Fig. 1.6, the output D_j $(j = 1.2 \dots)$ of the high-pass filters produces the detailed version of the high-frequency components of the decomposition, while the output A_j $(j = 1.2 \dots)$ of the low-pass filters gives the approximated version of the low-frequency components of the decomposition.

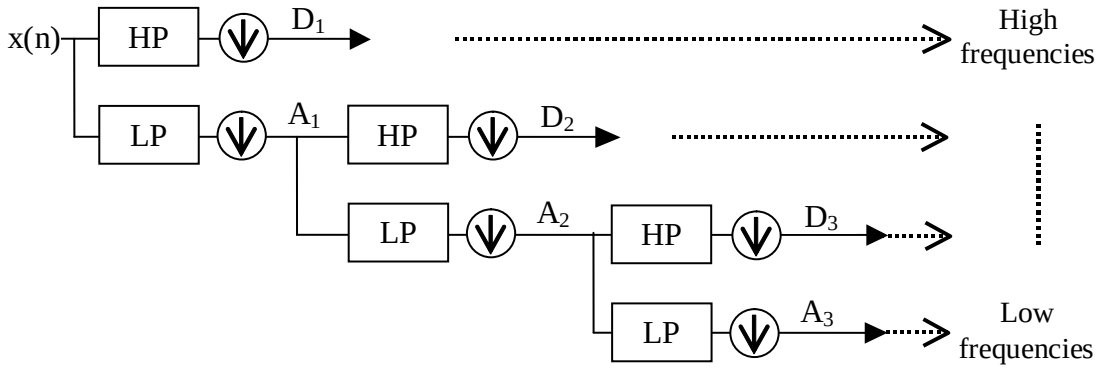

Figure 1.6 *– Fast DWT decomposition*

In a multi-resolution analysis, the DWT divides progressively the waveform to be analyzed in a discrete number of frequency bands at each decomposition level. At the first level of the decomposition, the waveform bandwidth is split into two parts constituted by low and high frequencies, respectively. At the second level, only the part made up of low frequency components is further split in a low frequency part and in a high frequency part. The process is then iteratively repeated, leading to an array of wavelet coefficients with *j* frequency bands and *k* coefficients that provide a representation of the original waveform.
Specifically, the coefficients D_j and A_j in Fig. 1.6 are computed through the following expressions [1,8]:

$$D_j\,(k) = \frac{1}{\sqrt{a_0^j}} \sum_{n=0}^{L-1} x(n)\check{\psi}\left(\frac{n-k}{a_0^j}\right). \tag{1.19}$$

$$A_j\,(k) = \frac{1}{\sqrt{a_0^j}} \sum_{n=0}^{L-1} x(n)\check{\varphi}\left(\frac{n-k}{a_0^j}\right). \tag{1.20}$$

where the symbol ˇ represents, again, the complex conjugate, k is related to the translation in time and j is linked to the j^{th} frequency bands, sorted from high to low frequencies.

Note that, as previously observed, the high frequency bandwidths are wide, thus providing a poor frequency resolution. Therefore, if detailed information is required for a specific spectral component, the DWT could not be effective. In general, the DWT is able to give only information on a particular frequency band, with a location that is strictly dependent on the selected parameters.

Wavelet packet transform (WPT) is another decomposition technique based on the wavelet application. WPT has a similar implementation to the DWT, since a sequence of filter pairs is utilized [7]. However, the main difference of the WPT with respect to the DWT is the decomposition at each level of all of the frequency bands obtained as output in the previous decomposition level; this is clear in the WPT tree-structure shown in Fig. 1.7. In this way, the frequency resolution is improved also for the high frequencies.

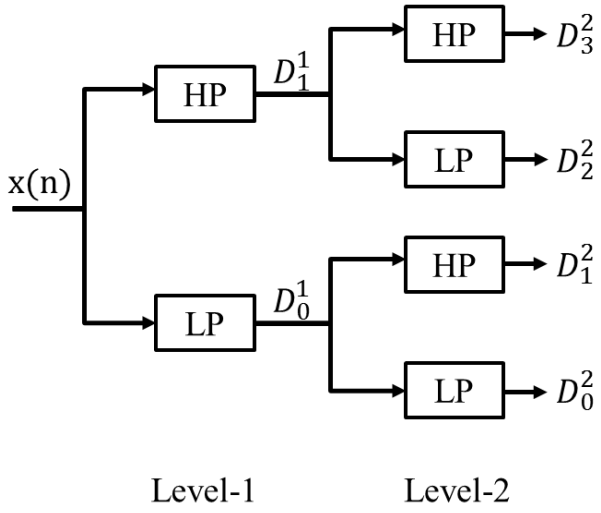

***Figure 1.7** – WPT decomposition structure*

The coefficients obtained at each level can be evaluated according the following equations:

$$D_{2j}^{m}(k) = \sum_{n=0}^{L-1} g(n) D_j^{m-1}(2k-n) \tag{1.21}$$

$$D_{2j+1}^{m}(k) = \sum_{n=0}^{L-1} h(n) D_j^{m-1}(2k-n) \tag{1.22}$$

where $g(n)$ and $h(n)$ are the impulse response of the low- and high-pass filter, respectively, and the index $j = 0,1,\dots,(2^{(m-1)}-1)$ represents each output frequency band at the $(m-1)^{th}$ level of decomposition. Then, each of these frequency bands becomes an input for the m^{th} level of decomposition. Note that the original sampled waveform $x(n)$ to be decomposed corresponds to D_0^0.

However, in each WT application, the choice of the mother wavelet has a fundamental role. The proper choice of the mother wavelet is strictly related to the particular application, so, in each case, a prior knowledge of the nature of the waveform to be analyzed is necessary and the experience in the field helps to select the most appropriate function. A wide number of mother wavelets has been used in PQ applications; the Daubechies wavelets are among the

most commonly ones. This wavelet family is characterized by orthogonality and compact support, as well as the absence of a closed analytical expression. Moreover, the lowest-order Daubechies derivatives are not always continuous functions [6,8].
Other commonly used mother wavelets, such as Morlet and Meyer mother wavelets, derive by a modulated Gaussian function and a harmonic waveform, both characterized by a smoothness that particularly allows them to provide amplitude information in the harmonic analysis. For example, the Meyer wavelet is suited for the visualization of time-varying spectral components in the discrete time domain, since this multi-resolution analysis can clearly show the oscillatory nature of different spectral components included in the waveform [6,8].
As previously stated, the WT multi-resolution analysis of the waveform proves to be a proper tool for the PQ applications. In relevant literature, many works have proposed an extension of different PQ indices, such as THD and k-factor, taking into account the main features of the WT. Specifically, the aforesaid indices are computed using the energy content of the frequency bands obtained through the DWT, instead of considering the spectral components. For example, a WT-based evaluation of the THD was proposed in [29]. Such kind of evaluation was effected by assigning different weights to each decomposition frequency level, with higher weights associated to the lower frequencies.
In [49] the WPT was proposed for the harmonic groups estimation defined in [40]. The WPT, in fact, is able to guarantee similar bandwidths across the entire frequency plane. The Vaidyanathan 24 and the Daubachies 20 were suggested as mother wavelets for that application, and a five-levels filter bank was used to obtain 32 uniform bands of 25-Hz width as output. Then, the filter bank output was post-processed in order to make the decomposition suitable to the grouping evaluation.
Note that WT-based techniques, as well as DFT-based ones and high resolution methods analysed in the next Section, have been extensively applied for the detection and the analysis not only of waveform distortion, but also of other PQ disturbances, such as voltage sags and transients [2]. An exhaustive overview of the application of WT-based methods for the spectral analysis in power system field is in [2,6,8,48,50-60].

1.2.3 Hilbert-Huang Transform

The Hilbert-Huang Transform (HHT) is another useful non-parametric technique. This is a relatively modern approach for the spectral analysis and consists in a two-steps method, based on the definition of instantaneous frequency [7,9].
The HHT decomposes the waveform to be analysed in Intrinsic Mode Functions (IMFs), by using the Empirical Mode Decomposition (EMD) in the first step. These IMFs are adaptive basis functions strictly related to the specific waveform to be analysed, unlike the basis functions used in both FT and WT that are prior selected. The EMD is realized by an iterative process that stops when the found IMFs fulfils the criteria on the decomposition residual, according to the block scheme in Fig. 1.8.

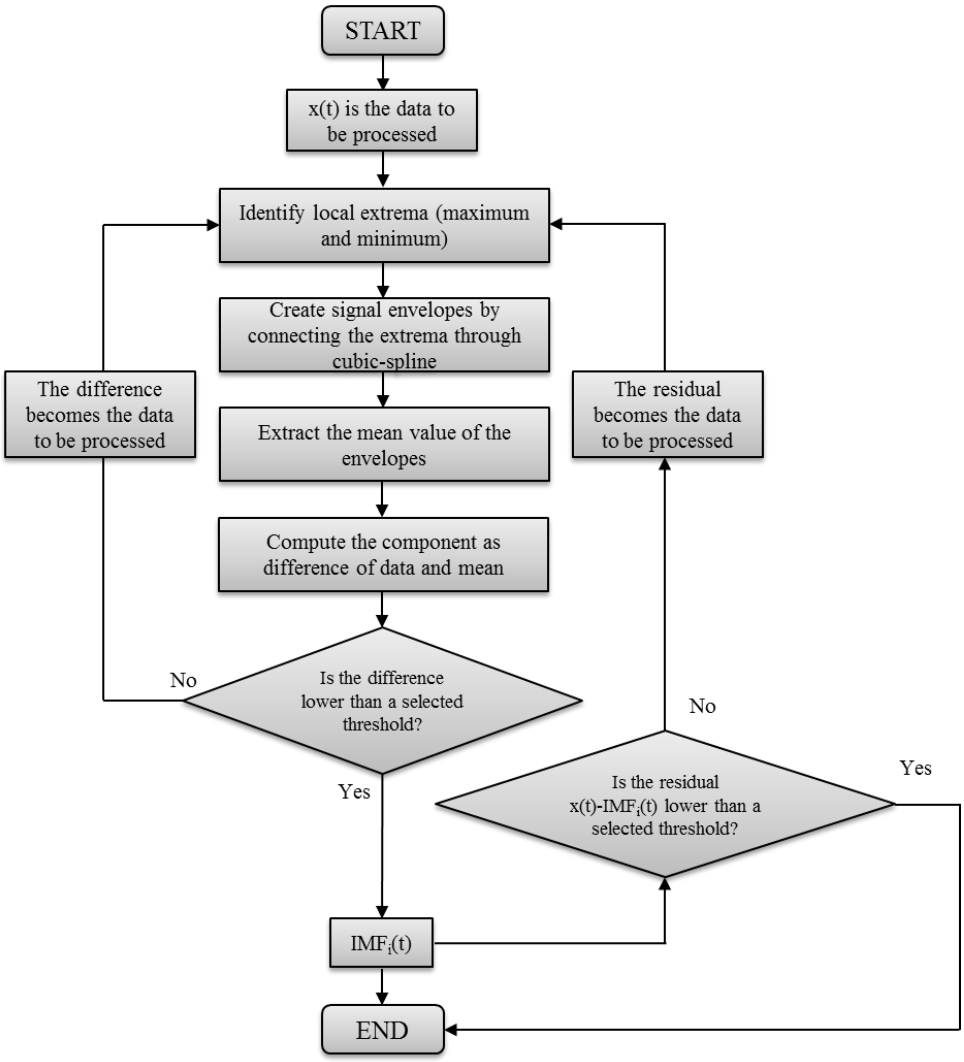

Figure 1.8 *– Block scheme of the HHT first step*

Specifically, the decomposition stops when the last residual obtained by the iteration becomes a constant, a monotonic function, or a function with only one maximum and one minimum, from which no more IMFs can be extracted [7,9].
Once the waveform $x(t)$ is fully decomposed, being $c_i(t)$ the *i-th* IMF and $r_n(t)$ the final residual, the waveform $x(t)$ to be analysed can be represented as [9]:

$$x(t) = \sum_{i=1}^{n} c_i(t) + r_n(t). \tag{1.23}$$

After the decomposition, in the second step, the HHT applies the Hilbert Transform (HT) to the IMFs according the Eq. (1.24) [9]:

$$\mathrm{H}(c_i(t)) = d_i(t) = \frac{1}{\pi} P \int_{-\infty}^{+\infty} \frac{c_i(t')}{t - t'} dt' \tag{1.24}$$

where $\mathrm{H}(c_i(t)) = d_i(t)$ represents the HT of the *i-th* IMF $c_i(t)$, and P is the Cauchy principal value.

Then, since $c_i(t)$ and $d_i(t)$ form a complex pair, an analytical signal $\varsigma_i(t)$ can be obtained as [9]:

$$\varsigma_i(t) = c_i(t) + jd_i(t) = A_i(t)e^{j\theta_i(t)} \tag{1.25}$$

where the instantaneous amplitude $A_i(t)$ and the instantaneous phase $\theta_i(t)$ can be evaluated as follows:

$$A_i(t) = \sqrt{c_i^2(t) + d_i^2(t)} \tag{1.26}$$

$$\theta_i(t) = \tan^{-1}\frac{d_i(t)}{c_i(t)} \tag{1.27}$$

In particular, the instantaneous frequency is defined as the derivative of the instantaneous phase $\theta_i(t)$:

$$f_i(t) = \frac{1}{2\pi}\frac{d\theta_i(t)}{dt} \tag{1.28}$$

Many HHT-based methods for the spectral component detection have been proposed in the last decade [61-63]. Indeed, due to the adaptive basis functions for decomposition, the HHT is particularly suitable also for the spectral analysis of nonlinear and non-stationary waveforms., An exhaustive overview of the application of HHT-based methods for the spectral analysis and the evaluation of PQ indices in power system field is in [48,62-69].

1.2.4 Chirp z-Transform

The chirp-z transform (CZT) is another important tool for the spectral analysis, and it is particularly indicated when the knowledge of only a small band of frequency is required with resolution higher than DFT [7,10]. Specifically, the CZT computes the z-transform of a finite number N of samples of a waveform along a general contour $\zeta_k = \Lambda W^{-k}$ in the z-plane, with $k = 0, \dots, K-1$. The symbols Λ and W represent two complex numbers, given by the following expressions:

$$\Lambda = \Lambda_0 e^{j2\pi\theta_0} \tag{1.29}$$

$$W = W_0 e^{j2\pi\phi_0} \tag{1.30}$$

where Λ_0, W_0, θ_0 and ϕ_0 are real numbers.
Given the contour, the CZT of a sampled waveform $x(n)$ is obtained by using two FFT and one inverse FFT, according to the following expression:

$$X_{CZ}(\zeta_k) = \sum_{n=0}^{N-1} x(n)\Lambda^{-n}W^{nk} \tag{1.31}$$

for $k = 0, \dots, K-1$.
Note that the CZT becomes the DFT if $\Lambda = 1$ and $W = e^{-j2\pi/N}$. In this case, the number of points K in the z-plane is equal to the total number of samples N of the waveform.
An exhaustive overview of the application of CZT-based methods for the spectral analysis and the evaluation of PQ indices in power system field is in [48,70-74].

1.3 Parametric Methods

The methods that have been dealt with in the previous Section descend from a "classical approach" to the spectral analysis, based on the use of analytic transformations having the waveform to be analysed as input and information about the waveform spectral content as output.
The "parametric approach" to the spectral analysis is discussed in this Section. This is an alternative approach to the classical one and it is based on the definition of a model for the waveform to be analysed. The waveform spectrum is known when the parameters of the model are evaluated.
Parametric methods overcome a lot of drawbacks of the non-parametric ones, thus allowing for a great accuracy in the spectral component estimation. For example, there is no definition of frequency resolution related to the time duration of the analysis window in the parametric framework, and therefore all of the main problems of the DFT-based methods are avoided [1-2].
Each parametric method assumes that the waveform model is constituted by a finite number of exponential functions. This means that the output spectrum is discrete and contains a finite number of spectral components, while the non-parametric methods could provide a spectrum constituted by an infinite number of spectral components.
Parametric methods can be used to characterize both stationary and non-stationary waveforms. In the first case, the parameter estimation can be obtained through an entire data sequence of the waveform to be analysed. In the second case, the spectrum variability in time can be detected by dividing the available sampled waveform into a proper number of blocks [1]. In this way, the same principle used for the STFT is repeated, since the analysis of the different data blocks of the waveform corresponds to the use of a time window that slides in time. These sliding-windows can be either overlapped or non-overlapped according to the particular application, and, for each window, the parameters of the model of the selected parametric method are evaluated. As a result, a representation of spectral component amplitudes and frequencies versus time (time-frequency representation) is obtained [1]. The Prony's method, the Estimation of Signal Parameters by Rotational Invariance Technique (ESPRIT), and the MUltiple SIgnal Classification (MUSIC) method are the most common examples of parametric methods applied to power system waveform distortion assessment.
Other parametric methods are developed according to the non-stationary data modelling approach. These methods apply a mathematical model of the system under study, and they utilize the voltage and current measurements in order to provide a dynamic correction to the model at any time. In this way, voltage and current phasors for different harmonic orders can be obtained by the state model, and their variations can be detected versus time in a measurement update step. The main method in this category is the Kalman filter [7,28].

A brief discussion of the theoretical background of Prony's method, ESPRIT method, MUSIC method and Kalman filter is presented in the next Sub-sections.

1.3.1 Prony's method

The Prony's method approximates the waveform samples with a linear combination of a finite number M of complex exponentials. The computation of the unknown parameters of each exponential function provides a spectral estimation of the waveform. These parameters are the amplitudes, the frequencies, the damping factors and the initial phases of the exponentials. Their estimation is obtained by solving linear equation systems which impose the minimization of the error between the waveform samples and their approximation provided by the model.

Let $x(n)$ be a L-point sequence of the waveform to be analysed; Prony's method uses the following model to achieve the approximation $\hat{x}(n)$ of each sample [1]:

$$\hat{x}(n) = \sum_{k=1}^{M} A_k e^{(\alpha_k + j\omega_k)nT_s + j\phi_k}, \quad n = 0,1,\dots,L-1 \tag{1.32}$$

where A_k, α_k, $\omega_k = 2\pi f_k$ and ϕ_k are the amplitude, the damping factor, the angular velocity, and the initial phase of the k-th exponential, respectively, and k is the exponential code. Since the waveform to be approximated is real, $M \leq L/2$ is an even number and the linear combination (1.32) is constituted by couples of complex conjugated exponentials. Introducing the following variables [1]:

$$z_k = e^{(\alpha_k + j\omega_k)T_s} \tag{1.33}$$

$$h_k = A_k e^{j\phi_k} \tag{1.34}$$

the Eq. (1.32) can be rewritten in the following, more compact form [1]:

$$\hat{x}(n) = \sum_{k=1}^{M} h_k z_k^n, \quad n = 0,1,\dots,L-1 \tag{1.35}$$

Considering only M equations and substituting $\hat{x}(n)$ with the actual waveform samples in the Eq. (1.35), the following system is obtained [1]:

$$\begin{bmatrix} x(0) \\ x(1) \\ \vdots \\ x(M-1) \end{bmatrix} = \begin{bmatrix} z_1^0 & z_2^0 & \cdots & z_M^0 \\ z_1^1 & z_2^1 & \cdots & z_M^1 \\ \vdots & \vdots & \vdots & \vdots \\ z_1^{M-1} & z_2^{M-1} & \cdots & z_M^{M-1} \end{bmatrix} \begin{bmatrix} h_1 \\ h_2 \\ \vdots \\ h_M \end{bmatrix} \tag{1.36}$$

Prony's approach is to separately calculate the variables z_k and h_k. This is possible by introducing a polynomial whose roots are the variables z_k, i.e. [1]:

$$z^M + a(1)z^{M-1} + \cdots + a(M-1)z + a(M) = 0; \tag{1.37}$$

obviously, the calculation of z_k by means the Eq. (1.37) requires the knowledge of the coefficients $a(m)$, $m = 1, \dots, M$. These can be evaluated by solving the following linear equation system obtained by manipulations of Eqs. (1.36) and (1.37) [1]:

$$\sum_{m=0}^{M} a(m)x(n-m) = 0, \quad n = M, M+1, \dots, L-1 \tag{1.38}$$

Once the variables z_k are known by solving Eqs. (1.38) and (1.37), the values h_k are evaluated by solving the linear equation system (1.36). Then, the unknown parameters of the M exponential components can be evaluated as:

$$\begin{aligned} f_k &= \frac{\omega_k}{2\pi} = \tan^{-1}\left[\frac{Im(z_k)}{Re(z_k)}\right] / (2\pi T_s), \; \alpha_k = \ln|z_k| / T_s, \\ A_k &= |h_k|, \qquad\qquad \phi_k = \tan^{-1}\left[\frac{Im(h_k)}{Re(h_k)}\right] \end{aligned} \tag{1.39}$$

As previously stated, the Prony's method can be applied both to an entire data sequence and to successive data blocks, applying a sliding-window on all available waveform. This sliding-window can be shifted in time either by overlapping the subsequent data blocks, or by non-overlapping them according to the required representation of model parameters (typically, amplitudes and frequencies) in time.

Note also that the data block size can be fixed or variable, depending on the particular nature of the waveform to be analysed. An adaptive sizing of the analysis windows was described in [11] for the sliding-window Prony's method. The usefulness of the adaptive windows in the detection of time-varying harmonic and interharmonic components is related to an evaluation of the proper width of each window, based on finding the best fit of the waveform in time.

Specifically, fixed the sampling rate f_s, if only L_j samples of the waveform $x(n)$ are considered for the *j*-th time window, the estimation error can be evaluated for each sample as:

$$e_n = |\hat{x}(n) - x(n)|, \quad n = 0,1, \dots, L_j - 1 \tag{1.40}$$

where $\hat{x}(n)$ is evaluated as in (1.32).

Evaluating the (1.40) for each of the L_j samples considered in the *j*-th time window, the mean square relative error ε_{j-curr}^2 can be defined in order to quantify the fidelity of the current model:

$$\varepsilon_{j-curr}^2 = \frac{1}{L_j}\sum_{n=0}^{L_j-1} \frac{|\hat{x}(n)-x(n)|^2}{x(n)^2}. \tag{1.41}$$

In particular, it is possible to individuate the most suitable length of the *j*-th time window when $\varepsilon_{j-curr}^2 \leq \varepsilon_{thr}^2$ occurs by properly selecting a threshold value ε_{thr}^2 for the mean square relative error ε_{j-curr}^2.

Moreover, as previously mentioned, the Prony's model requires the prior selection of the number of exponential functions in the linear combination (1.32). This number fixes univocally also the number of spectral components that could be evaluated by the method, so this selection is a fundamental aspect. The general principle is that a too smoothed spectrum is

obtained when a too small number of exponentials is selected, while some spurious low-amplitude spectral components could be introduced in the spectrum if a too high number of exponentials is chosen.
Different criteria were proposed in relevant literature in order to individuate the proper number of exponentials to be included in the Prony's model. Among them, Final Prediction Error (FPE), the Akaike Information Criterion (AIC), the Minimum Description Length (MDL) criterion, the autoregressive transfer criterion (CAT), and a criterion based on the eigendecomposition of the sample autocorrelation matrix are the most frequently applied [4-5,75-79].
In particular, the MDL criterion seems to properly evaluate the optimal number of exponential function in (1.32) when power system waveforms are analysed. The MDL method selects the value M corresponding to the minimum of the following MDL function:

$$MDL(M) = L\ln(\hat{\sigma}_M^2) + M\ln L \tag{1.42}$$

where L is the number of samples in the analysis window and $\hat{\sigma}_M^2$ is the estimated variance of the square prediction error [80].
Due to the great accuracy provided by the Prony's method, many other Prony-based methods and their applications have been proposed in relevant literature [80-89]. For example, a reduced Prony's algorithm was presented in [88-89], where damping factors and frequencies of all of the spectral components included in the waveform spectrum were supposed to be prior known. In this way, only the linear equation system for the estimation of h_k had to be solved, reducing global computational efforts. An exhaustive overview of the application of Prony-based methods for the spectral analysis and the evaluation of PQ indices in power system field is in [11,80,83-86,88,90-94].

1.3.2 ESPRIT method

The ESPRIT method belongs to the so-called "subspace methods", since is involves the linear algebraic concept of subspace in the model parameter estimation. The ESPRIT model assumes the waveform samples to be represented through a sum of $M/2$ couples of complex conjugated exponentials in the white noise. This is a background noise, and it represents the additive noise related to the measurement observations. The statistical characterization of the white noise is prior known in terms of mean value and co-variance. The unknown parameters of the model are, once again, the damping factors, the amplitudes, the initial phases and the frequencies of the exponentials.
Assuming the waveform sample vector to belong to a subspace, this vector can be used in the estimation of the auto-correlation matrix. In particular, two subspaces can be defined i.e., the waveform and the noise subspace. The fundamental principle of the ESPRIT method consists in the shift invariance between the discrete time series, which guarantees the rotational invariance between the corresponding subspaces.
Let $x(n)$ be a L-point sequence of the waveform; ESPRIT method uses the following model to achieve the approximation $\hat{x}(n)$ of each sample [1]:

$$\hat{x}(n) = \sum_{k=1}^{M} h_k e^{(\alpha_k + j\omega_k)nT_s} + r(n), \quad n = 0,1,\dots,L-1 \tag{1.43}$$

where $h_k = A_k e^{j\phi_k}$ and $r(n)$ represents the additive white noise.
Considering only $L_1 < L$ samples $x(n)$ of the waveform, and substituting them to $\hat{x}(n)$ in (1.43), the following relationship can be written:

$$\boldsymbol{x}(n) = \boldsymbol{V}\boldsymbol{\Phi}^n\boldsymbol{H} + \boldsymbol{r}(n), \tag{1.44}$$

where:

$$\begin{gathered}
\boldsymbol{x}(n) = [x(n) \quad x(n+1) \quad \cdots \quad x(n+L_1-1)]^T \\
\boldsymbol{V} = \begin{bmatrix} 1 & 1 & \cdots & 1 \\ e^{(\alpha_1+j\omega_1)} & e^{(\alpha_2+j\omega_2)} & \dots & e^{(\alpha_M+j\omega_M)} \\ \vdots & \vdots & \vdots & \vdots \\ e^{(\alpha_1+j\omega_1)(L_1-1)} & e^{(\alpha_2+j\omega_2)(L_1-1)} & \dots & e^{(\alpha_M+j\omega_M)(L_1-1)} \end{bmatrix} \\
\boldsymbol{H} = [h_1 \quad h_2 \quad \cdots \quad h_M]^T \\
\boldsymbol{\Phi} = \begin{bmatrix} e^{(\alpha_1+j\omega_1)} & 0 & \cdots & 0 \\ 0 & e^{(\alpha_2+j\omega_2)} & \dots & 0 \\ \vdots & \vdots & \vdots & \vdots \\ 0 & 0 & \cdots & e^{(\alpha_M+j\omega_M)} \end{bmatrix} \\
\boldsymbol{r}(n) = [r(n) \quad r(n+1) \quad \cdots \quad r(n+L_1-1)]^T.
\end{gathered} \tag{1.45}$$

The previous relationships show that the matrix $\boldsymbol{\Phi}$ provides information about the damping factors and the frequencies of the *M* components selected in the ESPRIT model. The evaluation of an estimation $\hat{\boldsymbol{\Phi}}$ of $\boldsymbol{\Phi}$, obtained by means of an estimation $\hat{\mathbf{R}}$ of the auto-correlation matrix $\mathbf{R}$ of the waveform, evaluated for the selected L_1 samples, is therefore necessary.
The eigenvectors of the auto-correlation matrix $\mathbf{R}$ of order L_1 can be divided between the matrix $\mathbf{S} = [\boldsymbol{s}_1 \quad \boldsymbol{s}_2 \quad \cdots \quad \boldsymbol{s}_M]$ and the matrix $\mathbf{E} = [\boldsymbol{e}_1 \quad \boldsymbol{e}_2 \quad \cdots \quad \boldsymbol{e}_{L_1-M}]$. The elements of $\mathbf{S}$ correspond to the *M* largest eigenvalues of $\mathbf{R}$, while the elements of $\mathbf{E}$ correspond to the remaining eigenvalues. In this way, two subspaces are constructed: signal and noise subspace, respectively.
Let $\mathbf{I}_{L_1-1}$ be the identity matrix of order $L_1 - 1$; two other matrices $\boldsymbol{\Gamma}_1 = [\mathbf{I}_{L_1-1} \quad 0]$ and $\boldsymbol{\Gamma}_2 = [0 \quad \mathbf{I}_{L_1-1}]$ are introduced to select the first $L_1 - 1$ rows and the last $L_1 - 1$ rows of $\mathbf{S}$, respectively; the following matrices $\mathbf{S}_1$ and $\mathbf{S}_2$ are thus obtained:

$$\begin{aligned} \mathbf{S}_1 &= \boldsymbol{\Gamma}_1\mathbf{S}, \\ \mathbf{S}_2 &= \boldsymbol{\Gamma}_2\mathbf{S}. \end{aligned} \tag{1.46}$$

These matrices allow the evaluation of the matrix $\boldsymbol{\Psi}$:

$$\mathbf{S}_2 = \mathbf{S}_1\boldsymbol{\Psi}. \tag{1.47}$$

According to the rotational invariance theory, the evaluation of the rotation matrix $\boldsymbol{\Phi}$ is equivalent to the calculation of matrix $\boldsymbol{\Psi}$. The total least-squares (TLS) approach (TLS-ESPRIT) is one of the most common methods for the estimation $\hat{\boldsymbol{\Psi}}$ of $\boldsymbol{\Psi}$:

$$\widehat{\mathbf{\Psi}} = (\hat{\mathbf{S}}_1^* \hat{\mathbf{S}}_1)^{-1} \hat{\mathbf{S}}_1^* \hat{\mathbf{S}}_2. \tag{1.48}$$

where $\hat{\mathbf{S}}_1$ and $\hat{\mathbf{S}}_2$ are estimations of $\mathbf{S}_1$ and $\mathbf{S}_2$, respectively.
As previously stated, the knowledge of the eigenvalues of $\widehat{\mathbf{\Phi}}$, that are the same eigenvalues of $\widehat{\mathbf{\Psi}}$, allows the evaluation of frequencies and damping factors of the M exponential functions in the ESPRIT model. Once frequencies and damping factors are known, also the M amplitudes and the M initial phases can be computed.
In particular, the amplitudes are obtained by solving a linear system of M equations related to the definition of the auto-correlation matrix $\mathbf{R}$:

$$\mathbf{R} = \mathbf{V}\mathbf{A}\mathbf{V}^H + \sigma_w^2 \boldsymbol{I}. \tag{1.49}$$

where the symbol ^{H} represents the Hermitian matrix, $\boldsymbol{I}$ is the identity matrix of order M, σ_w^2 is the variance of the white noise and:

$$\boldsymbol{A} = \begin{bmatrix} A_1^2 & 0 & \cdots & 0 \\ 0 & A_2^2 & \cdots & 0 \\ \vdots & \vdots & \vdots & \vdots \\ 0 & 0 & \cdots & A_M^2 \end{bmatrix}. \tag{1.50}$$

The initial phases can be then estimated through the vector $\boldsymbol{H}$ obtained by solving the (1.44) and imposing the white noise $\boldsymbol{r}(n)$ to be negligible.
Also the ESPRIT method can be applied to an entire data sequence or to several data blocks, with or without overlapping. Moreover, the adaptive technique introduced for the Prony's method can also be applied in the ESPRIT method [80]. An exhaustive overview of the application of ESPRIT-based methods for the spectral analysis and the evaluation of PQ indices in power system field is in [92,94-101].

1.3.3 MUSIC method

The MUSIC method is another subspace method, characterized by the same model (1.43) of the ESPRIT method. The parameters of the model are once again the amplitudes, the damping factors, the initial phases and the frequencies of the exponential functions.
Also the MUSIC method is based on the manipulation of the eigenvectors of an auto-correlation matrix estimation $\widehat{\mathbf{R}}$; these eigenvectors can be opportunely separated into signal and noise subspaces.
As previously seen, the ESPRIT method uses only the signal subspace in the procedure for the evaluation of the unknown parameters in the model (1.43). Instead, the MUSIC method uses only the noise subspace in its procedure for the estimation of the frequencies in the model (1.43). In particular, let $\mathbf{E} = [\boldsymbol{e}_1 \quad \boldsymbol{e}_2 \quad \cdots \quad \boldsymbol{e}_{L_1-M}]$ be the noise subspace; its elements are manipulated in order to obtain the following polynomial in the z-domain:

$$\hat{P}(\zeta) = \frac{1}{\sum_{i=M+1}^{L_1} E_i(\zeta) E_i^* \left(\frac{1}{\zeta^*}\right)} \tag{1.51}$$

with:

$$E_i(\zeta) = \sum_{r=0}^{L_1-1} e_i(r)\zeta^{-1} \tag{1.52}$$

where $e_i(r)$ is the *r*-th element of the *i*-th eigenvector in noise subspace.
Note that the polynomial $\hat{P}(\zeta)$ in (1.51) has *M* roots, two by two complex conjugate, along the unit circle. These roots provide the frequencies of the waveform spectral components. This technique for frequency detection is called the Root-MUSIC method.
Once the frequencies are known, the corresponding amplitudes can be evaluated by solving a linear equation system of dimension *M* obtained through the estimated autocorrelation matrix, as well as for the ESPRIT method. Similarly to ESPRIT method, also the initial phase estimation is performed.
As previously stated, the Root-MUSIC method can be applied to an entire data sequence or to several data blocks, with or without overlapping [80]. An exhaustive overview of the application of MUSIC-based methods for the spectral analysis and the evaluation of PQ indices in power system field is in [80,94,97,100-103].

1.3.4 Kalman filter

Kalman Filter [12] is an algorithm that considers a set of mathematical equations with added noise, and it assumes the availability of inaccurate measurement data. Kalman filter allows a recursive evaluation of past, present or future value estimations through the minimization of the mean square error.
The mathematical model is constructed by means of the state variable approach in discrete time domain. Assuming a fixed sampling rate T_s, at the generic time nT_s ($\forall\, n \in \mathbb{N}$) the model assumes the following expression [6-7]:

$$\boldsymbol{y}(n+1) = \boldsymbol{\Phi_{KF}}(n)\boldsymbol{y}(n) + \boldsymbol{w}(n) \tag{1.53a}$$

$$\boldsymbol{x}(n) = \mathbf{H_{KF}}(n)\boldsymbol{y}(n) + \boldsymbol{v}(n) \tag{1.53b}$$

where:

- $\boldsymbol{y}(n)$ and $\boldsymbol{x}(n)$ are the state vector and the measurement vector, respectively;
- $\boldsymbol{w}(n)$ and $\boldsymbol{v}(n)$ are the independent model and measurement white noise, respectively, with prior known probability density functions. They represent the inability of the model to properly fit the system under study and the measurement error, respectively;
- $\boldsymbol{\Phi_{KF}}(n)$ is generally a time dependent state transition matrix, that makes a connection between the state $\boldsymbol{y}(n+1)$ and the state $\boldsymbol{y}(n)$;
- $\mathbf{H_{KF}}(n)$ is generally a time dependent measurement matrix, that makes a connection between the measurement $\boldsymbol{x}(n)$ and the corresponding state $\boldsymbol{y}(n)$.

The Eqs. (1.53a) and (1.53b) are defined as state equations and measurement equations, respectively. Some examples of models for the description of sinusoidal waveform are provided in the next Sub-section.
Starting from an initial state estimation $\hat{\boldsymbol{y}}(0)$ and to its corresponding covariance error matrix estimation $\boldsymbol{P_{KF}}(0)$, Kalman filter recursively applies the following set of equation:

- *predictive time-update* equations:

$$\hat{\boldsymbol{y}}^{-}(n) = \boldsymbol{\Phi_{KF}}(n-1)\hat{\boldsymbol{y}}(n-1) \tag{1.54}$$

$$\boldsymbol{P_{KF}^{-}}(n) = \boldsymbol{\Phi_{KF}}(n-1)\boldsymbol{P_{KF}}(n-1)\boldsymbol{\Phi_{KF}}^{T}(n-1) + \boldsymbol{W_{KF}}(n-1) \tag{1.55}$$

- *corrective measurement-update* equations:

$$\mathbf{K_{KF}}(n) = \boldsymbol{P_{KF}^{-}}(n) \cdot \mathbf{H_{KF}}^{T}(n) \cdot (\mathbf{H_{KF}}(n) \cdot \boldsymbol{P_{KF}^{-}}(n) \cdot \mathbf{H_{KF}}^{T}(n) + \boldsymbol{V_{KF}}(n))^{-1} \tag{1.56}$$

$$\hat{\boldsymbol{y}}(n) = \hat{\boldsymbol{y}}^{-}(n) + \mathbf{K_{KF}}(n) \cdot (\mathbf{x}(n) - \mathbf{H_{KF}}(n)\hat{\boldsymbol{y}}^{-}(n)) \tag{1.57}$$

$$\boldsymbol{P_{KF}}(n) = (\boldsymbol{I} - \mathbf{K_{KF}}(n) \cdot \mathbf{H_{KF}}(n)) \cdot \boldsymbol{P_{KF}^{-}}(n) \tag{1.58}$$

where:

- $\hat{\boldsymbol{y}}(n)$ and $\hat{\boldsymbol{y}}^{-}(n)$ are the posterior (obtained after the measurement correction) and the prior (obtained without the measurement correction) estimation of the state variables at time nT_s, respectively;
- $\boldsymbol{P_{KF}^{-}}(n)$ and $\boldsymbol{P_{KF}}(n)$ are the prediction of the covariance error matrix at time $(n-1)T_s$ and the updated covariance error matrix at time nT_s, respectively;
- $\boldsymbol{W_{KF}}(n-1)$ and $\boldsymbol{V_{KF}}(n)$ are the process noise covariance matrix at time $(n-1)T_s$ and measurement noise covariance matrix at time nT_s, respectively;
- $\mathbf{K_{KF}}(n)$ is the Kalman gain evaluated at time nT_s.

Two common models for the description of sinusoidal waveform are generally reported in relevant literature. In particular, for a single component waveform, the first model is based on the concept of the harmonic oscillator, and its state equations can be represented as follow [6,104]:

$$\begin{aligned}\begin{bmatrix} y_{Re}(n+1) \\ y_{Im}(n+1) \end{bmatrix} = \boldsymbol{y}(n+1) &= \boldsymbol{\Phi_{KF}}\boldsymbol{y}(n) \\ &= \begin{bmatrix} \cos(\omega T_s) & \sin(\omega T_s) \\ -\sin(\omega T_s) & \cos(\omega T_s) \end{bmatrix} \begin{bmatrix} y_{Re}(n) \\ y_{Im}(n) \end{bmatrix}\end{aligned} \tag{1.59}$$

with obvious meaning of the symbols. In this case the state vector contains the real (cosinusoidal) and imaginary (sinusoidal) part of the actual voltage or current waveform. Moreover, in this model, the state transition matrix $\boldsymbol{\Phi_{KF}}$ is a time-constant matrix.
The corresponding measurement equation associated to the (1.59) is:

$$x(n) = \mathbf{H_{KF}}\boldsymbol{y}(n) = [1 \quad 0]\begin{bmatrix} y_{Re}(n) \\ y_{Im}(n) \end{bmatrix} \tag{1.60}$$

where the measurement is represented by the real part of the waveform under analysis.
The second model describes the sinusoidal waveform with a single spectral component by means of its phasor, so the state vector is represented by the direct and quadrature components of the phasor itself [6,104]:

$$\begin{bmatrix} y_{I-P}(n+1) \\ y_{Q-P}(n+1) \end{bmatrix} = \boldsymbol{y}(n+1) = \mathbf{\Phi_{KF}}\boldsymbol{y}(n) = \begin{bmatrix} 1 & 0 \\ 0 & 1 \end{bmatrix}\begin{bmatrix} y_{I-P}(n) \\ y_{Q-P}(n) \end{bmatrix} \tag{1.61}$$

In this case the state transition matrix $\mathbf{\Phi_{KF}}$ is an identity matrix, since the phasor ideally does not change in time.
The associated measurement equation is:

$$x(n) = \mathbf{H_{KF}}(n)\boldsymbol{y}(n) = [\sin(\omega n T_s) \quad \cos(\omega n T_s)]\begin{bmatrix} y_{I-P}(n) \\ y_{Q-P}(n) \end{bmatrix} \tag{1.62}$$

where the measurement matrix $\mathbf{H_{KF}}(n)$ is a time-dependent matrix, and the measurement is the same of the previous model.
Obviously, when the waveform to be analysed has more than one spectral component, the system has to be represented by an enlarged version of the models, where, the state vector dimension has to be M if $M/2$ is the total number of spectral component included in the waveform.
According to the different necessities of the specific applications, many modifications to the traditional Kalman filter have been proposed in relevant literature. Among these, the most relevant techniques are the Extended Kalman filter, the Unscented Kalman filter and the Ensemble Kalman filter. The aforesaid methods have the aim of overcoming the main limits of the traditional Kalman filter (mainly the low performances in presence of non-linear systems, and the high-computational effort) [105-106]. An exhaustive overview of the application of Kalman Filter-based methods for the spectral analysis and the evaluation of PQ indices in power system field is in [28,97,105-112].

1.4 Hybrid Methods

Many hybrid methods have been proposed in relevant literature [13-21], aiming to take the advantages of the original methods from which descend and to simultaneously overcome their main drawbacks [7].
Hybrid methods, as presented in [13-14], join different non-parametric methods. In [13], i.e., the proposed method detected transients by means of the WT, and then the FFT was used for the spectral analysis of the same waveform. Also the method proposed in [14] was based on WT and the FFT. In this case, the aim of the WT was to de-noise of the waveform before it was analysed through the FFT.

Similarly, also hybrid methods based only on parametric methods have been introduced in relevant literature. In [15], the authors combined the Kalman filter and the Prony method. In particular, the Prony method was used for the detection of the frequency spectral components included in the waveform, while the Kalman filter provided the corresponding amplitudes and initial phases. A Prony-ESPRIT based method for the assessment of the waveform distortion due to adjustable speed drive (ASD) was presented in [21]. This method was articulated in four step, and it was also based on the analytical knowledge of the frequencies introduced by the ASD, so only amplitudes and initial phases were evaluated for some bands of frequency.

The hybrid methods constituted of combinations of one or more non-parametric methods with one or more parametric methods are the most significant, since, generally, the resulting method is able to compensate the drawbacks of the original methods.

For example, the WT coupled to the Kalman filter was presented in [16]f or a real-time estimation of the spectral components. Specifically, the WT was used in order to reduce the tracking time of a Kalman filter-based method, applied for the detection of different harmonic amplitudes and phases. In [17], the WT was coupled to the Prony method; the WT was performed to individuate the transients and then, the transient frequency contents was evaluated through the Prony method.

The sliding-window hybrid methods based on the joint of parametric methods and DFT are particularly suitable when a spectrum detection characterized by high accuracy and reduced computational effort is required. Different sliding-window parametric-DFT methods have been proposed in relevant literature [18-20]. These hybrid methods can be double-steps [18-19] or three-steps [20], and are characterized by a decomposition of the waveform in two or more frequency bands, separately analysed through a parametric method or through the DFT.

Specifically, the method presented in [18] analysed the fundamental frequency and the interharmonics below the 100 Hz in the first step by means the ESPRIT method. Then, thanks to the knowledge of the fundamental period of the waveform, in the second step it was possible to use a synchronized time window for the spectral analysis effected through the DFT. In this second step, the DFT was applied for the analysis of the original waveform, curtailed of the frequency band analysed in the first step, providing only the harmonic components included in the original waveform.

Similarly to the method in [18], the hybrid method presented in [19] analysed the fundamental component in the first step by means of the Prony's method, then the harmonic components were obtained by a synchronized DFT.

Finally, the method presented in [20] was a sort of extension of the previous methods, since a step was added in order to estimate the interharmonics components above 100 Hz. Specifically, the waveform was divided also in this case in two frequency bands. In the first step, the spectral components up to 100 Hz were detected through the ESPRIT method. After this step, the estimated fundamental component was used for the synchronization of the DFT analysis window, that allowed, in the second step, the harmonic detection. In the third step, the ESPRIT method was again applied to the residual waveform (the original waveform without spectral component up to 100 Hz and without harmonic components), in order to estimate the interharmonics above 100 Hz.

Note that in these hybrid methods, thanks to the division in two bands of frequency, the parametric models require in each steps a more reduced number of exponentials than that

required using the parametric method for the spectral analysis of the whole waveform. Moreover, the use of a synchronized window for the DFT in the second step allows an increased accuracy in the harmonic detection. In this way, all of the aforesaid methods simultaneously guarantee a higher accuracy than the DFT and a lower computational effort than the parametric method.
The use of sliding-windows in the spectral analysis allows these parametric-DFT based methods to be applied also for the detection of time-varying spectral components and for the evaluation of PQ indices.

1.5 Filter bank-based Techniques

The wavelet based techniques can be considered as successive band-pass filters, so the signal processing has been greatly inspired also by different other filter bank-based techniques [6,113].
The multiscale analysis and synthesis filter banks are made up of combined versions of the basic module in Fig. 1.9, where $H_0(\zeta)$ and $H_1(\zeta)$ are the low-pass and high-pass filter of a two-channel analysis filter bank and $F_0(\zeta)$ and $F_1(\zeta)$ are the low-pass and high-pass filter of a two-channel synthesis filter bank.

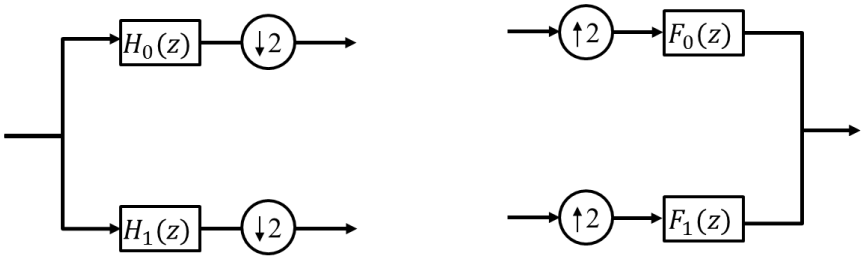

Figure 1.9 *– Basic module of (a) analysis filter bank and (b) synthesis filter bank*

Both filter banks require a resampling; a down-sampling of 2 is applied to the output waveforms for the analysis filters, while an up-sampling of 2 is needed for the input waveforms for the synthesis filters [2].
Basic modules can be combined in order to obtain full-length bandpass components of the original waveform. The sizing of both analysis and synthesis filter bank is based on the "perfect reconstruction" (PR) concept. This means that it is desirable that the waveform remains uncorrupted (except for possible time delay or amplification) after the analysis filter bank and the synthesis filter bank are applied. The PR condition is reached by verifying the following conditions in the z-domain:

$$F_0(\zeta)H_0(-\zeta) + F_1(\zeta)H_1(-\zeta) = 0 \tag{1.63}$$

$$F_0(\zeta)H_0(\zeta) + F_1(\zeta)H_1(\zeta) = 2\zeta^{-l} \tag{1.64}$$

with l representing the time delay. The Eqs. (1.63) and (1.64) are the aliasing cancellation condition and the no-distortion condition, respectively. In particular, from the (1.63) it descends that:

$$F_0(\zeta) = H_1(-\zeta) \quad F_1(\zeta) = -H_0(-\zeta) \tag{1.65}$$

Moreover, introducing the half-band filter $P_0(\zeta) = H_0(\zeta)F_0(\zeta)$ and substituting the (1.65) in the (1.64), the following relation can be obtained:

$$P_0(\zeta) - P_0(-\zeta) = 2\zeta^{-l} \tag{1.66}$$

The PR conditions guarantee the filter banks to be orthogonal; this means that the synthesis filter bank corresponds to the inverse of the analysis filter bank, i.e.:

$$\begin{bmatrix} F_0(\zeta) \\ F_1(\zeta) \end{bmatrix} \cdot \begin{bmatrix} H_0(\zeta) \\ H_1(\zeta) \end{bmatrix} = \boldsymbol{I} \tag{1.67}$$

Sometimes finite impulse response (FIR) filters are required both for the analysis and for the synthesis filter banks. In these cases, since the inverse of a FIR filter is often an infinite impulse response (IIR) filter, an additive condition between $H_0(\zeta)$ and $H_1(\zeta)$ in the filter bank sizing is required in order to make the two filters orthogonal [2].
Assuming an odd order N_f, a possible choice is to impose the coefficients of the high-pass filter $H_1(\zeta)$ as the alternating flip of the low-pass filter $H_0(\zeta)$:

$$H_1(\zeta) = -\zeta^{-N_f} H_0(-\zeta^{-1}) \tag{1.68}$$

Substituting the Eq. (1.68) in (1.65):

$$F_0(\zeta) = H_1(-\zeta) = \zeta^{-N_f} H_0(\zeta^{-1}) \tag{1.69}$$

$$F_1(\zeta) = -H_0(-\zeta) = \zeta^{-N_f} H_1(\zeta^{-1}) \tag{1.70}$$

So, given the low-pass analysis filter $H_0(\zeta)$, the Eqs. (1.68) – (1.70) have to be used to obtain the other filters of the orthogonal PR FIR filter banks.
In other cases, a filter bank with linear-phase is required. The impulse response of such a filter can be either symmetric :

$$H(\zeta) = \zeta^{-N_f} H(\zeta^{-1}) \tag{1.71}$$

or asymmetric:

$$H(\zeta) = -\zeta^{-N_f} H(\zeta^{-1}) \tag{1.72}$$

In particular, the following conditions have to be satisfied in order to obtain a two-channel bi-orthogonal PR filter bank with linear-phase:

$$H_0(\zeta) = \zeta^{-N_f} H_0(\zeta^{-1}) \text{ and } H_1(\zeta) = -\zeta^{-N_f} H_1(\zeta^{-1}) \quad (1.73)$$

for an even filter order N_f, or:

$$H_0(\zeta) = \zeta^{-N_f} H_0(\zeta^{-1}) \text{ and } H_1(\zeta) = \zeta^{-N_f} H_1(\zeta^{-1}) \quad (1.74)$$

for an odd filter order N_f.

The relationships (1.73) and (1.74) involve that both ζ_i and ζ_i^{-1} have to be roots of the filter.

This propriety has to be used in the factorization of $P(\zeta)$, in order to obtain $H_0(\zeta)$ and $F_0(\zeta)$ as linear-phase filters. Once $H_0(\zeta)$ and $F_0(\zeta)$ are obtained, the other two filters can be evaluated using the Eqs. (1.65).

Note that linear-phase filters cannot be also orthogonal filters for two-channel PR FIR filter banks. Therefore, a proper selection between the two possibilities is necessary on the basis of the specific applications.

An exhaustive overview of the application of filter banks for the spectral analysis and the evaluation of PQ indices in power system field is in [28,113-118].

1.6 Theoretical comparisons among the methods

The non-parametric methods perform a transformation of the sampled waveform and do not require a prior knowledge of the system under investigation. The DFT is the most popular non-parametric method, but it has many drawbacks, i.e.: (i) the frequency resolution is related to the selected time duration of the analysis window; (ii) spectral leakage problems and picket fence effects can occur; (iii) the FFT algorithm needs, for each analysis window, a number of samples equal to an integer power of 2 to be able to cover a integer number of cycles of the fundamental period. Windowing, interpolation and resampling techniques reduce some of the aforesaid DFT limitations, but the incompatibility to simultaneously have high time- and frequency-resolutions persists, making the DFT-based methods less accurate than other techniques. However, the main advantage of the DFT-based methods is the reduced computational burden, especially when the FFT algorithm is used.

The DWT and the WPT are able to provide multi-resolution spectral analyses, offering good time information about the analysed waveform, especially in the transient identification. Nevertheless, both DWT and WPT have very limited capability to provide accurate frequency detection; the WPT appears to show an improvement with respect to the DWT, since it has a more uniform frequency decomposition. However, the main drawbacks of the WT-based methods are the high computational effort, and difficulties in the result interpretation and in the proper selection of the mother wavelet.

The HHT is based on the decomposition of the waveform in IMFs, utilized as adaptive basis functions. This makes the HHT particularly suitable for the spectral analysis of both non-linear and non-stationary waveforms. Also the HHT requires adequate additional tools for the interpretation of the transformed parameters related, e.g., to the energetic content of the spectral component. The HHT accuracy is highly dependent on the choices and the approximations effected during the application of the EMD, and, an oversampling of the

waveform is often required in order to more-accurately identify the instantaneous frequency, thus hugely increasing the computational burden. However, the main drawback of the HHT is the unsuitable detection of closely-located spectral components, and, above all, the HHT applications are limited to narrow band-passed signals, that are very rare in modern electrical systems.

The CZT is another important method for the spectral analysis, but its application appears to be very limited since it is able to provide accurate information (even better than DFT) only on small frequency bands, although requiring higher computational burden than DFT.

Conversely to non-parametric methods, the parametric methods can provide very accurate results without frequency resolution problems, but their main drawback is the too high computational burden that limits their use for the only offline applications. In particular, the Prony's method, ESPRIT method and MUSIC method require a duration of the analysis window equal to at least one cycle of the fundamental period, but they are free from synchronized sampling or spectral leakage problems. Little inaccuracies of Prony's method can arise when the waveform to be analysed is heavily affected by noise. This problem is overcome by both the ESPRIT and the MUSIC method, that include the contribute of the white noise into their model. However, the MUSIC method requires too high storage potentiality for the analysis of large array, and it also appears to be less accurate than the ESPRIT method. Note also that the ESPRIT method error in the detection of the spectral component amplitudes is higher than the respective Prony's method error, while the frequency estimation is generally provided with the same accuracy. Difficulties can arise for the Prony's method, ESPRIT method and MUSIC method in the adequate selection of the model order, even if their adaptive versions are able to properly choose the number of exponentials to be included in the model.

The Kalman filter needs more information about the system to be observed than the previous parametric methods. It can suffer with problem related to the filter drop-off and related to sudden variations of state variables for invariance of the estimation parameters.

Hybrid methods try to overcome as much as possible the main problems of the basis method, still holding their advantages. In particular, the aim of the parametric-DFT-based hybrid methods is to guarantee a reduced computational effort than a parametric method, and higher accuracy than the DFT.

Finally, although the filter banks require a computational effort lower than DFT-based methods and DWT-based methods, their accuracy is generally poor, since filter outputs do not correspond to pure harmonic components, and overlapped spectral content is often included in each band.

1.7 References

[1] P. Caramia, G. Carpinelli, P. Verde, Power Quality Indices in Liberalized Market, John Wiley & Sons, Chichester, West Sussex (UK), 2009

[2] M. Bollen, I. Y. H. Gu, Signal Processing of Power Quality Disturbances, Wiley-IEEE Press, New Jersey, 2006

[3] S. M. Kay, Modern Spectral Estimation: Theory and Application, Prentice-Hall, New Jersey, 1988

[4] J.G. Proakis, D.G. Manolakis, Digital Signal Processing Principles, Algorithms, and Applications, Prentice-Hall, New Jersey, 1996

[5] P. Stoica, R. Moses, Introduction to Spectral Analysis, Prentice Hall, New Jersey, 1997

[6] P. F. Ribeiro, Time-Varying Waveform Distortions in Power Systems, Wiley, 2009

[7] S. K. Jain, S.N. Singh, Harmonics estimation in emerging power system: Key issues and challenges, Electric Power Systems Research, vol. 81, no. 9, 2011, 1754-1766

[8] S. Chen and H. Y. Zhu, Wavelet transform for processing power quality disturbances, EURASIP Journal on Advances in Signal Processing, vol. 2007, 2007

[9] N. E. Huang, M. L. Wu, W. Qu, S. R. Long, S. S. Shen, Applications of Hilbert–Huang transform to non-stationary financial time series analysis, Applied stochastic models in business and industry , vol.19, no.3, 2003, 245-268

[10] L. Rabiner, R. Schafer and C. Rader, The chirp z-transform algorithm, IEEE Transactions on Audio and Electroacoustics, vol. 17, no. 2, 1969, 86-92

[11] A. Bracale, P. Caramia, G. Carpinelli, Adaptive Prony Method for Waveform Distortion Detection in Power Systems, International Journal of Electrical Power & Energy Systems, vol. 29, no. 5, 2007, 371-379

[12] R.E. Kalman, A new approach to linear filtering prediction problems, Trans. ASME.J. Basic Eng., vol. 82, 1960, 35–45

[13] T. Tarasiuk, Hybrid wavelet-Fourier spectrum analysis, IEEE Trans. Power Del., vol. 19, 2004, 957–964

[14] C. Chen, T. Xu, Z. Piao, W. Liang, Y. Yuan, The study on FFT harmonic detecting method of rural network based on wavelet denoising, Int. Conf. Energy Environ. Technol., vol. 2, 2009, 365–368

[15] F.F. Costa, A.J.M. Darlan, A. Fernandes, Harmonic analysis based on Kalman filtering and Prony's method, Int. Conf. on Power Engineering, Energy and Electrical Drives, 2007, 696–701

[16] Y.Z. Liu, S. Chen, A wavelet based model for on-line tracking of power system harmonics using Kalman filtering, IEEE Power Eng. Soc. Summer Meet., vol. 2, 2001, 1237–1242

[17] T. Lobos, J. Rezmer, H.-J. Koglin, Analysis of power system transients using wavelets and Prony method, IEEE Power Technol. Proc., vol. 4,2001

[18] A. Bracale, G. Carpinelli, An ESPRIT and DFT-based new method for the waveform distortion assessment in power systems, 20th Int. Conf. and Exhibition on Electricity Distribution, CIRED, 2009, 1–4

[19] A. Bracale, P. Caramia, G. Carpinelli, A. Rapuano, A new, sliding-window Prony and DFT scheme for the calculation of power-quality indices in the presence of non-stationary waveforms, International Journal of Emerging Electric Power Systems, vol. 13, no. 5, 2013

[20] A. Bracale, G. Carpinelli, I.Y.-H. Gu, M.H.J. Bollen, A new joint sliding-window ESPRIT and DFT scheme for waveform distortion assessment in power systems, Electric Power Systems Research, vol. 88, 2012, 112-120

[21] A. Bracale, P. Caramia, P. Tricoli, F. Scarpa, L. Piegari, A new advanced method for assessment of waveform distortions caused by adjustable speed drives, IAS Annual Meeting, 2011, 1-10

[22] B. Barkat, B. Boashash, A high-resolution quadratic time-frequency distribution for multicomponent signals analysis, IEEE Transactions on Signal Processing, vol. 49, no. 10, 2001, 2232-2239

[23] B. Boashash, Time-frequency signal analysis, Advances in Spectrum Analysis and Array Processing, S. Haykin, Ed. Englewood Cliffs, NJ: Prentice-Hall, , vol. 1, ch. 9, 1991, 418–517

[24] M. G. Amin, W. J. Williams, High spectral resolution time-frequency distribution kernels, IEEE Trans. Signal Processing, vol. 46, 1998, 2796–2804

[25] B. Boashash, Time Frequency Signal Analysis, Melbourne, Australia: Longman Cheshire, 1992.

[26] D. König, J. F. Böhme, Wigner-Ville spectral analysis of automotive signals captured at knock, Appl. Signal Process., vol. 3, 1996, 54–64.

[27] H.I. Choi, W.J. Williams, Improved time-frequency representation of multicomponent signals using the exponential kernels, IEEE Trans. Acoust., Speech, Signal Processing, vol. 37, 1989, 862–871

[28] D. Granados-Lieberman, R.J. Romero-Troncoso, R.A. Osornio-Rios, A. Garcia-Perez, E. Cabal-Yepez, Techniques and methodologies for power quality analysis and disturbances classification in power systems: a review, IET Generation, Transmission & Distribution, vol. 5, no. 4, 2011, 519-529

[29] M.S. Kandil, S.A. Farghal, A. Elmitwally, Refined Power Quality Indices, IEE Proceedings - Generation, Transmission & Distribution, vol. 148, no. 6, 2001, 590-596

[30] P. Duhamel, M. Vetterli, Fast Fourier transforms: a tutorial review and a state of the art, Signal Process, vol. 19, 1990, 259–299

[31] F. J. Harris, On the Use of Windows for Harmonic Analysis with the Discrete Fourier Transform, Proceedings of IEEE, vol. 66, no. 1, 1978, 51-83

[32] D. Gallo, R. Langella, A. Testa, On the Processing of Harmonics and Interharmonics in Electrical Power Systems, IEEE PES Winter Meeting, Singapore, 2000

[33] P. Langlois, R. Bergeron, Interharmonic Analysis by a Frequency Interpolation Method, 2nd International Conference on Power Quality, Atlanta (USA), 1992

[34] D. Gallo, R. Langella, A. Testa, Interharmonic Analysis Utilising Optimised Harmonic Filtering, IEEE International Symposium on Diagnostics for Electric Machines, Power Electronics and Drives (SDEMPED), Gorizia (Italy), 2001

[35] D. Gallo, R. Langella, A. Testa, A Self Tuning Harmonics and Interharmonics Processing Technique", European Transaction on Electrical Power, vol. 12, no. 1, 2002, 25-31

[36] D. Gallo, R. Langella, A. Testa, On the Processing of Harmonics and Interharmonics: Using Hanning Window in Standard Framework, IEEE Trans. on Power Delivery, vol. 19, no. 1, 2004, 28-34

[37] D. Gallo, R. Langella, A. Testa, Desynchronized Processing Technique for Harmonic and Interharmonic Analysis, IEEE Trans. on Power Delivery, vol. 19, no. 3, 2004, 993-1001

[38] R.M. Hidalgo, J.G. Fernandez, R.R. Rivera, H.A. Larrondo, A simple adjustable window algorithm to improve FFT measurements, IEEE Transactions on Instrumentation and Measurement, vol.51, no.1, 2002, 31-36

[39] G. Andria, M. Savino, A. Trotta, Windows and interpolation algorithms to improve electrical measurement accuracy, IEEE Transactions on Instrumentation and Measurement, vol. 38, no. 4, 1989, 856-863

[40] IEC standard 61000-4-7, General guide on harmonics and interharmonics measurements, for power supply systems and equipment connected thereto, 2010

[41] Y. N. Chang, Y. C. Hsieh, C. S. Moo, Truncation effects of FFT on estimation of dynamic harmonics in power system, Proceedings. PowerCon 2000 International Conference on Power System Technology, vol. 3, 2000

[42] J. Barros, I.D. Ramon, On the use of the Hanning window for harmonic analysis in the standard framework, IEEE transactions on power delivery, vol. 21, no.1, 2006, 538-539

[43] Z. Ren, B. Wang, Estimation algorithms of harmonic parameters based on the FFT, IEEE Power and Energy Engineering Conference (APPEEC), Asia-Pacific, 2010

[44] F. Zhang, Z. Geng, W. Yuan, The algorithm of interpolating windowed FFT for harmonic analysis of electric power system, IEEE transactions on power delivery, vol. 16, no. 2, 2001, 160-164

[45] H. Qian, R. Zhao, T. Chen, Interharmonics analysis based on interpolating windowed FFT algorithm, IEEE Transactions on Power Delivery, vol. 22, no. 2, 2007, 1064-1069

[46] G. W. Chang, C. I. Chen, Y. J. Liu, M. C. Wu, Measuring power system harmonics and interharmonics by an improved fast Fourier transform-based algorithm, IET generation, transmission & distribution , vol. 2, no. 2, 2008, 193-201

[47] T. X. Zhu, Exact harmonics/interharmonics calculation using adaptive window width, IEEE Transactions on Power Delivery, vol. 22, no. 4, 2007, 2279-2288

[48] O. P. Mahela, A. G. Shaik, N. Gupta, A critical review of detection and classification of power quality events, Renewable and Sustainable Energy Reviews, vol. 41, 2015, 495-505

[49] J. Barros, R. I. Diego, Application of the Wavelet-Packet Transform to the Estimation of Harmonic Groups in Current and Voltage Waveforms, IEEE Trans. on Power Delivery, vol. 21, no. 1, 2006, 533-535

[50] Y. Chen, Harmonic detection in electric power system based on wavelet multi-resolution analysis, IEEE International Conference on Computer Science and Software Engineering, vol. 5, 2008

[51] V. L. Pham, K. P. Wong, Wavelet-transform-based algorithm for harmonic analysis of power system waveforms, IEE Proceedings-Generation, Transmission and Distribution , vol.146, no. 3, 1999, 249-254

[52] T. Keaochantranond, C. Boonseng, Harmonics and interharmonics estimation using wavelet transform, IEEE/PES Transmission and Distribution Conference and Exhibition , Asia Pacific, vol. 2, 2002

[53] E.Y. Hamid, K. Zen-Ichiro, Instrument for the quality analysis of power systems based on the wavelet packet transform, IEEE Power Engineering Review, vol. 22, no. 3, 2002, 52-54

[54] L. Eren, M. J. Devaney, Calculation of power system harmonics via wavelet packet decomposition in real time metering, Proceedings of the 19th IEEE Instrumentation and Measurement Technology Conference, IMTC/2002, vol. 2, 2002

[55] R. I. Diego, J. Barros, Global method for time–frequency analysis of harmonic distortion in power systems using the wavelet packet transform, Electric Power Systems Research, vol. 79, no. 8, 2009, 1226-1239

[56] A. Mazloomzadeh, M. Mirsalim, H. Fathi, Harmonic and inter-harmonic measurement using discrete wavelet packet transform with linear optimization, 4th IEEE Conference on Industrial Electronics and Applications, ICIEA 2009, 2009

[57] F. Vatansever, A. Ozdemir, A new approach for measuring RMS value and phase angle of fundamental harmonic based on wavelet packet transform, Electric power systems research, vol. 78, no. 1, 2008, 74-79

[58] S. Nath, A. Dey, A. Chakrabarti, Detection of power quality disturbances using wavelet transform, World Academy of Science, Engineering and Technology, vol. 49, 2009, 869-873

[59] C. H. Kim, R. Aggarwal, Wavelet transforms in power systems. I. General introduction to the wavelet transforms, Power Engineering Journal, vol. 14, no. 2, 2000, 81-87

[60] J. Barros, R. I. Diego, Analysis of harmonics in power systems using the wavelet-packet transform, IEEE Transactions on Instrumentation and Measurement, vol. 57, no. 1, 2008, 63-69

[61] J. Yu, L. Yang, Analysis of harmonic and inter-harmonic based on Hilbert–Huang Transform, Int. Conf. Comput. Intell. Software Eng., 2009, 1–4

[62] H. Chen, Y. Sun, Y. Cheng, Harmonic and inter-harmonic detection of grid connected DG based on modified mathematical morphology filter and HHT, IEEE Int. Conf. Power Electr. Motion Control, 2009, 1155–1160

[63] S. Zhang, Q. Wang, R. Liu, Power system harmonic analysis based on improved Hilbert–Huang Transform, Int. Conf. Electr. Meas. Instrum., 2009, 343–347

[64] D. S. Laila, A. R. Messina, B. C. Pal, A refined Hilbert–Huang transform with applications to interarea oscillation monitoring, IEEE Transactions on Power Systems, vol. 24, no. 2, 2009, 610-620

[65] N. Senroy, S. Suryanarayanan, P. F. Ribeiro, An improved Hilbert–Huang method for analysis of time-varying waveforms in power quality, IEEE Transactions on Power Systems, vol. 22, no. 4, 2007, 1843-1850

[66] S. Kizhner, T.P. Flatley, N.E. Huang, K. Blank, E. Conwell, On the Hilbert-Huang transform data processing system development, IEEE Proceedings Aerospace Conference, vol. 3, 2004

[67] X. Wang, Z. Yan, Multiple scale identification of power system oscillations using an improved Hilbert-Huang transform, IEEE/PES Power Systems Conference and Exposition, PSCE'09, 2009

[68] A. R. Messina, M. A. Andrade, J. H. Hernández, R. Betancourt, Analysis and characterization of power system nonlinear oscillations using Hilbert Spectral Analysis, The Open Electrical & Electronic Engineering Journal , vol.1, 2007, 1-8

[69] D. Granados-Lieberman, M. Valtierra-Rodriguez, L.A. Morales-Hernandez, R.J. Romero-Troncoso, R.A. Osornio-Rios, A hilbert transform-based smart sensor for detection, classification, and quantification of power quality disturbances, Sensors, vol. 13, no. 5, 2013, 5507-5527

[70] M. Aiello, A. Cataliotti, S. Nuccio, A chirp-z transform-based synchronizer for power system measurements, IEEE Transactions on Instrumentation and Measurement, vol. 54, no. 3, 2005, 1025-1032

[71] P. Daponte, D. Menniti, A. Testa, Segmented chirp Z-transform and multiple deep dip windows for electrical power system harmonic analysis, Measurement, vol. 18, no. 4, 1996, 215-224

[72] M. Aiello, A. Cataliotti, S. Nuccio, An induction motor speed measurement method based on current harmonic analysis with the chirp-Z transform, IEEE Transactions on Instrumentation and Measurement, vol. 54, no. 5, 2005, 1811-1819

[73] L. I. Hua, L. I. Shang-bai, Z. H. O. U. Wei, Z. H. E. N. G. Gao-qun, Chirp-z Transform and its Applicationsin in Power System Harmonic Analysis [J], Electrical Measurement & Instrumentation , vol. 3, 2005

[74] F.V. Topalis, I.F. Gonos, G.A. Vokas, Arbitrary waveform generator for harmonic distortion tests on compact fluorescent lamps, Measurement, vol. 30, no. 4, 2001, 257-267

[75] H. Akaike, A New Look at the Statistical Model Identification, IEEE Trans. on Automatic Control, vol.19, no. 6, 1974, 716-723

[76] R. Kashyap, Inconsistency of the AIC Rule for Estimating the Order of Autoregressive Models, IEEE Trans. on Automatic Control, vol. 25, no. 5, 1980, 996-998

[77] M. Wax, T. Kailath, Detection of Signals by an Information Theoretic Criteria, IEEE Trans. on Acoustics, Speech and Signal Processing, vol. 33, no. 2, 1985, 387-392

[78] X. D. Zhang, Y. S. Zhang, Determination of the MA Order of an ARMA Process Using Sample Correlations, IEEE Trans. on Signal Processing, vol. 41, no. 6, 1993, 2277-2280

[79] G. Liang, D. Mitchell Wilkes, J. A. Cadzow, ARMA Model Order Estimation Based on the Eigenvalues of the Covariance Matrix, IEEE Trans. on Signal Processing, vol. 41, no. 10, 1993, 3003-3009

[80] A. Bracale, P. Caramia, G. Carpinelli, Optimal Evaluation of Waveform Distortion Indices with Prony and RootMusic methods, International Journal of Power & Energy Systems (IJPES), vol. 27, no. 4, 2007

[81] L. Marple, Spectral line analysis by Pisarenko and Prony methods, IEEE Int. Conf. Acoustics, Speech, and Signal Process, vol. 4, 1979, 159–161

[82] Z. Leonowicz, T. Lobos, J. Rezmer, Advanced spectrum estimation methods for signal analysis in power electronics, IEEE Trans. Ind. Electron., vol. 50, 2003, 514–519

[83] F.F. Costa, A.J.M. Cardoso, Harmonic and interharmonic identification based on improved Prony's method, Ann. Conf. IEEE Ind. Electr., 2006, 1047–1052

[84] Z. Hu, J. Guo, M. Yu, Z. Du, C. Wang, The studies on power system harmonic analysis based on extended Prony method, Int. Conf. Power Syst. Technol., 2006, 1–8

[85] L. Qi, L. Qian, S. Woodruff, D. Cartes, Prony analysis for power system transient harmonics, Eurasip. J. Adv. Signal Process, 2007, 1–12

[86] C.-I. Chen, G.W. Chang, An efficient Prony's method for time-varying power system harmonic estimation, IEEE Int. Symp. Circuits and Systems, 2009, 1701–1704

[87] G.W. Chang, Cheng-I. Chen, An accurate time-domain procedure for harmonics and interharmonics detection, IEEE Trans. Power Del., vol. 25, 2010, 1787–1795

[88] J. Zygarlicki, M. Zygarlicka, J. Mroczka, K.J. Latawiec, A reduced Prony's methodin power-quality analysis—parameters selection, IEEE Trans. Power Deliv., vol. 25, 2010, 979–986

[89] J. Zygarlicki, J. Mroczka, Variable-Frequency Prony Method in the Analysis of Electrical Power Quality, Metrology and Measurement Systems, vol. 19, no. 1, 2012, 39–48

[90] S. Y. Sun, H. C. Shu, J. Dong, Z. J. Liu, Analysis of low frequency oscillation mode based on PMU and PRONY method, IEEE Electric Power Conference, EPEC 2008, Canada, 2008

[91] P. Tripath, S. C. Srivastava, S. N. Singh, An improved Prony method for identifying low frequency oscillations using synchro-phasor measurements, International Conference on Power Systems, ICPS'09, 2009

[92] A. Bracale, G. Carpinelli, D. Lauria, Z. Leonowicz, T. Lobos, J. Rezmer, On some spectrum estimation methods for analysis of nonstationary signals in power systems. Part I. Theoretical aspects, 11th International Conference on Harmonics and Quality of Power, 2004

[93] A. Andreotti, A. Bracale, P. Caramia, G. Carpinelli, Adaptive Prony method for the calculation of power-quality indices in the presence of nonstationary disturbance waveforms, IEEE transactions on Power Delivery, vol. 24, no. 2, 2009, 874-883

[94] A. Bracale, G. Carpinelli, Z. Leonowicz, T. Lobos, J. Rezmer, Measurement of IEC groups and subgroups using advanced spectrum estimation methods, IEEE Transactions on Instrumentation and Measurement, vol. 57, no. 4, 2008, 672-681

[95] I.Y.H. Gu, M.H.J. Bollen, Estimating interharmonics by using sliding-window ESPRIT, IEEE Transactions on Power Delivery, vol. 23, no. 1, 2008, 13-23

[96] I.Y.H. Gu, E. Styvaktakis, Bridge the gap: signal processing for power quality applications, Electric Power Systems Research, vol. 66, no. 1, 2003, 83-96

[97] M.H. Bollen, I.Y. Gu, S. Santoso, M.F. McGranaghan, P.A. Crossley, M.V. Ribeiro, P. F. Ribeiro, Bridging the gap between signal and power, IEEE Signal Processing Magazine, vol. 26, no. 4, 2009

[98] Z. Leonowicz, T. Lobos, Analysis of traction system time-varying signals using ESPRIT subspace spectrum estimation method, 32nd Annual IEEE Conference on Industrial Electronics, IECON 2006, 2006.

[99] R. Zolfaghari, Y. Shrivastava, V.G. Agelidis, Evaluation of windowed ESPRIT virtual instrument for estimating Power Quality Indices, Electric Power Systems Research, vol. 83, no. 1, 2012, 58-65

[100] C.I. Chen, G.W. Chang, Virtual instrumentation and educational platform for time-varying harmonic and interharmonic detection, IEEE Transactions on Industrial Electronics, vol. 57, no. 10, 2010, 3334-3342

[101] Z. Leonowicz, T. Lobos, Parametric spectral estimation for power quality assessment, The International IEEE Conference on Computer as a Tool, EUROCON, 2007

[102] P. Stoica, A. Eriksson, MUSIC estimation of real-valued sine-wave frequencies, Signal processing, vol. 42, no. 2, 1995, 139-146

[103] Z. Leonowicz, Analysis of sub-harmonics in power systems, 9th International IEEE Conference on Environment and Electrical Engineering, EEEIC, 2010

[104] A.A. Girgis, W.B. Chang, E. B. Makram, A digital recursive measurement scheme for online tracking of power system harmonics, IEEE Transactions on Power Delivery, vol. 6, no. 3, 1991, 1153-1160

[105] A. Kumar, B. Das, J. Sharma, Dynamic State Estimation of Power System Harmonics with Bad Data, Electric Power Components and Systems, vol. 33, no. 12, 2005

[106] G. Valverde, V. Terzija, Unscented kalman filter for power system dynamic state estimation, IET Generation, Transmission & Distribution, vol.5, no.1, 2011, 29-37

[107] P. K. Ray, B. Subudhi, Ensemble-Kalman-Filter-Based Power System Harmonic Estimation, IEEE Transactions on Instrumentation and Measurement, vol.61, no.12, 2012, 3216-3224

[108] H. Ma, A.A. Girgis, Identification and tracking of harmonic sources in a power system using a Kalman filter, IEEE Transactions on Power Delivery, vol. 11, no. 3, 1996, 1659-1665

[109] H.M. Beides, G.T. Heydt, Dynamic state estimation of power system harmonics using Kalman filter methodology, IEEE Transactions on Power Delivery, vol. 6, no. 4, 1991, 1663-1670

[110] K. Kennedy, G. Lightbody, R. Yacamini, Power system harmonic analysis using the Kalman filter, IEEE Power Engineering Society General Meeting, vol. 2, 2003

[111] K.K.C.Yu, N.R. Watson, J. Arrillaga, An adaptive Kalman filter for dynamic harmonic state estimation and harmonic injection tracking, IEEE Transactions on Power Delivery, vol. 20, no. 2, 2005, 1577-1584

[112] J.A.R. Macias, A. Gomez Exposito, Self-tuning of Kalman filters for harmonic computation, IEEE Transactions on Power Delivery, vol. 21, no. 1, 2006, 501-503

[113] T.C.O. Carvalho, C.A. Duque, P.M. Silveira, M.A.S. Mendes, P. F. Ribeiro, Review of signal processing techniques for time-varying harmonic decomposition, IEEE Power and Energy Society General Meeting, San Diego (CA), 2012, 1-6

[114] C.A. Duque, P.M. Silveira, P.F. Ribeiro, Visualizing time-varying harmonics using filter banks, Electric Power Systems Research, vol. 81, no.4, 2011, 974-983

[115] Y.B. Lim, S.W. Sohn, J.J. Yun, H.D. Bae, H. Choi, Time varying harmonics estimation of power signal based on filter banks and adaptive filtering, IEEE Instrumentation and Measurement Technology Conference (I2MTC), 2010.

[116] S. W. Sohn, Y. B. Lim, J. J. Yun, H. Choi, H. D. Bae, A filter bank and a self-tuning adaptive filter for the harmonic and interharmonic estimation in power signals, IEEE Transactions on Instrumentation and Measurement, vol. 61, no. 1, 2012, 64-73

[117] H. Sun, G.H. Allen, G.D. Cain, A new filter-bank configuration for harmonic measurement, IEEE transactions on instrumentation and measurement, vol. 45, no. 3, 1996, 739-744

[118] Z. Chen, P. Urwin, Power quality detection and classification using digital filters, IEEE Porto Power Tech Proceedings, Porto, vol. 1, 2001

Chapter 2.
Modified parametric methods for the spectral analysis of time-varying waveforms in power systems

2.1 Introduction

The state of art of methods for the spectral analysis of power system waveforms was summarized in Chapter 1. The comparison of the different traditional techniques available in relevant literature brought out the main characteristics and issues related to the spectral analysis methods applied in the power system field. Also the need of new advanced methods for the spectral analysis of voltage and current waveforms in modern power systems emerged from that investigation. Specifically, the new advanced methods should have the following characteristics: (i) a computational effort that is comparable to that of the traditional STFT-based methods, and (ii) adequate accuracy in the assessment of the waveform spectral components. Starting from the consideration that the damping factors and the frequencies of the spectral components in power system applications slightly vary in time [1-11], and inspired by the method presented in [12], a new sliding-window modified ESPRIT method that fully meets the above requirements is presented in this Chapter [13].

In particular, as stated in the Chapter 1, the method proposed in [12] assumed that in the Prony's model the damping factors of the spectral components are equal to zero and the frequencies are constant. In a successive version of the same method [14], the possibility of varying the frequencies for each analysis window is considered, using as input of the procedure a frequency matrix instead of a frequency vector. Moreover, in both cases, the application of the method requires that the frequencies of all spectral components, the number of components used in the model and the duration of the analysis window must be prior known; clearly, these are serious flaws in the method. In addition, Prony's method is known to behave poorly when a signal is corrupted with an added noise.

Motivated by the issues indicated above, the method presented in this Chapter introduces the following substantial improvements:

(i) it is based on the use of the ESPRIT method that is known to behave better than Prony's method when a signal is corrupted by added noise;

(ii) it does not assume that the frequencies of all of the spectral components are constant all over the analysed waveform and prior known; rather, it calculates the frequencies of the spectral components at least once and, at most, only a few times along the entire signal that is being analysed;

(iii) it does not assume that the damping factors of all of the spectral components are equal to zero all over the analysed waveform; rather, it calculates the damping factors of the spectral components at least once and, at most, only a few times along the entire signal that is being analysed;

(iv) a duration equal to some cycles of the fundamental period is selected for the analysis window in order to guarantee a proper evaluation of both the fixed frequencies and the fixed damping factors of the spectral components;
(v) also the number of components used in the model and the order of the correlation matrix are not fixed a priori, but based on an evaluation performed at least once and, at most, only a few times along the entire signal that is being analysed.
Obviously, the proposed approach is not generally applicable, but it is particularly beneficial for many waveforms due to the accuracy of the results and the low computational effort required. Thus, it can be used in practical applications for the rapid and accurate computation of PQ indices [15].
The remainder of this Chapter shows the details of new sliding-window modified ESPRIT method, highlighting the benefits it provides and the results of several experiments.

2.2 Sliding-window modified ESPRIT method

As stated in the Chapter 1, the sliding-window ESPRIT method provides very accurate results in the spectral analysis of the waveforms of power systems, but its computational time is usually very high because equations (1.48) and (1.49) must be solved for each window inside the whole signal to be analyzed, and the size of the involved systems can be so large that their solution becomes burdensome, depending on the correlation matrix size L_1 (linked to window size L) and the number M of exponentials [4,16].
In this Section, a novel scheme is presented with the aim of providing accurate estimation of the spectral components of waveforms while keeping the computational cost significantly lower than the efforts required by not only the sliding-window ESPRIT method but also by both the other main traditional parametric methods and the hybrid methods.
The novel scheme modifies ESPRIT's original approach by (i) evaluating the frequencies of the exponentials one time or, at most, only a few times; (ii) evaluating the damping factors of the exponentials one time or, at most, only a few times; (iii) evaluating the amplitudes and initial phases of the exponentials in all the time windows but with a significant reduced computational effort. Moreover, the waveform is appropriately sampled to increase the accuracy of the results.
In the next Sub-Sections, these choices are motivated and illustrated with details. The block diagram of the proposed new scheme (Fig. 2.1) is also described and discussed.

2.2.1 Model formulation and solving procedure

a) Frequency evaluation
The analysis of time-varying waveforms in several power system applications has shown that in most cases the spectral components of the waveform are characterized by frequencies that are much less variable versus time than amplitudes, so only the variations of the spectral component amplitudes are often detected in the time or taken into account [1-11].

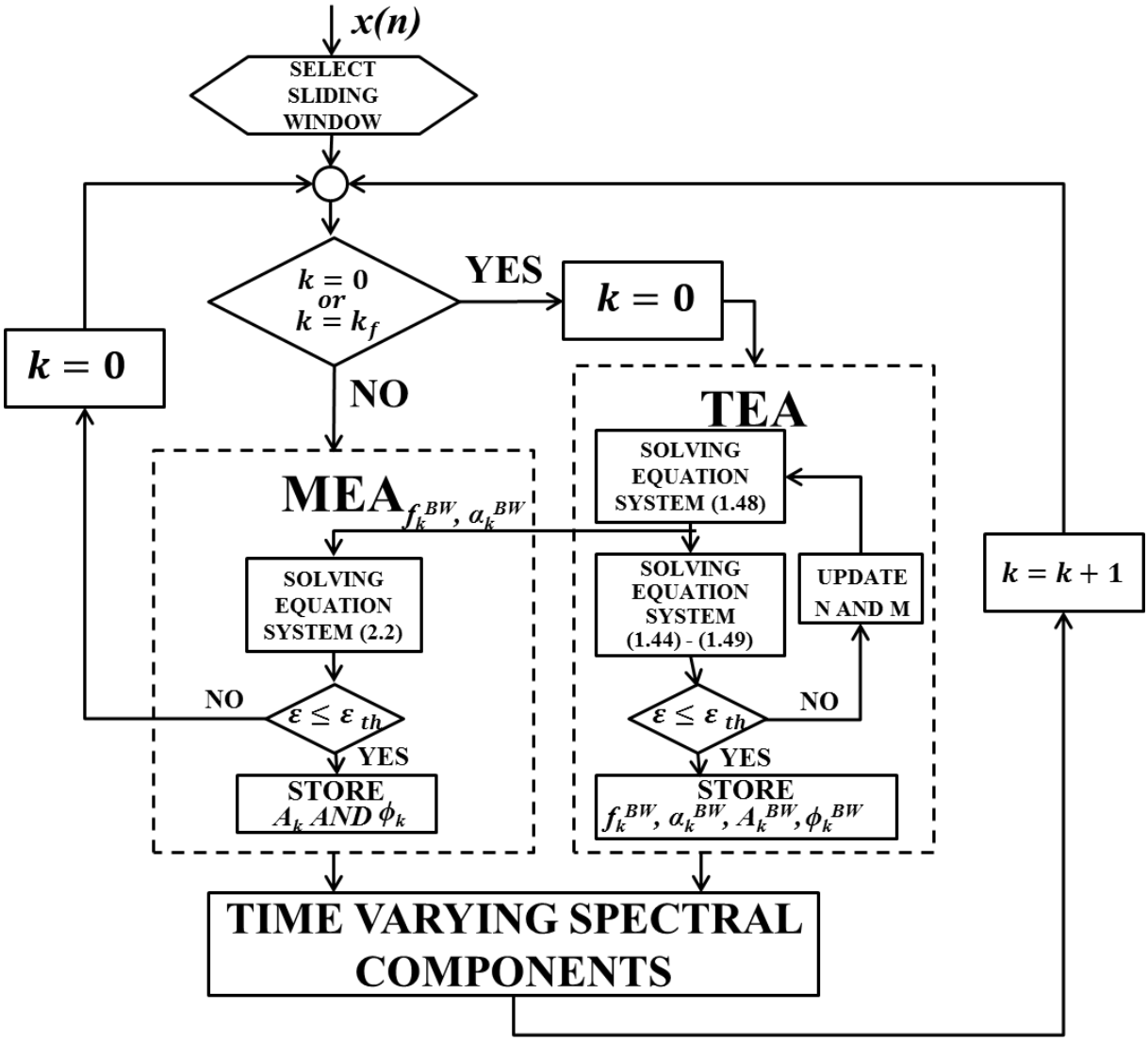

Figure 2.1 *- Block diagram of the new, modified, sliding-window, ESPRIT scheme*

As an example, Figures 2.2, 2.3, and 2.4 show some spectral components of measured waveforms of a wind-turbine generator during soft starting (Fig. 2.2), an industrial load (autoclave) (Fig.2.3) and a photovoltaic plant (Fig. 2.4). As shown in Figs. 2.2, 2.3, and 2.4, the main spectral components are harmonics, the frequencies (Figs. 2.2a, 2.3a, and 2.4a) of which vary slowly with time. This behavior depends mainly on the correlation between the harmonic frequencies and the frequency of the fundamental component, which is slowly and slightly variable with time in modern, interconnected power systems. Also, interharmonic frequencies, if present, vary slowly.

Note that similar behavior is not the general rule, mainly for the frequencies of interharmonics. For example [8,11], adjustable speed drives, cycloconverters or arc furnaces can be characterized by interharmonics the frequencies of which are determined by factors that are not correlated with the fundamental frequency, so significant temporal frequency variations can be experienced. Moreover, the modern diffusion of static converters, utilized by both distributed power plants and end-user equipment for the connection to the grid, as well as the use of power line communication sources have determined also the introduction of spectral components at high-frequency (from 2 to 150 kHz) in voltage and current waveforms [17-23].

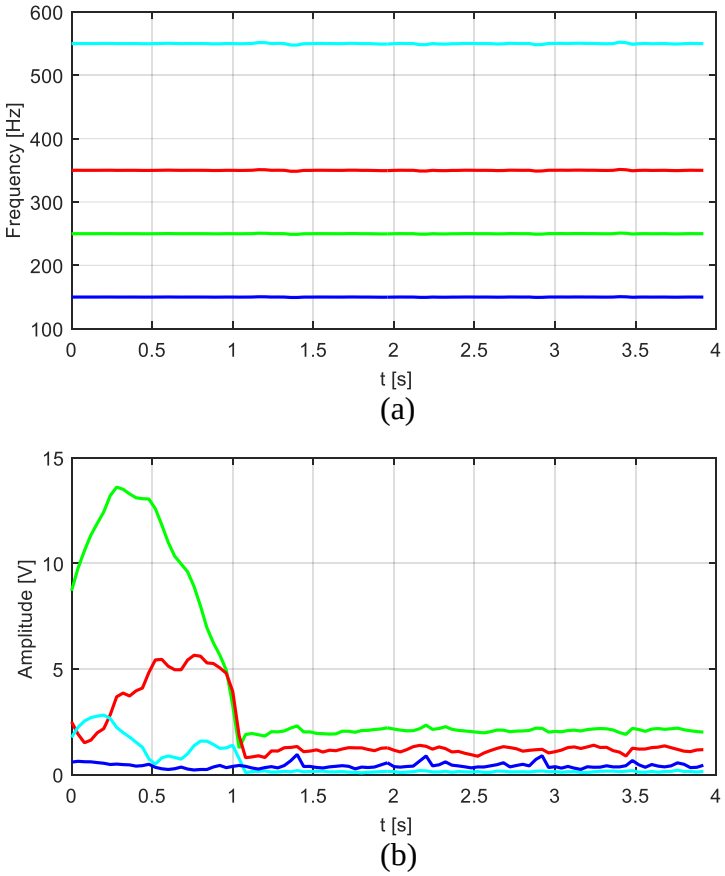

Figure 2.2 *- Frequencies (a) and amplitudes (b) of the spectral components of the measured waveform of a wind-turbine generator during soft starting*

These high-frequency spectral components (supraharmonics) are characterized by high non-stationarity with fast dynamics in time, and consequently with frequencies and amplitudes that can rapidly vary vs. time [23].

Despite this, in many practical applications, the spectral component frequencies with a good approximation can be considered slowly and slightly variable versus time.

Motivated by the aforesaid consideration, instead of [12] where the frequencies are constant or instead of both [12,14] where the frequencies are known a priori, the novel scheme presented in this Chapter calculates initially the frequencies of the spectral components of the waveform from the analysis of the first sliding window, the *basis window*, and initially assumes that the frequencies in the successive sliding windows, i.e., the *no-basis windows*, can be considered constant.

Moreover, in order to avoid masking effects when frequencies are significantly varying, the novel method repeats periodically the calculation of all of the ESPRIT model parameters in a new *basis window* and performs a check on the spectral analysis results. In this way, for example, if the reconstruction error of the waveform or the difference between the values calculated in two consecutive *basis windows* are greater than a tolerance value, the frequencies are updated and the spectral analysis can proceed.

Specifically, as shown in Fig. 2.1, if k is the window counter with an initial value of 0 and the first analysis window ($k = 0$) is a *basis window*, an integer number k_f is introduced to define the distance between two successive *basis windows*. The first choice of the value k_f

can be determined heuristically based on the knowledge of the waveforms to be analyzed. After the first interval $[0, k_f]$, the choice of the successive values of k_f can be updated using different criteria. For example, one of the following criteria could be applied: (i) k_f could be an integer number that is inversely proportional to the value of the maximum difference between the values of frequencies calculated in the new *basis window* and those obtained previously; (ii) k_f could be an integer number that grows as the reconstruction error value, evaluated in each analysis window, is kept below a fixed threshold value. Eventually, with the assumption of constant frequencies inside the *no-basis windows*, the Sliding-window modified ESPRIT method is able to reduce the unknowns to be obtained and the computational effort significantly, as will be described in more detail in the next Sub-Sections.

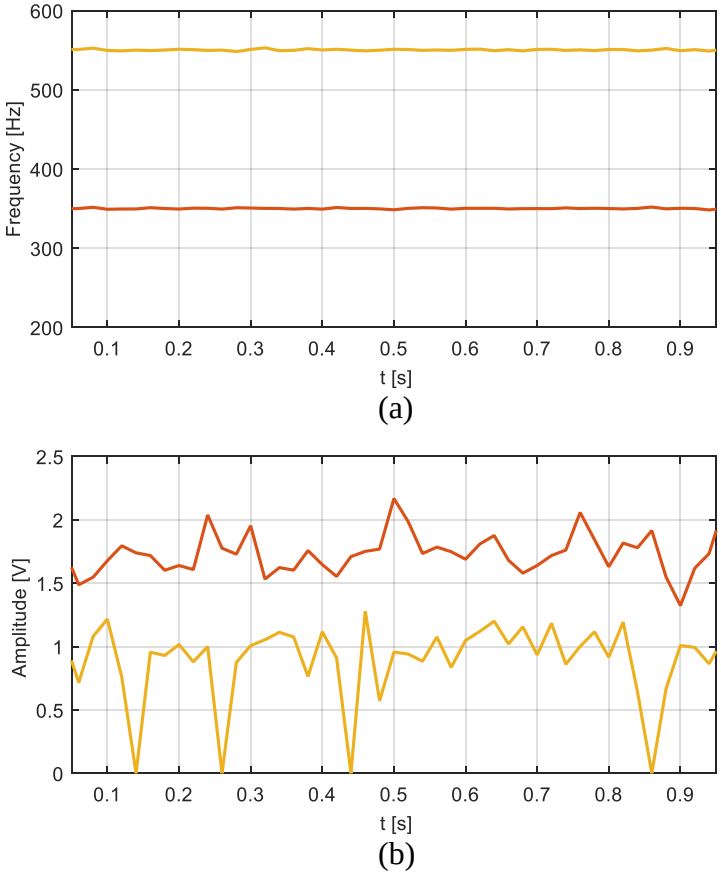

Figure 2.3 *- Frequencies (a) and amplitudes (b) of the spectral components of the measured waveform of an industrial load*

b) Damping factor evaluation

As observed in the Chapter 1, in the traditional Prony's approach the damping factors have an important role; however, in [12] they became less significant, since in the case of very short duration of the windows, the damping factors usually have very small values (close to zero).

In the novel scheme analyzed in this Chapter, instead, since the damping factors contribution to the model grows with increasing of the analysis window duration, it is proposed to assume the values of the damping factors of the spectral components inside the *no-basis windows* equal to the values computed in the *basis window*, because the ESPRIT model requires a slightly larger value of L than the Prony's model for two reasons:

1. the ESPRIT performance improves with increasing of the order L_1 of the correlation matrix, so, since $L_1 < L$, the value of L has to be a proper number of times the waveform's fundamental period;
2. differently to the Prony's method, the ESPRIT algorithm doesn't require the research of the optimal duration L of the window under examination to improve the estimation of the waveform spectral components, so the L value is constant.

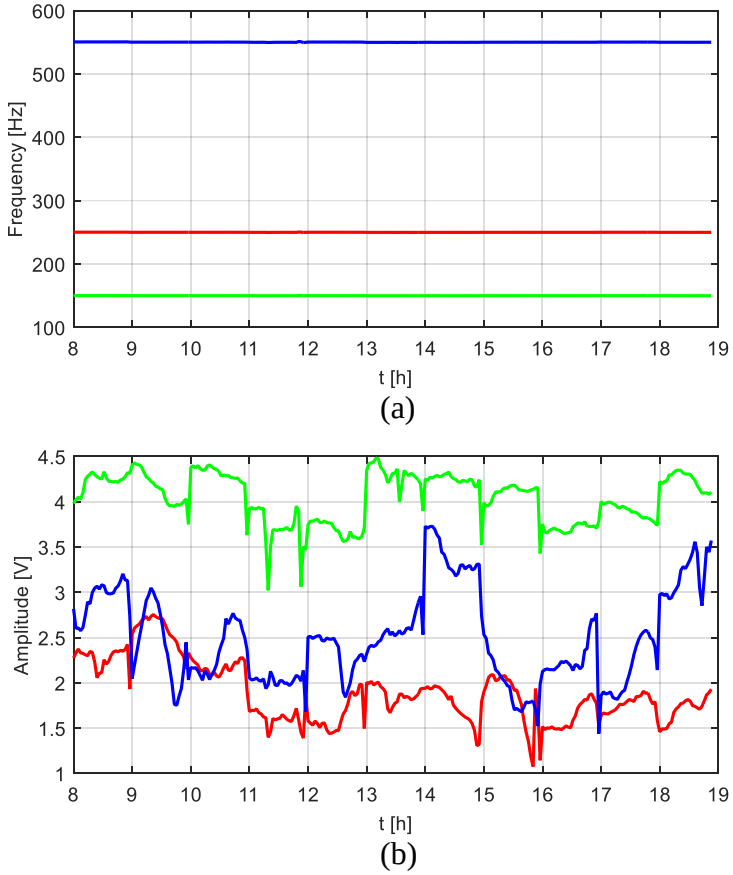

Figure 2.4 *- Frequencies (a) and amplitudes (b) of the spectral components of the measured waveform of a photovoltaic plant*

In these circumstances, the aforesaid fixed value of L determines that damping factors cannot be neglected in the ESPRIT model (1.43). However, since the selection of a unique duration for all of the analysis window, a stationary damping trend of the spectral components can be supposed in time, and consequently the damping factor values can be assumed almost constant along the windows.

Then, the novel method assumes that in addition to the frequencies also the damping factors of the exponentials (i) are calculated by applying the traditional ESPRIT method in the *basis windows*; and (ii) are assumed constant along the *no-basis windows*.

Obviously, once again the problem of masking effects is avoided by making use of the same principles applied for the frequencies, i.e. check on the reconstruction error of the waveform or on the difference between the evaluated parameters in two consecutive *basis window*. So, also when the damping factors evaluated for the spectral components in a *basis window* don't prove to be adequate for all of the successive *no-basis windows*, a proper check guarantees

both the updating of the value of k_f and the generation of a new *basis window* that recalculates the parameters for the following *no-basis windows*.

c) Amplitudes and initial phases evaluation

With reference to the remaining parameters of the ESPRIT model (i.e., the amplitudes and initial phases of the exponentials), the novel scheme assumes that they are calculated (i) by applying the traditional ESPRIT method in the *basis windows* and (ii) with a new scheme along the *no-basis windows*.

The required new scheme modifies ESPRIT model (1.43) in the *no-basis windows* in such way as:

$$\hat{x}(n) = \sum_{k=1}^{M} A_k e^{j\phi_k} e^{(\hat{\alpha}_k^{BW} + j2\pi\hat{f}_k^{BW})nT_s} + r(n), \;\; n = 0,1,\dots,L-1 \qquad (2.1)$$

where the frequencies $\hat{f}_k^{BW}$ and the damping factors $\hat{\alpha}_k^{BW}$ are known from the analysis of the *basis windows* performed with the traditional ESPRIT method, where the eigenvalues $\hat{\lambda}_k^{BW} = e^{(\hat{\alpha}_k^{BW} + j2\pi\hat{f}_k^{BW})}$ are computed.

With $\hat{\lambda}_k^{BW}$ known, the linear equation system (1.48) has no longer to be solved in the *no-basis windows*, which results in significant reduction of the computational efforts. Only the linear equation system obtained by (1.49) and (1.44) must be solved in order to obtain amplitudes and initial phases in the *no-basis windows*; the result is:

$$\boldsymbol{H} = (\boldsymbol{V}_{BW}^H \boldsymbol{V}_{BW})^{-1} \boldsymbol{V}_{BW}^H \, \boldsymbol{x} \qquad (2.2)$$

where the meaning of the symbols is obvious.

Note also that the order L_1 and the number of exponentials *M* involved in the analysis of the basis windows also are imposed for the analysis of the *no-basis windows*, resulting in further improvement in the computational efficiency.

d) Resampling

Usually, parametric methods require an adequate sampling rate in order to avoid inaccuracies in the evaluation of the spectral components. These methods, in fact, are able to accurately detect spectral components until a maximum value of frequency that is strictly linked to the sampling rate of the waveform [12,24-26]. Specifically, in [26] it was shown that ESPRIT method is able to detect spectral components with frequencies up to $f_s/2$, where f_s is the sampling rate, but, in some cases the estimation of the components near $f_s/2$ was revealed unstable, so it is recommended to consider the accurately estimated maximum frequency equal to $f_s/4$.

Then, in the novel method presented in this Chapter, the sampling frequency is selected heuristically as follows:

- if the characteristics of the waveform to be studied are prior known, the sampling frequency is assumed to be four times the maximum expected frequency of the spectral component; otherwise,
- the sampling frequency is assumed to be four times the maximum frequency of interest.

It should be noted that an inadequate sampling rate produces very high reconstruction errors due to the inability of the method to adequately approximate the waveform. Then, when the reconstruction error is high, the sampling frequency must be increased. It should also be noted that an adequate choice of the sampling frequency allows a faster research of the optimal L_1 and M values, which also contributes to reducing the computational burden.

e) Description of the block diagram of the sliding-window modified ESPRIT method
Fig. 2.1 shows the block diagram of the proposed approach.
The first waveform window (*basis window*) is analyzed with the traditional ESPRIT algorithm (TEA), and all of the parameters obtained ($A_k^{BW}, f_k^{BW}, \phi_k^{BW}, \alpha_k^{BW}$, L_1 and M) are stored. Then, the *no-basis windows* are analyzed with the modified ESPRIT algorithm (MEA), in which only the unknown amplitudes A_k and initial phases ϕ_k of the spectral components are calculated, solving the equation system (2.2).
It should be noted that when the number of *basis windows* increases, the Modified ESPRIT Method (MEM) approaches the Traditional ESPRIT Method (TEM) in terms of the accuracy of the results and of the computational time.
According to previous Sub-Sections, in order to verify the slight variability of the fixed model parameters (f_k^{BW}, α_k^{BW}, L_1 and M) in time and in order to improve accuracy of the spectral analysis: (i) the difference between the frequency values calculated in two successive *basis windows*; or (ii) the time domain reconstruction error should be calculated. In the following, the time domain reconstruction error is applied for the check on the results reliability and for the evaluation of k_f, since the reconstruction error provides contemporary information about all of the model parameters (i.e., L_1, M, damping factor and frequencies) variations and the adequacy of the chosen sampling frequency.
In particular, the time-domain reconstruction error is calculated for each sliding window (both *basis* and *no-basis window*) to ensure that its value is less than a pre-determined threshold (ε_{th}). This check, in the *no-basis windows*, ensures the identification of the significant time-variations of the model of the signal determined in the *basis window*. In other words, the modified ESPRIT algorithm is applied only until the reconstruction error does not exceed the threshold value in the *no-basis windows*. Otherwise, a new basis window is generated and also the value of k_f is update in order to set again the expected future distance between two consecutive *basis window*. Note that the above-mentioned reconstruction error check is one of the elements that make the proposed method robust and prevents inaccuracies in the model. Another important element that ensures the reliability of the proposed approach is that the value of L is chosen so that it is equal to the number of samples included in a few cycles of the fundamental period. In fact, in a such restrained time interval, the variation of the detected spectral components is expected to be negligible, so the assumption of constant frequencies and damping factors between two consecutive windows becomes more reasonable.

2.2.2 Numerical applications

Several numerical experiments were conducted by analysing both synthesized and measured waveforms in order to evaluate the performances of the modified ESPRIT method. In particular, the results of MEM were compared with the results obtained by applying TEM, the sliding-window Joint ESPRIT-DFT method (JEDM) proposed in [7] and the STFT method

(STFTM). In all of the numerical experiments, comparisons were made between both the accuracy of the spectral component and computational time.

For the sake of brevity, only five case studies are presented in this Sub-Section. Specifically, the results obtained from the analysis of three synthesized signals and of two measured waveforms are shown. In particular, the first two synthesized signals were generated in order to facilitate the comparisons between the MEM scheme and the other considered methods using the ground truth' values of the spectral components. These signals were characterized by the presence of different harmonic and interharmonic components superimposed to the fundamental component in order to observe the behavior of the MEM in the detection of the most common types of low-frequency spectral components, in presence of slight time-varying trends. Moreover, in both the cases, an interharmonic close to the fundamental frequency was introduced in the signal in order to test also possible failures or the achievements of the proposed method in the identification of neighboring components. The measured waveforms are a voltage waveform recorded at a low-voltage bus supplying a laser printer and a current waveform of a wind-turbine generator during soft starting. Finally, the last synthesized signal was chosen in order to highly stress the proposed method, showing its inability in the detection of time-varying spectral components at high-frequency, when wide-spectrum waveforms are analyzed.

Note that the case studies 1 and 2 aimed also to show the high accuracy of the TEM in the component estimations and the high speed of the STFTM analysis, justifying the choice to use them in the two subsequent case studies 3 and 4 as references for the other two methods' evaluations in term of results accuracy and computational burden, respectively.

Note also that TEM and MEM selected N and M dynamically on the basis of the reconstruction error [5,16] in each analysis window of fixed duration. STFTM was applied with an analysis window of duration equal to 10 cycles of the fundamental period, according to the IEC standards [15,27]. Eventually, in the case studies related to synthesized signals, the results were obtained by setting a very low threshold value for the reconstruction error for the parametric methods, since the interest in strongly emphasizing both the maximum allowable precision and the computational time associated with the methods that were used. In particular, the value of this reconstruction error threshold as well as the duration of the analysis window assumed different values in each case study and they were chosen by taking into account both the different source of the waveforms (synthesized or measured signals) and the degree of variability in time of the waveforms. For example, a slightly-time-varying synthesized waveform can be analysed by using window with higher duration and by fixing a lower reconstruction error threshold than a measured waveform, affected by high noise.

All of the programs were conducted in MATLAB, and they were not optimized for computational speed because we were interested only in obtaining a rough and relative quantification of the efficiency of the different methods. MATLAB programs were developed and tested on a Windows PC with an Intel i7-3770 3.4 GHz and 16 GB of RAM.

a) Case study 1

The first signal analyzed was a 4 s, acid-test, synthetic waveform. The signal, shown in Fig. 2.5, included:

- a fundamental component at 50.03 Hz with an initial amplitude of 100 p.u. that increased by 1.2% for each interval of 0.24 s;
- 3^{rd}, 5^{th}, 7^{th}, 11^{th}, and 13^{th} order harmonics of amplitude, respectively, 3%, 4%, 3%, 1%, and 1% of the fundamental;
- an interharmonic at 86 Hz with an amplitude that was 0.5% of the fundamental.

A white noise, with a standard deviation of 0.001, was added in order to make the waveform more realistic. The sampling rate was 5000 Hz and, for TEM and MEM, reconstruction error thresholds of 10^{-11} were used. TEM, JEDM and MEM were applied to analyze progressively data blocks of the same duration and time location. In particular, the duration of the analysis windows was chosen equal to 0.04 s in order to yield smoother results through the windows. Moreover, the second step of JEDM was applied with a DFT window sizes of 3 cycles of the fundamental period. Note that, since the waveform varied slowly with time, just one basis window was required for MEM, since a reconstruction error thresholds of 10^{-5} were used in the *no-basis* windows. The percentage errors in the estimates of the spectral components were calculated by using the results obtained from all data blocks and by evaluating their deviation from the actual values.

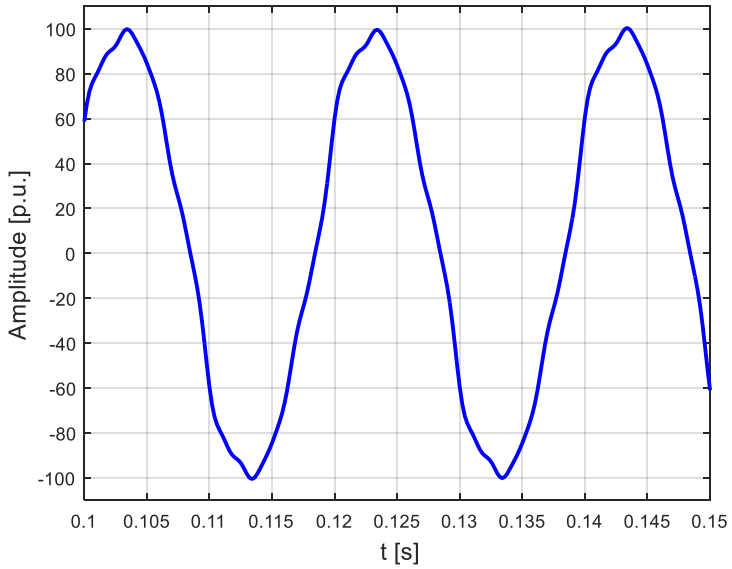

***Figure 2.5** – MEM - Case study 1: trend of the analysed synthetic waveform*

Table 2.1 shows the average percentage errors in the amplitudes and frequencies of the spectral components that were obtained by applying all the selected methods.
From the analysis of the results reported in Table 2.1, it is evident that TEM and MEM performed similarly and were characterized by errors lower than those for JEDM and STFTM. STFTM furnishes, usually, the higher errors due to the well-known spectral leakage caused by both fundamental desynchronization and presence of interharmonics.
Note that JEDM furnished accurate results for fundamental and interharmonic but, as foreseeable, had spectral leakage problems in the estimation of the harmonic components due to the presence of residual 86Hz interharmonic component in the second step of the method [7]. However, globally, JEDM provided more accurate estimations of all spectral components than STFTM.

Table 2.2 shows the computational time of the aforesaid spectral analyses performed by each method, in per unit of the computational time required by STFTM, that analyzed the whole signal in 0.36 s.

From the analysis of Table 2.2, it is evident that using TEM the high accuracy was paid with a great time computation. On the other hand, JEDM furnished acceptable results with a significant reduction of computational burden. Conversely, MEM had a computational time significantly lower than TEM and just one order of magnitude higher than that of STFTM.

Thus, the proposed method obtained in this case-study accuracy as TEM and time computation comparable to STFTM.

***Table 2.1** – MEM - Case study 1: averages errors (%) on amplitudes, frequencies, and initial phases obtained by TEM, JEDM, MEM, and STFTM: (a) fundamental and interharmonic; (b) 3rd, 5th, and 7th harmonics; (c) 11th and 13th harmonics*

	Average error [%]			
	Amplitude		Frequency	
	Fundamental	Interharmonic	Fundamental	Interharmonic
TEM	$420 \cdot 10^{-6}$	0.070	$46 \cdot 10^{-6}$	0.0060
JEDM	$590 \cdot 10^{-6}$	0.060	$36 \cdot 10^{-6}$	0.0050
MEM	$190 \cdot 10^{-6}$	0.16	$81 \cdot 10^{-6}$	0.0030
STFTM	0.23	12	0.060	1.2

(a)

	Average error [%]					
	Amplitude			Frequency		
	3^{rd}	5^{th}	7^{th}	3^{rd}	5^{th}	7^{th}
TEM	0.0090	0.0080	0.010	$390 \cdot 10^{-6}$	$160 \cdot 10^{-6}$	$180 \cdot 10^{-6}$
JEDM	0.64	0.22	0.19	0.0080	0.0080	0.0080
MEM	0.0070	0.0040	0.0030	$360 \cdot 10^{-6}$	$47 \cdot 10^{-6}$	$20 \cdot 10^{-6}$
STFTM	0.33	0.27	0.38	0.060	0.060	0.060

(b)

	Average error [%]			
	Amplitude		Frequency	
	11^{th}	13^{th}	11^{th}	13^{th}
TEM	0.030	0.030	$290 \cdot 10^{-6}$	$230 \cdot 10^{-6}$
JEDM	0.40	0.34	0.0080	0.0080
MEM	0.050	0.050	$65 \cdot 10^{-6}$	$400 \cdot 10^{-6}$
STFTM	0.50	0.99	0.060	0.060

(c)

***Table 2.2** – MEM - Case study 1: computational time by TEM, JEDM and MEM in p.u. of time required by STFTM*

	Computational time [p.u.]
TEM	410
JEDM	74
MEM	10
STFTM	1

Also the effects of the sinusoidal variation of the fundamental frequency with deviations from 0.01% to 0.1% in the synthetic waveform mentioned earlier were analyzed. In particular,

Tables 2.3 and 2.4 show the results, in term of average percentage errors, referred to the 0.01% and 0.1% deviations, respectively.

Table 2.3 *- MEM - Case study 1: variable fundamental frequency and maximum deviation equal to 0.01%. Averages errors (%) on amplitudes, frequencies, and initial phases obtained by TEM, JEDM, MEM, and STFTM: (a) fundamental and interharmonic; (b) 3rd, 5th, and 7th harmonics; (c) 11th and 13th harmonics*

	Average error [%]			
	Amplitude		Frequency	
	Fundamental	Interharmonic	Fundamental	Interharmonic
TEM	$480 \cdot 10^{-6}$	0.095	0.0098	0.0077
JEDM	0.074	8.5	0.0097	0.17
MEM	0.0065	0.95	0.0061	0.0086
STFTM	0.24	12	0.067	1.2

(a)

	Average error [%]					
	Amplitude			Frequency		
	3rd	5th	7th	3rd	5th	7th
TEM	0.010	0.0070	0.012	0.0099	0.0098	0.0098
JEDM	0.73	0.24	0.21	0.0098	0.0098	0.0098
MEM	0.012	0.024	0.028	0.0058	0.0065	0.0062
STFTM	0.35	0.29	0.38	0.067	0.067	0.067

(b)

	Average error [%]			
	Amplitude		Frequency	
	11th	13th	11th	13th
TEM	0.036	0.032	0.0098	0.0098
JEDM	0.42	0.35	0.0098	0.0098
MEM	0.054	0.074	0.0062	0.0065
STFTM	0.58	1.1	0.067	0.067

(c)

The orders of magnitude of the average percentage errors increased for all of the methods that were used, but, in the comparison of the methods, similar observations were made for the waveform with a constant fundamental frequency. Specifically, when the maximum deviation of frequency was 0.01% (Table 2.3), the average percentage errors of MEM have the same orders of magnitude of the average percentage errors of TEM, and they increase by only one order of magnitude with respect to those obtained for the waveform with a constant fundamental frequency (Table 2.1). When the maximum deviation of frequency was 0.1% (Table 2.4), the average percentage errors of the frequencies of TEM and MEM increased by about two orders of magnitude with respect to those obtained for the waveform with a constant fundamental frequency (Table 2.1). For the estimates of amplitude, the errors of MEM were one order of magnitude greater than those of TEM, and they were two orders of magnitude greater than those presented in Table 2.1. However, in term of the accuracy, the results provided by MEM approached those provided by TEM better than any other model for every operative condition. With reference to the computational efforts, also in case of the considered variations of fundamental frequency, the methods confirmed the trend shown in Table 2.2. The above experiments were repeated also increasing the frequency of the sinusoidal variations of the fundamental frequency, with growing errors. Anyway, the

calculation of the waveform reconstruction error in each no-basis window helps in the immediate identification of significant time-variations of the signal model. In fact, when the reconstruction error becomes significant, the model is updated, applying the ESPRIT algorithm without assumptions on frequency values in a new basis window. Obviously, the computational efforts grow with the number of basis windows.

Table 2.4 *- MEM - Case study 1: variable fundamental frequency and maximum deviation equal to 0.1%. Averages errors (%) on amplitudes, frequencies, and initial phases obtained by TEM, JEDM, MEM, and STFTM: (a) fundamental and interharmonic; (b) 3rd, 5th, and 7th harmonics; (c) 11th and 13th harmonics*

	Average error [%]			
	Amplitude		Frequency	
	Fundamental	Interharmonic	Fundamental	Interharmonic
TEM	0.0021	0.45	0.098	0.036
JEDM	0.061	8.0	0.094	0.27
MEM	0.0065	1.4	0.079	0.036
STFTM	0.24	21	0.13	1.2

(a)

	Average error [%]					
	Amplitude			Frequency		
	3^{rd}	5^{th}	7^{th}	3^{rd}	5^{th}	7^{th}
TEM	0.027	0.013	0.024	0.098	0.098	0.098
JEDM	0.77	0.29	0.37	0.096	0.096	0.096
MEM	0.13	0.067	0.34	0.078	0.079	0.079
STFTM	0.67	0.71	1.7	0.13	0.13	0.13

(b)

	Average error [%]			
	Amplitude		Frequency	
	11^{th}	13^{th}	11^{th}	13^{th}
TEM	0.042	0.052	0.098	0.098
JEDM	0.79	0.67	0.096	0.096
MEM	0.22	0.17	0.079	0.079
STFTM	3.9	5.7	0.13	0.13

(c)

b) Case study 2

The 5 s test waveform, shown in Fig. 2.6, was constituted by:

- a fundamental component at 49.98 Hz with an amplitude of 100 p.u.;
- 5^{th} and 7^{th} order harmonic of amplitude that was 2% of the fundamental;
- two interharmonics at 72 Hz and at 423 Hz with amplitudes that were 0.5% of the fundamental decreasing by 1.1% for each 0.24 s interval.

A white noise with a standard deviation of 0.01 was also added. The sampling rate was 5000 Hz and, for TEM and MEM, reconstruction error thresholds of 10^{-9} were used. TEM, JEDM and MEM were applied to analyze progressively data blocks of the same duration and time location. In particular, the duration of the analysis windows was chosen equal to 0.04 s in order to yield smoother results through the windows. Moreover, the second step of JEDM was applied with a DFT window sizes of 5 cycles of the fundamental period.

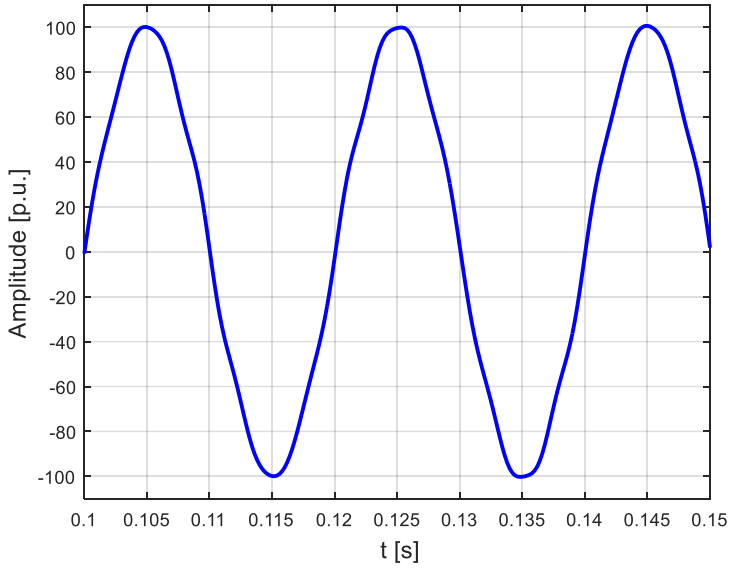

***Figure 2.6** – MEM - Case study 2: trend of the analysed synthetic waveform*

Note that, since the waveform varied slowly with time, just one basis window was required for MEM, since a reconstruction error thresholds of 10^{-5} were used in the *no-basis* windows. Table 2.5 shows the average percentage errors for the fundamental and interharmonics amplitudes and frequencies. From the analysis of the results provided in Table 2.5, MEM and TEM provided more accurate and very similar results. It can be noted that TEM and MEM's errors related to the 72Hz interharmonic are greater than the ones related to the 423Hz interharmonic. This behavior can be explained considering that the 72Hz interharmonic was near to the fundamental frequency leading to the two components interfered with each other. For the 423Hz interharmonic, the interference was negligible.

***Table 2.5** - MEM - Case study 2: averages errors (%) on amplitudes, frequencies, and initial phases obtained by TEM, JEDM, MEM, and STFTM*

	Average error [%]					
	Amplitude			Frequency		
	Fundamental	72Hz	423Hz	Fundamental	72Hz	423Hz
TEM	0.0080	2.3	0.65	0.0010	0.16	0.0090
JEDM	0.0060	1.4	26	$750 \cdot 10^{-6}$	0.14	0.22
MEM	0.0080	2.0	0.21	$190 \cdot 10^{-6}$	$530 \cdot 10^{-6}$	0.0020
STFTM	0.020	21	25	0.040	2.8	0.47

In addition, in some cases, MEM errors are lower than TEM errors; this can be explained observing that, in some windows, TEM's results can be unstable for the high number of variable parameters. On the other hand, the reduced number of variables in non-basis windows of MEM determines a more stable behavior leading to reduced values of errors.
As expected, it clearly appears that STFTM's errors in the estimation of both 72Hz and 423Hz interharmonics were globally the greatest in terms of amplitude and frequency due to the spectral leakage caused by both fundamental desynchronization and the presence of interharmonics.

Eventually, with reference to JEDM results, the fundamental and 72Hz interharmonic errors were about the same order of magnitude of TEM and MEM. Once again, due to spectral leakage, JEDM errors increase for 423Hz interharmonic.
Table 2.6 provides the computational time by all of the methods in per unit of time required by STFTM, that spent 1.18 s for the analysis of the whole waveform. Table 4 shows that MEM had a computational time that was about one order of magnitude less than that JEDM and that was about the same as the time required by STFTM demonstrating the effectiveness of the proposed approach also in presence of fundamental desynchronization and multiple interharmonics.

***Table 2.6** - MEM - Case study 2: computational time by TEM, JEDM and MEM in p.u. of time required by STFTM*

	Computational time [p.u.]
TEM	422
JEDM	80
MEM	9.8
STFTM	1

c) Case study 3
A 3 s voltage waveform measured at a low voltage bus supplying a laser printer was analyzed. The sampling rate was 25 kHz, and it was adequate for estimating the low-frequency components until 5 kHz that was the maximum frequency of our interest. Fig. 2.7 shows the analyzed voltage waveform.

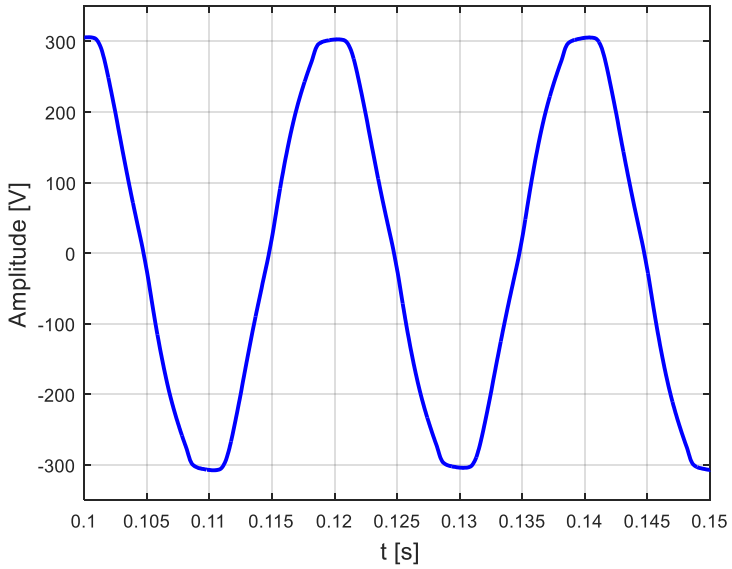

***Figure 2.7** – MEM - Case study 3: trend of the analysed waveform*

TEM, JEDM and MEM were used to analyze the same number of data blocks with sliding window length of 0.025 s. For TPM and for the basis window of MPM, a reconstruction error threshold equal to 10^{-5} was used. Moreover, the second step of JEDM was applied with window sizes of 3 times the fundamental period. Note that, since the waveform varied slowly with time also in this case study, just one basis window was required for MEM, since a reconstruction error thresholds of 10^{-3} were used in the *no-basis* windows.

In addition to the fundamental component, many harmonics were detected by all of the methods, the most significant being the 3rd, 5th, 7th, 9th, 11th, 13th, and 15th-order harmonics.
The results of the analysis are shown in Table 2.7. Specifically, Table 2.7.a shows the average values of the amplitudes and frequencies of the most significant spectral components evaluated by TEM, JEDM, MEM and STFTM. In Table 2.7.b, for the same components, JEDM's, MEM's and STFTM's average percentage errors for amplitudes and frequencies are shown by comparing them with the results obtained by TEM. In fact, as mentioned before, since the previous two test cases showed that TEM globally provided the best estimation of the spectral components, in this case study, as well as in the following one, TEM was assumed as references for the evaluation of the accuracy of all of the other applied methods.

Table 2.7 - *MEM - Case study 3:a) average values of the amplitudes and frequencies of the most significant spectral components detected by TEM, JEDM, MEM and STFTM; b) amplitude and frequency average errors (%) by JEDM, MEM and STFTM*

	Average value									
	Amplitude [V]					Frequency [Hz]				
	Fundamental	3th	5th	7th	9th	Fundamental	3th	5th	7th	9th
TEM	224.13	2.85	4.94	3.21	1.25	49.96	150.00	250.11	349.89	449.98
JEDM	220.80	3.06	5.04	3.23	1.30	50.00	149.97	249.92	349.94	449.92
MEM	219.92	2.51	5.16	3.33	1.24	49.95	149.16	250.25	349.85	450.34
STFTM	221.44	2.98	5.02	3.27	1.28	50.00	150.00	250.00	350.00	450.00

(a)

	Average error [%]									
	Amplitude					Frequency				
	Fundamental	3th	5th	7th	9th	Fundamental	3th	5th	7th	9th
JEDM	1.5	7.4	2.0	0.62	4.0	0.080	0.020	0.080	0.010	0.010
MEM	1.9	12	4.5	3.7	0.80	0.020	0.56	0.060	0.010	0.080
STFTM	1.3	18	2.3	1.5	9.2	0.13	0.29	0.080	0.060	0.12

(b)

Note that, as shown in Table 2.7, in this analysis, the STFTM results and errors are particularly comfortable, since in this waveform the significant components are slowly varying harmonics. Specifically, from Table 2.7.b, it appears that STFTM, JEDM and MEM provided similar results for all the components in terms of both amplitude and frequency, with percentage errors having globally the same order of magnitude. This can be explained also with the absence of significant interharmonics in the measured waveform.
Eventually, Table 2.8 compares the computational time by all of the methods in per unit of time required by STFTM. Once again, MEM was significantly faster than the other two methods; in addition it worked much better in this case study 3 than in case studies 1 and 2.

Table 2.8 - *MEM - Case study 3: computational time by TEM, JEDM and MEM in p.u. of time required by STFTM*

	Computational time [p.u.]
TEM	2918
JEDM	30
MEM	4.2
STFTM	1

d) Case study 4

A current waveform measured during the soft starting of a fixed-speed wind turbine asynchronous generator was analyzed (Fig. 2.8). The duration of the analyzed waveform was about 5 s. The sampling rate was 2048 Hz, so, as discussed in Sub-Section 2.2.1, a resampling was necessary to allow a proper spectral analysis of the TEM and the MEM, so a sampling rate equal to 10 kHz was chosen.

TEM, JEDM and MEM were used to analyze the same number of data blocks with analysis windows of duration equal to 0.02 s. For TEM and for the basis windows of MEM, a reconstruction error threshold of 10^{-7} was used. This is a waveform with a high time-varying nature in the first 2 s, so MEM was set to analyze a basis window whenever the reconstruction error exceeded 10^{-3}.

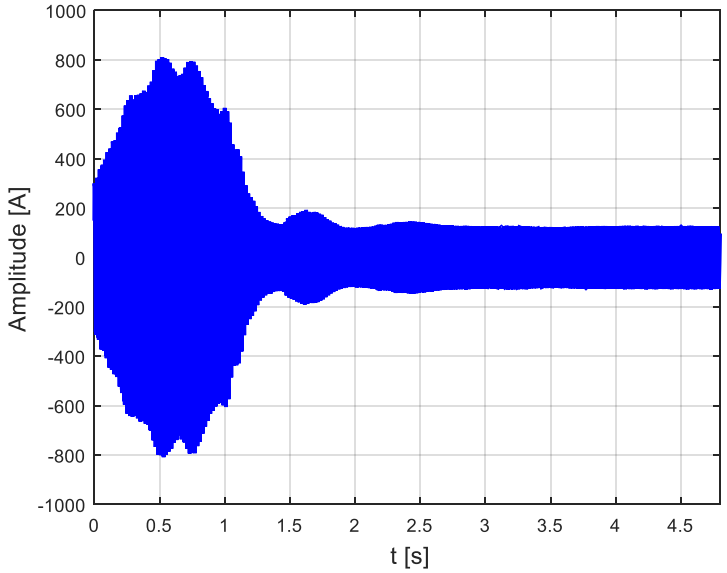

***Figure 2.8** – MEM - Case study 4: trend of the analysed waveform*

The most meaningful components detected by all of the methods were the 3rd, 5th, 7th, and 11th-order harmonics, in addition to the fundamental component. Their presence is justified since the fixed-speed wind turbine systems are equipped with an electronic soft starter aimed to avoid the increase of current during the start-up phase. The spectral emissions of this system primarily are caused by the action of this soft starter, which introduces odd harmonic components at low frequency. Fig. 2.9 shows the amplitude of the fundamental harmonic (Fig. 2.9.a), the 5th-order harmonic (Fig. 2.9.b), and the 7th-order harmonic (Fig. 2.9.c) obtained by using TEM, JEDM, MEM and STFTM. All of the methods provided globally a similar behavior of the detected spectral components versus time, though TEM, JEDM, and MEM seemed to identify better than STFTM the variability in time of all the detected spectral components. In fact, a lack of detail in the STFTM estimations was highly evident, caused by both the spectral leakage problem (due to the use of an analysis window with duration not synchronized with the fundamental period) and the poor time resolution.

Assuming once again the TEM values as the reference, the mean percentage errors in the estimations of the spectral components for JEDM, MEM and STFTM were calculated, and they are shown in Table 2.9. MEM and JEDM provided globally the same results in terms of amplitudes and frequencies. It's fair to say that in this case study STFTM has more problems

in the components estimation (i.e. the average error on the 7th harmonic amplitude is more than 24%), since the highly time-varying nature of the waveform.

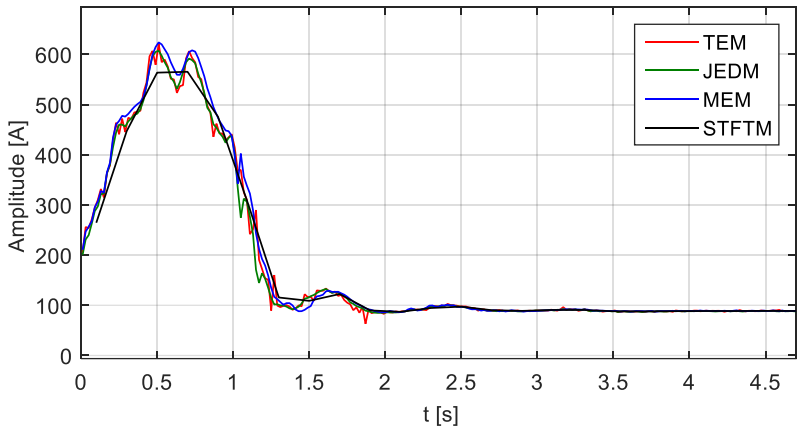

(a)

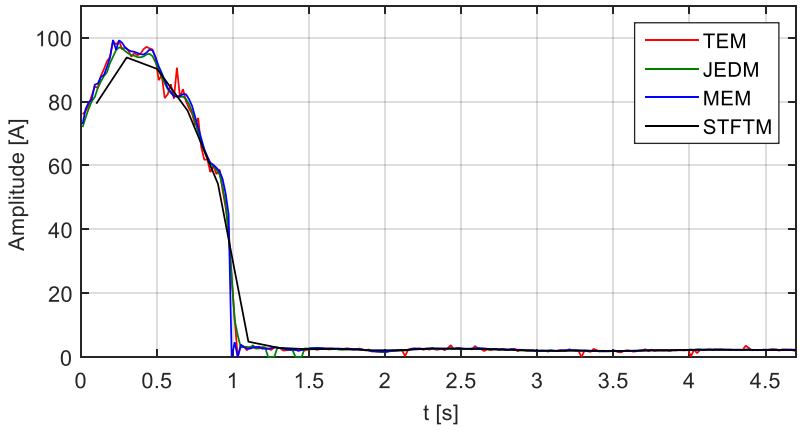

(b)

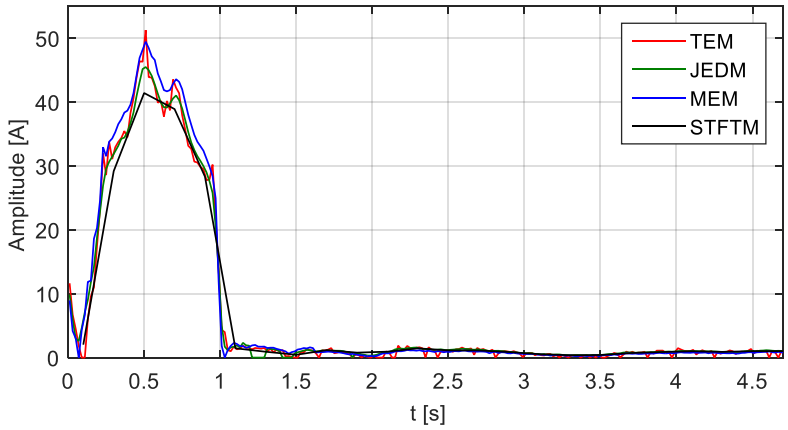

(c)

Figure 2.9 *- MEM - Case study 4: a) fundamental, b) 5th, and c)7th-order harmonic components versus time evaluated by TEM, JEDM, MEM and STFTM*

Note that this case study was characterized by an important issue that occurred in some of our applications, i.e., TEM's results furnished spectral components characterized by very low amplitudes that frequently change versus time, in a non-linear behavior. This phenomenon,

physically difficult to explain, seems to be linked to numerical problems due to the very low values of spectral component amplitudes. In order to guarantee the best investigation upon the selected spectral analysis methods, the percentage errors in Table 2.9 are evaluated by taking into account the aforesaid TEM problem. Specifically, when the spectral components detected by TEM presented in time an amplitude below the 2% of the corresponding fundamental component amplitude, the spectral estimations in those time intervals were not included in the evaluation of percentage errors for JEDEM, MEM and STFTM.

It has to be emphasized that JEDM, MEM and STFTM partially exceeded the above problem that characterizes TEM. In fact, JEDM and STFTM were always able to detect the low-amplitude harmonic components, since they were evaluated by the DFT algorithm. Also MEM was always able to detect the aforesaid low-amplitude spectral components, since, being the corresponding frequencies evaluated in the *basis window* and then imposed also in the *no-basis windows*, even if the amplitudes decreased in a *no-basis window*, solving the Eq. (2.2), the small amplitude values were still identified.

Table 2.10 shows a comparison of the computational time by all of the methods in per unit of time required by STFTM. MEM was faster than the other two methods, and it approached STFTM better than they did; in particular, in this case study MEM approached STFTM much better than in the previous case studies, indicating that MEM is very powerful in the presence of long waveforms, since, in these cases, the computational burden of the basis windows is more mediated.

***Table 2.9** - MEM - Case study 4: average percentage errors of the most significant spectral components detected by JEDM and MEM*

	Average error [%]					
	Amplitude			Frequency		
	Fundamental	5^{th}	7^{th}	Fundamental	5^{th}	7^{th}
JEDM	2.2	6.8	7.0	0.26	0.27	0.13
MEM	4.1	6.5	12	0.50	0.30	0.11
STFTM	4.4	7.1	24	0.51	0.17	0.39

***Table 2.10** - MEM - Case study 4: computational time by TEM, JEDM, and MEM in p.u. of time required by STFTM*

	Computational time [p.u.]
TEM	126
JEDM	8.4
MEM	1.6
STFTM	1

e) Case study 5

A synthetic 3 s waveform that emulates a current at the PCC of a PV system equipped with a full-bridge, unipolar inverter, is analyzed (Fig. 2.10). Specifically, the waveform was assembled assuming a fundamental current of 40 A at 50.02 Hz and a frequency modulation index m_f of the inverter PWM technique equal to 200; then, all odd harmonics up to the 27th order (low-frequency components) and a white noise with a standard deviation of 0.001 were added.

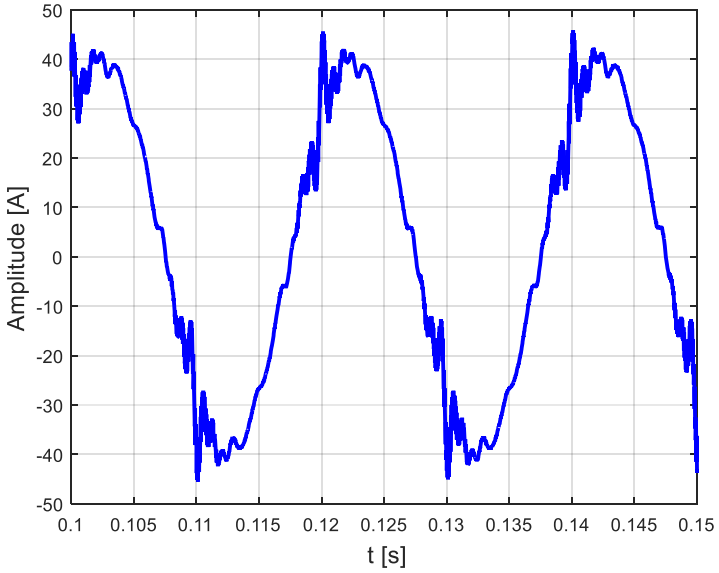

***Figure 2.10** – MEM - Case study 5: trend of the analysed synthetic waveform*

The sampling frequency of the waveform was 50 kHz, in order to provide the most appropriate operating conditions for the parametric methods; this choice allowed the detection of the spectral components around the order $2m_f$, that are the most significant introduced by the inverter PWM and whose amplitudes were fixed up to 2% of the fundamental, in order to emulate the behavior of the PV system during high-irradiance conditions [28].

Moreover, a frequency-modulated, high-frequency spectral component was added to the aforesaid spectral components. This was made in order to both emulate the presence of secondary emission and to test the performance of the proposed method in the detection of time-varying spectral components, that are typical in the high-frequency range. The added spectral component $s_{tv}(t)$ was a tone at $f_{tv} = 17598\,Hz$ with a sinusoidal modulation in frequency, according to Eq. (2.3):

$$s_{tv}(t) = A_{tv}\cos(2\pi f_{tv}t + \varphi_{tv}(t)), \tag{2.3}$$

where:

$$\varphi_{tv}(t) = A_{\varphi}\sin(2\pi f_{\varphi}t), \tag{2.4}$$

and A_{tv} was fixed equal to the 0.5% of the fundamental amplitude, A_{φ} was 5 Hz and f_{φ} was 1 Hz.

For the TEM, JEDM and MEM the error threshold was fixed equal to 10^{-5}, and the window of analysis moves by 0.04 s without overlap. Moreover, the second step of JEDM was applied with a DFT window size of 3 times the fundamental period. Note also that MEM was set to analyze a basis window whenever the reconstruction error exceeded 10^{-3} in order to allow the detection of the high-frequency time-varying spectral component.

Table 2.11 shows the average percentage errors of the frequencies (Tab. 2.11a) and of the amplitudes (Tab. 2.11b) for four selected spectral components. These spectral components are the fundamental and the 11th harmonic (low-frequency components), the component of order $2m_f + 1$ linked to the inverter switching frequency and the frequency-modulated component (high-frequency components).

The average percentage errors in Table 2.11 once again prove the better accuracy of the low-frequency component estimations obtained through TEM and MEM; above all, the results

obtained through STFTM are sensibly poorer. However, the considered methods appear to behave differently in the estimation of high-frequency, time-invariant components and in the estimation of high-frequency, time-varying components. Specifically, TEM and MEM still provided the best estimations of the high-frequency time-invariant spectral components; the MEM errors for the high-frequency time-varying components became higher than STFTM errors both for the amplitude and the frequency in time. The loss of accuracy of the MEM was due the too-high duration of the analysis window, with respect to the period of f_{tv}. Indeed, the most significant low-frequency components hid the frequency modulation on high-frequency components, since the effect of these high-frequency components on the whole waveform was marginal. For this reason, the MEM reconstruction error obtained in the *no-basis window* was often lower than the selected threshold, even if MEM assumed the modulated frequency to be constant in several analysis windows. On the other hand, as well known, the use of a smaller analysis window (i.e., at least one hundred times smaller than the one actually used) would not allow an accurate estimation of the low-frequency spectral components.

Table 2.11 *- MEM - Case study 5: (a) average percentage errors of frequency; (b) average percentage errors of amplitude for: the fundamental, the 11th harmonic, the component of order* $\mathbf{2m_f + 1}$ *and the frequency-modulated component estimated by TEM, JEDM, MEM and STFTM*

Average Errors of Frequency [%]				
	Fundamental	11th harmonic	$2m_f + 1$	Modulated
TEM	$32 \cdot 10^{-6}$	$44 \cdot 10^{-6}$	$4.0 \cdot 10^{-6}$	0.0044
JEDM	0.013	0.015	0.0036	0.52
MEM	$33 \cdot 10^{-6}$	$31 \cdot 10^{-6}$	$5.1 \cdot 10^{-6}$	0.45
STFTM	0.040	0.040	0.040	0.010

(a)

Average Errors of Amplitude [%]				
	Fundamental	11th harmonic	$2m_f + 1$	Modulated
TEM	$180 \cdot 10^{-6}$	0.0054	0.011	24
JEDM	2.4	0.059	47	95
MEM	$23 \cdot 10^{-6}$	0.0021	0.016	95
STFTM	0.060	0.25	82	19

(b)

Note that TEM still provided the best accuracy also in the estimation of high-frequency time-varying spectral components, but the corresponding percentage errors significantly grew (about three orders of magnitude) with respect to the estimation of the low-frequency and high-frequency, time-invariant spectral components. This means that also TEM was highly stressed when it was used to analyze a wide-spectrum waveform that contains time-varying spectral components; this was due to the different requirements of low- and high-frequency spectral components in terms of duration of the analysis window. Also JEDM provided a great inaccuracy in the high-frequency spectral component estimation in this case study; this was due to the spectral leakage that affected the second step of JEDM, and that avoided the correct detection of the low-amplitude spectral components that were not synchronized with the duration of the analysis window. Obviously, this is the same problem of the STFTM; however, since STFTM and the second step of JEDM used a different analysis window, the different frequency resolution of these two methods determined dissimilar percentage errors

in the detection of the high-frequency spectral components, according to their proximity to the multiples of the frequency resolution of each method. Eventually, the significant amplitude percentage error of JEDM in the fundamental component estimation was related both to the low-pass filtering and to the down-sampling procedure performed in the first step of JEDM, that caused an unavoidable loss of information.
Table 2.12 shows a comparison of the computational time required by all of the methods in per unit of the time required by STFTM. The computational burden of TEM was the highest of all of the considered methods; JEDM and MEM completed the analysis in about half of the time required by TEM, but their computational burden is still high with respect to the STFTM. This was coherent with the previous considerations on the difficulties suffered by both methods in the detection of spectrum that was characterized by both low- and high-frequency spectral components, with different behavior in time. In particular, MEM in this case required the generation of several *basis windows* due to the variability of the modulated frequency, thus increasing the computational burden.

Table 2.12 - *MEM - Case study 5: computational time by TEM, JEDM, and MEM in p.u. of time required by STFTM*

	Computational time [p.u.]
TEM	217.76
JEDM	132.37
MEM	125.86
STFTM	1

2.3 Conclusions

In this chapter, an advanced, new ESPRIT-based scheme for the accurate assessment of waveform distortions in power systems at relatively low computational cost was presented.
The proposed scheme was tested and evaluated on waveform recordings measured in the power system and on synthetically-generated data sequences.
The method was based on the assumptions that the frequencies of the spectral components can be calculated once or, at most, a few times along the analyzed waveform and that the damping factors too can be assumed almost constant along the windows, thereby significantly reducing the computational effort that is required.
The main outcomes of the scheme were:

- guaranteed a sufficiently accurate estimation of the spectral components for many waveforms, significantly reducing the estimation error.
- Resulted in a significant reduction of the computational time compared to the conventional ESPRIT method without sacrificing the performance of estimation.
- Resulted in a significant reduction of the computational time compared to the recent hybrid ESPRIT-DFT methods, guaranteeing better performance of estimation.
- Resulted in a significant improvement of the accuracy of the results compared to the DFT method, guaranteeing sometimes quite similar and sometimes similar computational time.

The presented method is particularly beneficial for many waveforms, in terms of both the accuracy of the results and the reduced computational efforts, however, as previously stated

and demonstrated in this Chapter, such approach cannot be considered to be generally applicable. In particular, the presented method provides some inaccuracies in the presence of wide-spectrum waveforms that have time-varying high-frequencies spectral components. Moreover, the estimation problems in presence of time-varying wide-spectrum are also matched to a significant growing of the computational time with respect to the analysis of waveforms with low-frequencies that vary slightly with time.
It is worth noting that the problems related to the spectral analysis of these wide-spectrum waveforms can be observed not only in the presented method, but also in the other methods considered in the numerical application of this Chapter. This remark underlines and endorses that the high-frequency disturbances are currently an important and non-trivial issue and that adequate analysis tools are required for their detection.
In the following Chapter, some hybrid methods for the spectral analysis will be presented, and also the detection of high-frequencies disturbances will be further dealt.

2.4 References

[1] G.W. Chang, C.I. Chen, Measurement Techniques for Stationary and Time-varying Harmonics, Proc. of IEEE PES General Meeting, 2010, 1-5

[2] T. Lobos, Z. Leonowicz, J. Rezmer, P. Schegner, High-resolution spectrum estimation methods for signal analysis in power systems, IEEE Trans. Instr. Measurement, vol. 55, no. 1, 2006, 219–225

[3] A. Bracale, G. Carpinelli, Z. Leonowicz, T. Lobos, J. Rezmer, Measurement of IEC Groups and Subgroups using Advanced Spectrum Estimation Methods, IEEE Trans. on Instr. and Meas., vol. 57, no. 4, 2008, 672–681

[4] I.Y.H. Gu, M.H.J. Bollen, Estimating interharmonics by using sliding-window ESPRIT, IEEE Transaction Power Delivery, vol. 23, no. 1, 2008, 13–23

[5] A. Bracale, P. Caramia, G. Carpinelli, Adaptive Prony Method for Waveform Distortion Detection in Power Systems, Int. Journal of Electrical Power & Energy Systems, vol. 29, no. 5, 2007, 371–379

[6] C.I. Chen, G.W. Chang, An efficient Prony-based solution procedure for tracking of power system voltage variations, IEEE Transactions on Industrial Electronics, 2013, 2681-2688

[7] A. Bracale, G. Carpinelli, I.Y.H. Gu, M.H.J. Bollen, A new joint sliding-window ESPRIT and DFT scheme for waveform distortion assessment in power systems, Electric Power Systems Research, vol. 88, 2012, 112-120

[8] A. Bracale, P. Caramia, G. Carpinelli, A new joint sliding-window Prony and DFT scheme for the Calculation of Power Quality Indices in the Presence of Non-Stationary Disturbance Waveforms, Int. J. of Emerging Electric Power Systems, vol. 13, no. 5, 2012

[9] P. Nayak, B. N. Sahu, A robust extended Kalman filter for the estimation of time varying power system harmonics in noise, IEEE Power, Communication and Information Technology Conference (PCITC), Bhubaneswar, 2015, 635-640

[10] A. Testa, M.F. Akram, R. Burch, G. Carpinelli, G. Chang, V. Dinavahi, C. Hatziadoniu, W. M. Grady, E. Gunther, M. Halpin, P. Lehn, Y. Liu, R. Langella, M. Lowenstein, A. Medina, T. Ortmeyer, S. Ranade, P. Ribeiro, N. Watson, J. Wikston, W. Xu, Interharmonics: Theory and Modeling, IEEE Trans. on Power Del., vol. 22, no. 4, 2007, 2335-2348

[11] A. Bracale, P. Caramia, P. Tricoli, F. Scarpa, and L. Piegari, A new advanced method for assessment of waveform distortions caused by adjustable speed drives, Proc. of the 46th Annual IAS Meeting, Orlando (FL), 2011

[12] J. Zygarlicki, M. Zygarlicka, J. Mroczka, K.J. Latawiec, A reduced Prony's method in power-quality analysis—parameters selection, IEEE Trans. Power Deliv., vol. 25, no. 2, 2010, 979–986

[13] L. Alfieri, G. Carpinelli, A. Bracale, New ESPRIT-based method for an efficient assessment of waveform distortions in power systems, Electric Power Systems Research, vol. 122, 2015, 130-139

[14] J. Zygarlicki, J. Mroczka, Variable-Frequency Prony Method in the Analysis of Electrical Power Quality, Metrology and Measurement Systems, vol. 19, no. 1, 2012, 39–48

[15] IEC standard 61000-4-30, Testing and measurement techniques – Power quality measurement methods, 2015

[16] P. Caramia, G. Carpinelli, P. Verde, Power Quality Indices in Liberalized Market, John Wiley & Sons, Chichester, West Sussex (UK), 2009

[17] J. Meyer, M. Bollen, H. Amaris, A.M. Blanco, A. Gil de Castro, J. Desmet, M. Klatt, Ł. Kocewiak, S. Rönnberg, K. Yang, Future work on harmonics - some expert opinions Part II - supraharmonics, standards and measurements, Proceedings of 16th IEEE ICHQP, Bucharest, 2014, 909-913

[18] CIGRE WG 37–23, Impact of increasing contribution of dispersed generation on the power system, 1999

[19] E.O.A. Larsson, M.H.J. Bollen, Measurement result from 1 to 48 fluorescent lamps in the frequency range 2 to 150 kHz, Proceedings of 14th Int. Conf. on Har. and Qual. of Pow. (ICHQP), Bergamo, 2010, 1-8

[20] D. Gallo, R. Langella, A. Testa, J.C. Hernandez, I. Papic, B. Blazic, J. Meyer, Case studies on large PV plants: Harmonic distortion, unbalance and their effects, IEEE PES Gen. Meet., Vancouver, 2013

[21] A. Moreno-Munoz, A. Gil-de-Castro, E. Romero-Cavadal, S. Rönnberg, M. Bollen, Supraharmonics (2 to 150 kHz) and multi-level converters, Proceedings of IEEE 5th Int. Conf. on P. Eng., En. and Elect. Dr. (POWERENG), Riga, 2015, 37-41

[22] S.K. Ronnberg, M. Wahlberg, E.O.A. Larsson, M.H.J. Bollen and C.M. Lundmark, Interaction between equipment and power line Communication: 9-95 kHz, IEEE Bucharest PowerTech, Bucharest, 2009, 1-5

[23] M. Bollen, M. Olofsson, A. Larsson, S. Ronnberg, M. Lundmark, Standards for supraharmonics (2 to 150 kHz), IEEE Electromagnetic Compatibility Magazine, vol. 3, no. 1, 2014, 114-119

[24] P. Stoica, R. Moses, Introduction to Spectral Analysis, Prent. Hall, New Jersey, 1997

[25] O.Y. Bushuev, O.L. Ibryaeva, Choosing an optimal sampling rate to improve the performance of signal analysis by Prony's method, 35th Int. Conf. on Telecom. and Sig. Proc. (TSP), 2012, 634-638

[26] L. Alfieri, A. Bracale, P. Caramia, G. Carpinelli, Advanced Methods for the Assessment of Time Varying Waveform Distortions Caused by Wind Turbine Systems. Part II: Experimental Applications, 13th IEEE International Conference on Environment and Electrical Engineering, Wroclaw, Poland, 2013

[27] IEC standard 61000-4-7, General guide on harmonics and interharmonics measurements, for power supply systems and equipment connected thereto, 2010

[28] D. Gallo, C. Landi, M. Luiso, AC and DC power quality of photovoltaic systems, Proceedings of IEEE Int. Inst. and Meas. Tech. Conf. (I2MTC), Graz, 2012, 576-581

Chapter 3.
Proposed hybrid methods for the spectral analysis of time-varying waveforms in power systems

3.1 Introduction

As observed in Chapter 1, hybrid methods for the waveform distortion analysis were proved to be important tools in order to overcome the problems of the methods from which they derive [1-9]. In particular, the hybrid methods based on the joint of parametric and non-parametric methods are particularly suitable to detect the spectrum with high accuracy and reduced computational effort [1-3]. Motivated by the above considerations, three new hybrid methods that properly match both parametric and non-parametric methods are presented in this Chapter [10-12].

The first method is a three-step method (*Sliding-window Prony-DFT-Prony method*) that combines the Prony's method with the DFT [10-11]. The second method (*Sliding-window Parametric-DFT-analytical-parametric method*) is a four-step method and is addressed for an accurate and fast assessment of current waveform distortions caused by adjustable speed drives [11]. Finally, the last method (*Sliding-window Wavelet-modified ESPRIT method*) is based on a DWT step, followed by the application of the modified ESPRIT method in the successive step [12]. This last method, differently to the previous ones, is expressly designed for the modern requirements in term of spectral analysis of waveforms with wide spectra that include frequencies exceeding 2 kHz up to 150 kHz[4].

The remainder of this chapter is organized as follows. Section 3.2 describes in detail the sliding-window Prony-DFT-Prony method. Section 3.3 deals with the sliding-window parametric-DFT-analytical-parametric method. Section 3.4 provides a description of the sliding-window Wavelet-modified ESPRIT method. Both the theoretical aspects and numerical applications of the aforesaid methods are presented in each Section. Finally, the conclusion are in Section 3.5.

[4] This spectral content was initially indicated as "high-frequency distortion", but recently the term "supraharmonic" is generally used. The supraharmonics have currently gained great interest since this range of frequencies still require not only appropriate analysis tools, but also adequate standardizations, which allow to define proper indices and maximum thresholds for the evaluation and the limitation of these high-frequency spectral components [13-17].

3.2 Sliding-window Prony-DFT-Prony Method

As well known, in order to calculate the waveform spectral components in the low-frequencies range, IEC 61000 4-7 [18] recommends DFT applied over successive rectangular time windows of 10 or 12 cycles of fundamental period, respectively for 50 or 60 Hz system. However, while the standard method is useful to globally quantify the waveform distortions, it is of limited use for accurately extracting detailed information on individual components, mainly in presence of time-varying waveforms. In fact, DFT spectral leakage can be relevant when: (i) time window length is not exactly an integer-multiple of power system fundamental and secondary (ii) in presence of interharmonics [1,19-20]. Thus, parametric high-performance signal-analysis techniques were proposed in the relevant literature, allowing to identify the spectral components without spectral leakage problems (and, then, with high resolution), leading to an accurate evaluation of time varying waveforms. However, these methods are usually characterized by higher computational efforts than the DFT-based method [2,20-22].

Some recent contributions in the relevant literature proposed hybrid methods based on the contemporaneous use of both DFT method and high resolution parametric methods with the aim of providing accurate estimation of spectral components while keeping a relatively low computational effort, mainly in case of non-stationary waveforms [2-3]. In particular, as shown in the Chapter 1, in [3] a three-step sliding-window (SW) scheme was proposed that applies successively a SW ESPRIT, a SW DFT[5], and a further SW ESPRIT in different pass-bands for separately estimating the power system fundamental, harmonics and interharmonics, respectively. Using the strategy of divide and conquer, the SW ESPRIT is employed to estimate the fundamental component and a reduced number of interharmonic spectral components while harmonics are estimated using the SW DFT with a synchronized window to mitigate spectral leakage. In [2] a two-step sliding-window scheme is proposed to calculate new energy-based PQ indices in non-stationary conditions. Prony method is applied at first to estimate only the fundamental component while the SW DFT is applied in the second step to evaluate the remaining waveform distortions.

The novel three-step SW scheme presented in [10,23] is described in this Section. This method applies successively a SW Prony, a SW DFT, and a SW Prony in different pass-bands for separately estimating the power system fundamental, harmonics and interharmonics. Even though the novel SW scheme adopts the same three-step strategy of divide and conquer of [3], it differs substantially from [3] since the SW Prony method is applied instead of SW ESPRIT, in order to improve the estimation of the spectral component amplitudes. The SW Prony is focused on estimating only the power system fundamental and a reduced number of high frequency interharmonics. In such a way, the joint SW Prony and DFT method (JPDM) may significantly reduce the computational cost in comparison with conventional parametric methods applied to the whole waveform.

The following Sub-sections firstly describe the proposed scheme in detail, then, several case studies are analysed with reference to synthetic and actual waveforms.

[5] The SW DFT corresponds to the Short Time Fourier Transform (STFT). See Chapter 1 for further clarifications.

3.2.1 Model formulation and solving procedure

The JPDM, as previously evidenced, alternatively applies a sliding-window Prony and a sliding-window DFT in different pass-bands for separately estimating the power system fundamental, harmonics and interharmonics. In each step, different spectral components are estimated with the aim of reducing the problems of spectral leakage and high computational efforts that can arise in SW DFT and SW Prony method application, respectively. In particular, this hybrid method avoids spectral leakage problems constraining the size of the window of the SW DFT to be an integer multiple of the fundamental period, estimated applying SW Prony to a low-pass filtered signal.

The presented new scheme consists of a three-step procedure. The block diagram of the scheme for the analysis of a signal $x(n)$ is reported in Fig. 3.1.

a) First step

In the first step, a SW Prony is applied to the low-pass filtered waveform to estimate basically the power system fundamental component. The filter low-pass band is from 0 to 100 Hz.

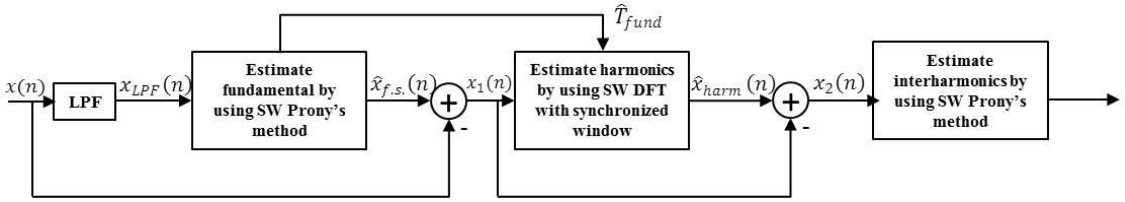

Figure 3.1 *– Block diagrams of the SW Prony-DFT-Prony scheme*

Specifically, the SW Prony is applied to each L^*-point window of the filtered waveform $x_{LPF}(n)$. The filtered waveform is approximated, according to the Prony's model presented in the Chapter 1, with the linear combination of $M^* \leq L^*/2$ exponentials [24]:

$$\hat{x}_{LPF}(n) = \sum_{k=1}^{M^*} h_k e^{(\alpha_k + j2\pi f_k)nT_s}, \qquad n = 0,1,\dots,L^* - 1 \tag{3.1}$$

where $\hat{x}_{LPF}(n)$ is the estimated value of $x_{LPF}(n)$, $h_k = A_k e^{j\phi_k}$, and A_k, ϕ_k are the amplitude and the initial phase, respectively, f_k is the frequency, α_k is the damping factor of the $k-th$ exponential.

Obviously, in the first step of the proposed scheme, a small integer even and positive number of exponentials, i.e., $M^* = 2$, is assigned in (3.1), since the first step was only concerned about the fundamental component and the interharmonic components from 0 to 100 Hz. For non-stationary waveform-distortion sequences, the use of a SW Prony method guarantees a proper time-dependent estimation of the spectral components in the selected range of frequency. The presented method applies also the adaptive technique proposed in [1] that allows to implement the Prony's model as correctly as possible, since the adaptive technique performs an optimal and adjustable choice both of the duration L^* of the sliding window size versus time and of the number of exponential M^* required in the model (3.1).

As well known, the computational burden of the Prony's method is strictly dependent on the cubic order of the size of the matrices related to the equation systems (1.36) and (1.38) to be

solved (see also Chapter 1). These sizes are $M \times M$ and $(L - M) \times M$, respectively, where M is the number of spectral components included in the full-band signal $x(n)$, and L is the number of samples related to the duration of the sliding-window utilized when the full-band signal $x(n)$ has to be analysed. Based on the previous considerations, it's obvious that the computational requirement for the first step of JPDM is significantly less than that for the SW Prony method applied to the full-band signal $x(n)$, since: (i) as previously evidenced, the first step was concerned about only few spectral components, that are the fundamental and the interharmonics from 0 to 100 Hz, so number of exponentials M^* required in the first step of JPDM is necessarily significantly lower than M; (ii) the filtered signal $x_{LPF}(n)$ can be also down-sampled, according to the Nyquist-Shannon theorem, in order to reduce the number of samples L^* related to the duration of the sliding-window utilized in the first step of JPDM.
At the end of the first step, using the estimated parameters associated with the fundamental and the interharmonics in the band from 0 to 100 Hz, the reconstructed first step components, $\hat{x}_{f.s.}(n)$, is obtained (Fig. 3.1). The waveform obtained as difference $x_1(n) = \hat{x}_{f.s.}(n) - x(n)$, as well as the estimated period of the fundamental component $\hat{T}_{fund}$, are used as input for the second step of JPDM.

b) Second step

In the second step, the SW DFT is used to achieve an accurate and fast evaluation of the harmonic components included in the waveform to be analyzed. In fact, the knowledge of $\hat{T}_{fund}$ allows to perform the analysis of the waveform $x_1(n)$ by using a SW DFT with a window size synchronized with the harmonic components included in $x_1(n)$. Specifically, the duration of the analysis window in this step can be set to 10 cycles (12 cycles) of the estimated fundamental period $\hat{T}_{fund}$, for 50-Hz systems (60-Hz systems), according to the IEC recommendations, but, if it is required, it also is possible to select a different number of cycles [3].
Note that, as stated in Chapter 1, setting the duration $\hat{T}_w$ of the SW DFT to be an integer multiple of the estimated fundamental period $\hat{T}_{fund}$, the spectral leakage from other harmonics is minimized. Hence, the aforesaid synchronization of the time-window in the SW DFT guarantees a very accurate estimation of the harmonic components, since the spectral leakage becomes significantly limited, being due only to the possible presence of interharmonics at frequencies $f > 100\ Hz$ in $x_1(n)$. Moreover, also in this case, for non-stationary waveform-distortion sequences, the use of a SW DFT guarantees a proper time-dependent estimation of the harmonic components included in the waveform.
Simultaneously, the spectral analysis of $x_1(n)$ is also obtained with a reduced computational effort, since the SW DFT, as observed in Chapter 1, can be performed using very fast algorithms as the FFT.
Summing the reconstructed harmonic components, the waveform $\hat{x}_{harm}(n)$ can be found. This waveform $\hat{x}_{harm}(n)$ has to be subtracted to $x_1(n)$ in order to obtain the residual $x_2(n)$ (Fig. 3.1). This residual $x_2(n)$ is usually constituted by a low number of components [3]. In particular, based on the described decomposition of the original waveform $x(n)$, the spectral components included in $x_2(n)$ are the only interharmonic components at frequencies $f > 100\ Hz$.

c) Third step

The residual is analyzed in the third step, where the interharmonic components at frequencies $f > 100\ Hz$ are estimated using the SW Prony again. Also in this step, the presented method applies the adaptive technique proposed in [1], in order to perform an optimal and adjustable choice both of the size L^{**} of the sliding window versus time and of the number of exponential M^{**} required in the Prony's model:

$$\hat{x}_2(n) = \sum_{k=1}^{M^{**}} h_k e^{(\alpha_k + j2\pi f_k)nT_s}, \qquad n = 0,1,\dots,L^{**}-1 \tag{3.2}$$

with obvious meaning of the symbols.

In particular, the relationships (1.36) and (1.38) in Chapter 1, as well as in the first step of the method, are recursively applied, starting from initial values for M^{**} and L^{**} heuristically selected according to: (i) the expected number of components included in the waveform to be analyzed and (ii) the number of samples included in some cycles of the fundamental period, respectively. Then, the aforesaid values of M^{**} and L^{**} are iteratively increased of ΔM and ΔL, respectively. The values of ΔM and ΔL are even numbers heuristically chosen, based on the particular application. Eventually, the JPDM uses a fast iterative procedure that minimizes the mean square relative reconstruction error. This, in the third step, is obtained as follow:

$$\varepsilon_{curr}^2 = \frac{1}{L^{**}} \sum_{n=1}^{L^{**}} \frac{|x_2(n) - \hat{x}_2(n)|^2}{x_2^2(n)} \tag{3.3}$$

where $x_2(n)$ are the measured samples and $\hat{x}_2(n)$ are given by (3.2). Fixed a priori a threshold value ε_{th}^2 for the aforesaid error, the iteration that provides $\varepsilon_{curr}^2 \leq \varepsilon_{th}^2$ determines also the optimal value of M^{**} and L^{**}, and, similarly to the first step, the corresponding estimated spectral components are the output of the third step.

It should be noted that, once again, the reduced number M^{**} of model (3.2) and the opportune choice of the window size L^{**} provide low time computation.

d) Performances of JPDM

As stated before, the JPDM, combining the SW DFT and SW Prony, overcomes the limits of SW Prony and SW DFT too. In fact, the JPDM is able to: (i) improve the DFT accuracy in the harmonic estimations; (ii) guarantee a reduced computational effort, since the sum of computational efforts in the first and third steps is significantly less than that for the SW Prony method applied for the full-band signal.

In particular, the aforesaid goals are reached by reducing the dimension of the linear system involved in the SW Prony application, and synchronizing the sliding-window size in the DFT with the actual fundamental frequency of the waveform. These choices cause respectively a more low computation than the SW Prony applied for the full-band waveform and a significant reduction of the spectral leakage problem involved in the SW DFT application.

Hence, the JPDM appears as a good compromise in term both of accuracy and computational burden for the estimation of the waveform spectral components in the low-frequencies range.

3.2.2 Numerical applications

To evaluate the effectiveness and performances of the proposed JPDM, several numerical experiments were performed on both waveforms with data being acquired from the power systems as well as from synthetically-generated waveforms.

For the sake of brevity, the following subsections show only three case studies, one from the synthetic waveforms and two from the measured waveforms.

In the case of the waveform generated synthetically, the aim is to compare the JPDM performances with those of the STFT method (STFTM) according to IEC recommendations, the joint SW ESPRIT and DFT method presented in [3] (JEDM), the traditional Prony's method (TPM), using the ground truth values of the spectral components. Comparisons were effected on both results accuracy and computational efforts.

The measured waveforms are a voltage waveform during a signalling by the distributor and an arc furnace voltage supply waveform. These two waveforms were analysed only by the JPDM.

For all cases, the low-pass filter was formed by a linear-phase FIR filter with a cut-off frequency of 200Hz. MATLAB programs were developed and tested on a Windows PC with an Intel® Core™ 2 Duo 2.66-GHz processor and 2048 MB of RAM. It should be noted that all programs are implemented by MATLAB and are not optimized for computational speed; then, the computational time only gives a rough and relative comparison of efficiency in different methods.

a) Case study 1

The synthetic waveform was an "acid test", consisting of a 50.03 Hz fundamental component of amplitude 100 p.u., 2nd and 4th harmonic components of amplitude 1 p.u., 5th and 7th harmonic components of amplitude 5 p.u., 11th and 13th harmonic components of amplitude 3 p.u. and two interharmonic components of amplitude 0.5 p.u. at frequencies 82 Hz and 182 Hz, respectively. The sampling rate was set to be 5 kHz. The fundamental frequency value introduces a de-synchronization comparable with the maximum permissible error of IEC instruments [18].

All methods (JPDM, STFTM, JEDM and TPM) were applied analysing a certain number of data blocks. Neighbouring data blocks are chosen with 0.04 s overlap in order to yield more smooth results through windows. Table 3.1 shows the average percentage errors of some spectral component amplitudes/frequencies estimated by TPM, JEDM, JPDM and STFTM. In particular, Table 3.1.a shows the average percentage errors for the fundamental, 82 Hz interharmonic and 182 Hz interharmonic, while Table 3.1.b shows the average percentage errors for the 2nd, the 7th and the 13th harmonics.

The results of Table 3.1 show that the proposed scheme has yielded an accurate estimation for all spectral components in terms of both amplitudes and frequencies. Moreover, the following considerations arise:

(i) the estimated interharmonic frequencies with STFTM are 80 Hz and 180 Hz, as a consequence of the 5-Hz frequency resolution of DFT. In addition, significant errors arise in the spectral component amplitudes, mainly in case of interharmonic components.

(ii) TPM yielded highly accurate estimation for all spectral components, in terms of both amplitudes and frequencies.

(iii) JEDM and JPDM furnish very good results in terms of both amplitudes and frequencies, with errors similar to TPM for frequencies and slightly less accurate for amplitudes.

(iv) JPDM seems to provide higher accuracy than JEDM in the amplitude estimations obtained in the first and third step, although a worsening in the corresponding frequency estimation occurs.

Further, the efficiency of the proposed scheme was evaluated by comparing the computational time.

Table 3.1 - *JPDM - Case study 1: average percentage errors of estimated amplitudes and frequencies of: (a) fundamental, 82Hz interharmonic and 182Hz interharmonic; (b) 2^{nd},7^{th} and 13^{th} harmonics, obtained with TPM, JEDM, JPDM and STFTM*

	Average error [%]					
	Amplitude			Frequency		
	Fundamental	82Hz	182Hz	Fundamental	82Hz	182Hz
TPM	$38\cdot10^{-12}$	$170\cdot10^{-12}$	$73\cdot10^{-12}$	$0.13\cdot10^{-12}$	$0.13\cdot10^{-12}$	$0.14\cdot10^{-12}$
JEDM	0.014	0.12	0.14	$22\cdot10^{-12}$	$21\cdot10^{-12}$	$60\cdot10^{-6}$
JPDM	0.0053	0.0030	0.048	$0.061\cdot10^{-12}$	0.0080	0.0030
STFTM	0.026	24	26	0.060	2.4	1.1

(a)

	Average error [%]					
	Amplitude			Frequency		
	2nd	7th	13th	2nd	7th	13th
TPM	$31\cdot10^{-12}$	$240\cdot10^{-12}$	$69\cdot10^{-12}$	$0.026\cdot10^{-12}$	$0.018\cdot10^{-12}$	$0.056\cdot10^{-12}$
JEDM	0.48	0.051	0.28	$1700\cdot10^{-12}$	$22\cdot10^{-12}$	$22\cdot10^{-12}$
JPDM	0.44	0.10	0.22	$0.061\cdot10^{-12}$	$0.051\cdot10^{-12}$	$0.057\cdot10^{-12}$
STFTM	7.1	0.38	1.2	0.060	0.060	0.060

(b)

Table 3.2 shows the computational time required for the analysis performed by all of the methods in p.u. of time required by STFTM, assumed as reference. From the analysis of Table 3.2 results, it clearly appears that the computational time for JEDM and JPDM is greater than STFTM but significantly lower than TPM. Moreover, the computational time of JPDM is reduced by more than one scale level in comparison to TPM; a reduction of about 30% arises in comparison to JEDM.

Table 3.2 - *JPDM - Case study 1: computational time by TEM, JEDM, and JPDM in p.u. of time required by STFTM*

	Computational time [p.u.]
TPM	822
JEDM	72
JPDM	54
STFTM	1

b) Case study 2

The analyzed waveform was a measured voltage recording, that was carried out during a signaling by the distributor. The sampling rate was set to be 7.2 kHz. An anti-aliasing filter was present in the measurement device before analog to digital conversion. Figures 3.2 show

the time-dependent parameters (frequencies and amplitudes) of waveform components estimated by JPDM.

The same number marked on the curve in Figs 3.2.a) and 3.2.b) implies that they correspond to the same component. In particular, Figs 3.2 show the following significant spectral components present in the waveform: 3rd, 4th, 5th, 7th, 9th, 11th, 13th and 15th harmonics and two interharmonics at frequency of about 183 Hz (amplitude below 4 V) and 283 Hz (amplitude below 2 V). All amplitudes fluctuate with time. The fundamental component (amplitude about 231 V) and a 2nd harmonic with magnitude lower than 0.1% of the fundamental are not shown.

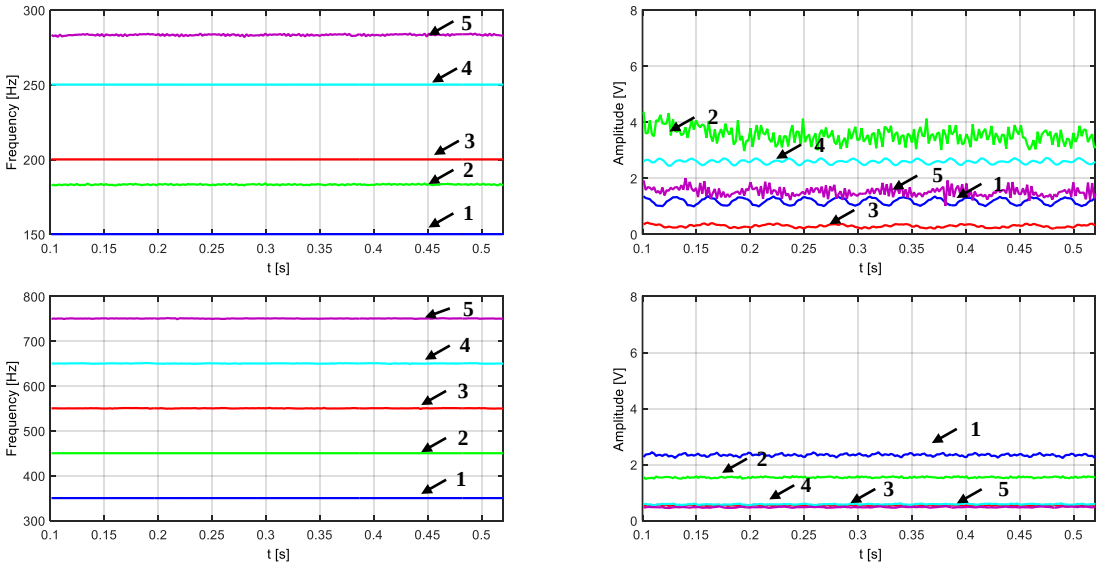

***Figure 3.2** – JPDM - Case study 2: estimated spectral components: (a) frequencies (b) amplitudes*

The same waveform was analyzed in [3] using JEDM. With reference to the band from 0 to 300 Hz, JEDM evidenced a spectral line splits when estimating 50Hz fundamental frequency; this splitting determines the presence of two interharmonics that are not evidenced in JPDM analysis where they are responsible of the fundamental amplitude modulation. With reference to the band from 300 to 800 Hz, JPDM analysis furnished similar results as in [3]; on the other hand, the interharmonic amplitudes obtained by JEDM are more stable than JPDM, shown in Fig. 3.2.b. The slightly different behavior of JEDM and JPDM can be justified by observing the different approach of the ESPRIT and the Prony's methods in the detection of the unknown parameters included in their models (see also Chapter 1). For example: (i) differently to the Prony's method, in the ESPRIT method the white noise is added in the noise; (ii) in the Prony's method the detection of the model parameters mainly depends on the number of spectral components included in the model and on the number of samples included in the selected analysis window, while in the ESPRIT method the aforesaid detection depends also on the order of the correlation matrix. This different approach of these two parametric methods involves different equation systems to be solved and, consequently, a slightly different spectrum detection.

c) Case study 3

The analyzed waveform was a measured voltage recording of 40s, obtained close to an AC arc furnace. The sampling rate was set to be 3 kHz. Once again, an anti-aliasing filter was present in the measurement device before analogical to digital conversion. Figures 3.3 show the time-dependent parameters (frequencies and amplitudes) of waveform components estimated by JPDM.

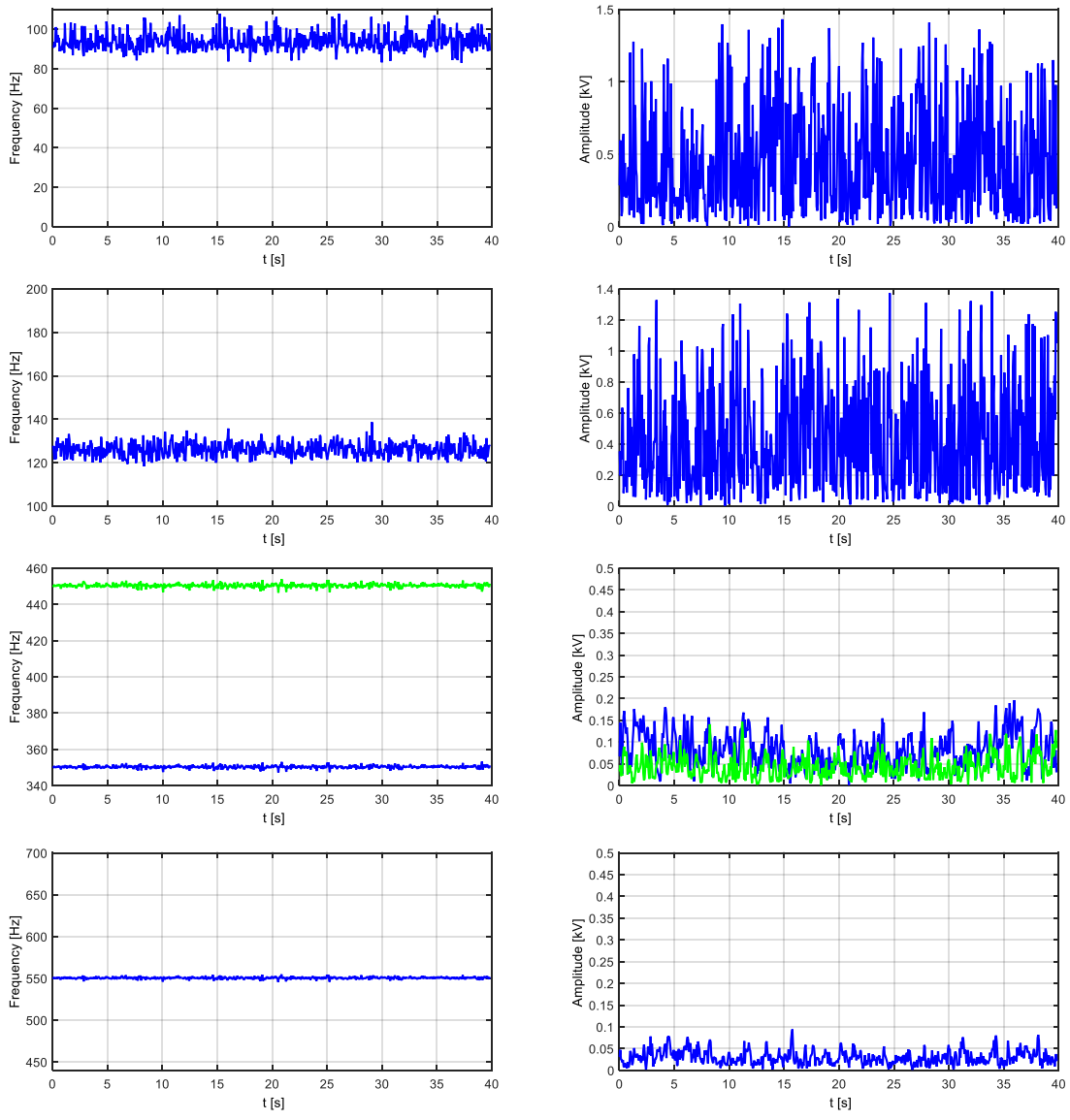

***Figure 3.3** – JPDM - Case study 3: estimated spectral components: (a) frequencies (b) amplitudes*

In particular, Figs 3.3 show the following significant spectral components present in the waveform: 7th, 9th and 11th harmonics and two interharmonics at frequency of about 95 Hz (amplitude below 1.5 kV) and 125 Hz (amplitude below 1.5 kV). All amplitudes fluctuate with time as well as the interharmonic frequencies. The fundamental component (amplitude about 11.5 kV) is not shown.

The same waveform was analyzed in [3] using JEDM. With reference to the band from 0 to 110 Hz, JEDM evidenced two interharmonics around 75 Hz and 95 Hz while JPDM found only one interharmonic component around 95Hz (first row of Fig. 3.3.a) characterized by a

larger amplitude. With reference to remaining bands, JPDM analysis furnished similar results as in [3], except for interharmonic amplitudes that in JPDM is usually slightly larger. This is linked to the differences between the estimation of $x_2(n)$ signal (input of the third step procedures) in JPDM and JEDM methods. In fact, as observed in the previous case study, the different approach of the ESPRIT and the Prony's methods in the detection of the unknown parameters included in their models involve little differences in the spectrum obtained by JEDM and JPDM (see also Chapter 1).

3.3 Sliding-window Parametric-DFT-Analytical-Parametric methods

The growing number of perturbing loads in modern electrical systems has generated increased interest in PQ issues and, consequently, expanding studies of the disturbances that characterize PQ [24-26].

Adjustable speed drives (ASDs) are one of the most prevalent disturbing loads in industrial systems, since ASDs cause heavy distortions in the supply-side at the point of common coupling (PCC) [24-26]. Thus, they have been modelled extensively in the relevant literature with the aim of quantifying the harmonic and interharmonic components of the current waveforms [1,27-31]. The analysis of literature indicated that the waveforms on the AC supply-side of the Pulse-Width Modulation (PWM) ASDs are characterized by several harmonic and interharmonic components that, depending on the particular operating conditions of the motors, can vary with time both in amplitude and in frequency [1,26].

In these conditions, it is well known that some difficulties can arise in the analysis of the harmonic and interharmonics components if inadequate techniques are selected for the spectral analysis [24-25]. For example, as previously observed, IEC 61000 4-7 [18] recommends the use of the DFT with fixed-size rectangular windows that slide in the time on the waveform, but this method is helpful only for a very fast and global quantification of the waveform distortions. In particular, the method becomes inefficient in obtaining more detailed information about the spectral components when the spectral leakage phenomenon arises. The problems of IEC method mentioned above can be overcome by using advanced DFT-based methods or parametric methods, such as the Prony and ESPRIT methods [1,3,21,32-36]. In particular, as seen in the Chapter 1, the parametric methods are able to provide reliable results, especially in the detection of spectral components included in the low-frequency range. However, they generally need a too huge computational burden, in opposition to the modern requirements in term of PQ monitoring.

In [1], the authors proposed an advanced method for the assessment of waveform distortions caused by ASDs. In particular, the method draws inspiration by the modulation theory used in [28], that provides an analytical way to forecast the harmonic and interharmonic frequencies up to 2 kHz due to synchronous, sinusoidal PWM drives. Moreover, the method is based on the cascade application of the ESPRIT and Prony methods in a three-step procedure. In the first and third steps, parametric methods are applied to bands of signals that contain reduced numbers of components, which leads to less computational efforts. In the second step, the frequencies of the harmonics and interharmonics are calculated by the closed-form formulas reported in [28]. Although the combination of these three steps resulted in accurate estimation

with reduced computational requirements, unfortunately those requirements are still significantly greater than those of the DFT method suggested by the IEC Standard.
The sliding-window Parametric-DFT-Analytical-Parametric methods presented in [11] have been designed with the aim of overcoming the aforesaid problems. They are described in this Section. These new methods are based on proper combinations of the Prony, ESPRIT, and DFT methods as well as the analytical formulas in [28] for the analysis of the distortions of current waveforms caused by ASDs. These new methods guarantee high accuracy in the calculation of the spectral components, and they require computational time that is significantly less than that of [1] and that is similar to that of the IEC method. The methods involve a four-step procedure, i.e.: i) a parametric method (either the Prony or the ESPRIT method) is used to estimate the fundamental and the low frequency interharmonics up to 100 Hz; ii) thanks to the estimation of the actual fundamental frequency in first step, a synchronized DFT is used to compute the harmonic components in the waveform; iii) the modulation theory used in [28] is enforced to forecast the frequency interharmonics in the band from 100 Hz to f_{max}, where generally $f_{max} \leq 2\,\text{kHz}$; iv) once again, a parametric method is used to calculate the amplitudes of the high-frequency interharmonics. The advantages of the sliding-window Parametric-DFT-Analytical-Parametric methods are that: (i) in the first and last step, the computational burden is reduced drastically due to the presence of a filter and due to the subsequent decompositions of the waveform, which decrease the spectral content that must be analyzed in each step, and, consequently, decrease the number of exponentials required by the parametric methods; (ii) in the fourth step, the computational effort also is reduced significantly due to the analytical knowledge of the interharmonic frequencies, which reduces the variables of the signal model by 50%; and (iii) in the second step, the accuracy is maximized since the spectral leakage problems are contained due to the synchronization of the analysis window duration and the fundamental period.
The following Sub-sections first describe the proposed scheme in detail; then, several case studies are analysed with reference to synthetic and actual waveforms.

3.3.1 Model formulation and solving procedure

The parametric methods applied in [11] for the first and last steps of the proposed procedure are the SW ESPRIT and SW Prony methods, used in all their possible combinations, i.e., SW Prony in the first step and SW ESPRIT in the last step; SW Prony in both steps; SW ESPRIT in both steps; SW ESPRIT in the first step and SW Prony in the last step. Figure 3.4 shows the block diagram of the general scheme of the sliding-window Parametric-DFT-Analytical-Parametric methods in which each frequency band is analysed separately by a different method in order to optimize the performance and obtain accurate results with a computational effort comparable to that of the IEC method.
In particular, two low-pass filters are used preliminarily on the original waveform $x(n)$*:* the first filter has a band from 0 to 200 Hz, and it leaves only the fundamental component and the low-frequency components in the waveform, obtaining the signal $x_{LPF1}(n)$; the second filter has a band from 0 to 5000 Hz and its aim is to clean up the analysed original waveform by the noise eventually introduced by the measuring instrument, obtaining the waveform $x_{LPF2}(n)$.

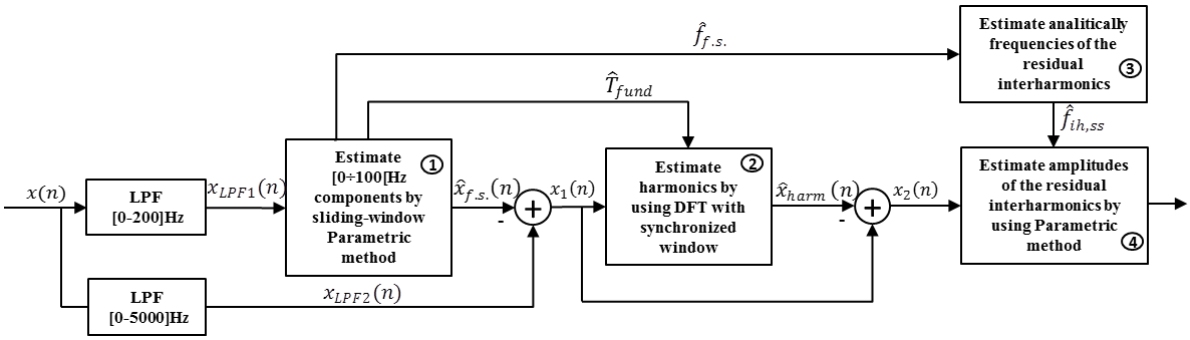

***Figure 3.4** – Block scheme of the presented sliding-window Parametric-DFT-Analytical-Parametric methods*

a) First step

In this step, the waveform $x_{LPF1}(n)$, concerned by spectral content from 0 to 200 Hz, is analysed using a parametric method (either SW Prony or SW ESPRIT), and an accurate analysis is conducted in order to obtain a reliable estimation of the low-frequency components. If the sampling rate f_s of the waveform is too high for the considered band according to the Nyquist-Shannon theorem, a decimation of the data block can be performed in order to reduce the number of samples *L* (and, consequently, the order L_1 chosen for the correlation matrix for SW ESPRIT application). A containment of *L* also leads to a reduction of *M* so that either the SW ESPRIT method or the SW Prony method can provide accurate estimations of the amplitudes and frequencies of the spectral components in the considered range of frequency with less computational effort. Only the estimated spectral components in the frequency band from 0 to 100 Hz are used to construct the waveform $\hat{x}_{f.s.}(n)$ according to the model used by the parametric methods, and the difference $x_1(n)$ between the waveforms $x_{LPF2}(n)$ and $\hat{x}_{f.s.}(n)$ is sent to the second step of the method. The choice of the frequency band from 0 to 100 Hz is a compromise between the need of having components that are not distorted by the filter and the need to estimate the frequencies of all of the components used in the next steps.

b) Second step

In the second step, the waveform $x_1(n)$ is analysed by a synchronized DFT. In fact, the fundamental frequency accurately estimated in the first step allows us to choose a duration $\hat{T}_w$ for the DFT analysis window that is exactly an integer multiple of the effective fundamental cycle, reducing significantly the spectral leakage problems, which remain only due to the presence of interharmonics above 100 Hz. $\hat{T}_w$ is set to 10 cycles of the fundamental period $\hat{T}_{fund}$ for 50-Hz systems and to 12 cycles of the fundamental period for 60-Hz systems, according to IEC's standard requirements [37]. The second step of the method just provides the evaluation of the amplitudes and frequencies of the harmonics, which are then summed in the time domain to yield the waveform, $\hat{x}_{harm}(n)$. The application of DFT in this step guarantees a very rapid computation.

c) Third step

Once the maximum frequency f_{max} of interest is fixed, the frequencies $\hat{f}_{f.s.}$ obtained by the first step of the proposed scheme are used in the third step to compute analytically the

frequencies of the interharmonics in the range from 100 Hz to f_{max} using the mathematical model of the ASD with a double-stage converter presented in [28]. In particular, considering the configuration in Figure 3.5, the interharmonic components on the supply-side of the system are produced by the interaction between the harmonics generated by the rectifier and the harmonics on the DC link side due to the inverter.

The frequencies $f_{h,ss}$ of the supply-side harmonic components linked to the rectifier can be estimated as:

$$f_{h,ss} = |(\upsilon - 1)q_r - 1| \cdot f_{ss} \qquad \upsilon = 1, \dots, q_r \tag{3.4}$$

where f_{ss} is the fundamental frequency of the supply system, and q_r is the number of rectifier pulses. At the same time, in the DC link side, if we know the fundamental frequency f^{os} of the voltage of the output side, the frequencies $f_{h,dc}^{os}$ of the harmonics introduced by the inverter can be computed as:

$$f_{h,dc}^{os} = \left| j\, m_f \pm r \right| \cdot f^{os} \tag{3.5}$$

where m_f is the ratio between the carrier and the modulating frequency, which, in this case, is an integer because a synchronous PWM modulation is considered. The values of j and r are chosen according to Table 3.3, where they are given based on their dependence on m_f. Once the frequencies of the harmonics are known, i.e., $f_{h,ss}$ and $f_{h,dc}^{os}$, the frequencies of the interharmonics, i.e., $f_{ih,ss}$, on the supply side can be obtained as:

$$f_{ih,ss} = \left| f_{h,ss} \pm f_{h,dc}^{os} \right| \tag{3.6}$$

Note that the previous relationships indicate that interharmonic components are always present on the AC supply system side in this type of configuration, except when it can be verified that $f^{os} = f_{ss}$. In the same circumstances, it is also possible for the interharmonics to degenerate into harmonics.

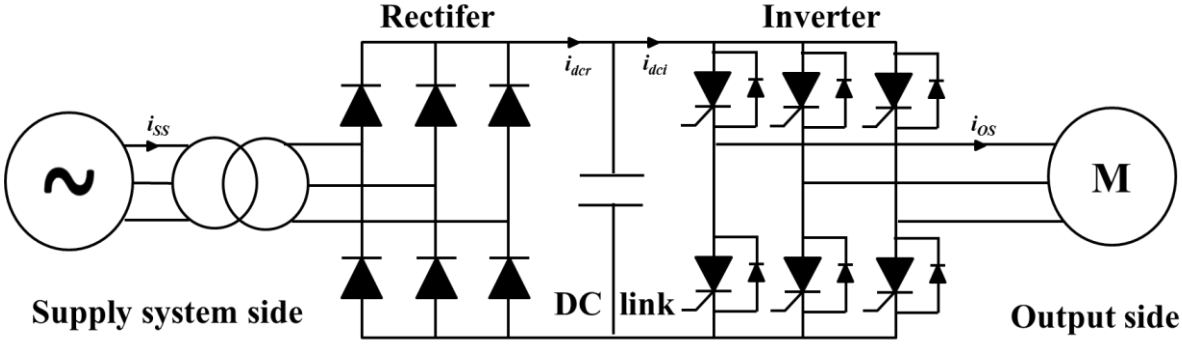

***Figure 3.5** – Scheme of an ASD with a double-stage converter*

The Eqs. (3.4)-(3.6) allow to calculate, in closed form, frequencies of the spectral components. In particular, according to equation (3.6), the interharmonic frequencies can be calculated once the fundamental frequency f_{ss} of the supply system and the fundamental frequency f^{os} of the inverter output voltage are known.

To estimate the fundamental frequency, $\hat{f}^{os}$, of the inverter output voltage, the results of the first step were used in the following procedure:

a) an estimation of the frequencies $\left(\hat{f}_{h,dc}^{os}\right)^{LPF_1}$ (the harmonics in the DC link) is obtained using the frequencies $\hat{f}_{f.s.}$ calculated in step 1 and by solving relationship (3.6), i.e., $\left(\hat{f}_{ih,ss}\right)^{LPF_1} = \left|\hat{f}_{ss} \pm \left(\hat{f}_{h,dc}^{os}\right)^{LPF_1}\right|$;

b) an estimation of the fundamental frequency, $\hat{f}_{os}$, of output voltage of the PWM inverter is obtained by equation (3.5) applied to LF waveform i.e., $\left(\hat{f}_{h,dc}^{os}\right)^{LPF_1} = \left|jm_f \pm r\right|\hat{f}^{os}$ with $\left(\hat{f}_{h,dc}^{os}\right)^{LPF_1}$ obtained in a).

The application of simple relationships to calculate the interharmonic frequencies from 100 Hz to f_{max} reduces the computational efforts required in the last step dramatically.

Table 3.3 - *Dependence of the values of* $\boldsymbol{j}$ *and* $\boldsymbol{r}$ *on* $\boldsymbol{m_f}$

	Odd m_f		**Even m_f**	
Not Triple	j	r	j	r
	Even integers → Odd integers →	Even integers Odd integers	Even integers → Odd integers →	Integers
Triple	j	r	j	r
	Even integers → Odd integers →	Even triple integers Odd triple integers	Even integers → Odd integers →	Triple integers

d) Fourth step

Once the interharmonic frequencies from 100 Hz to f_{max} are calculated, their values are imposed in the fourth step of the sliding-window Parametric-DFT-Analytical-Parametric methods. In this step the waveform $\hat{x}_2(n)$, obtained as the difference between $\hat{x}_1(n)$ and $\hat{x}_{harm}(n)$, is analysed by a simplified algorithm of a parametric method (once again either ESPRIT or Prony) in order to estimate *only* the corresponding amplitudes of the interharmonics.

Specifically, assuming the damping factors to be zero:

- if the SW ESPRIT parametric method is used, the imposed interharmonics' frequencies determine the diagonal elements $\hat{\lambda}_i$ of the rotation matrix **Φ**; then it is possible to obtain the interharmonics' amplitudes using only equation (1.49) (see Chapter 1);
- if the SW Prony parametric method is used, the imposed interharmonics' frequencies determine the polynomial roots z_k, and, then, it is possible to obtain the interharmonics' amplitudes with simple relationships solving only equation (1.36) (see Chapter 1).

Note that the computational effort in this fourth step of the sliding-window Parametric-DFT-Analytical-Parametric schemes is very low due to the reduced value of the number of exponentials *M* required in the model by the parametric methods. This is because *only* the interharmonic components from 100 Hz to f_{max} are included in the waveform to be analysed. At the same time, the computational burden also is reduced since the number of unknown parameters is reduced by 50%. This is because the frequencies were assigned as the output of

the third step, so both of the parametric methods just require the solution of one system of equations.

In addition, if the sampling rate f_s is elevated with respect to the maximum frequency to be analysed, guaranteeing the respect of the parametric methods bound ($f_{M.E.} \leq f_s/4$, with $f_{M.E.}$ the maximum frequency that can be detected by the parametric method [38]), a decimation of the data block can be applied to further reduce the computational efforts.

3.3.2 Numerical applications

Several numerical experiments were conducted analysing many operating conditions of the PWM ASD in order to test the performances and the benefits of the sliding-window Parametric-DFT-Analytical-Parametric methods. For the sake of brevity, only three cases are shown in this Section. Specifically, the results obtained from the analysis of two test signals and a measured AC supply current are shown.

The analysis of the first two case studies, i.e., synthetic ASD supply currents is described in greater detail. These synthetic ASD supply currents were obtained according to Eqs. (3.4)-(3.6) and by summing the harmonic and interharmonic components in the time domain, and their analytical expressions were obtained on the basis of our experience with actual ASDs.

In the third case study, a measured ASD supply current with a constant load is considered. This measured waveform was obtained on a hardware test system constituted by a synchronous, sinusoidal PWM ASD.

Figure 3.6 shows the test bench used for the AC current measurements, which was equipped as follows:

- Supply system 400 V, 50 Hz;
- Inductive input filter of 500 μH;
- LEM Hall effect transducers LA50-S, coupled with a data acquisition (DAQ) unit, that was a National Instruments 6071E PCI board;
- VSI controlled by a 40-MHz Texas Instruments DSP TMS320C30, programmed in C-language to have a traditional sub-oscillation PWM technique, where the carrier frequency was set to achieve an integer modulation ratio (specifically, $m_f = 21$ in the following applications);
- Four-pole pairs induction motor of 5.5 kW, connected mechanically to a DC motor operated by a controlled rectifier that regulates the resistance torque.

All of the case studies were analysed using the STFT method (STFTM) according to the IEC recommendations, the traditional ESPRIT method (TEM), the traditional Prony method (TPM), the Three Step Method (TSM) proposed in [1] and all combinations of the four-step proposed methods, i.e.,:

- Prony + DFT + Analytical frequencies + Prony (PDAPM);
- Prony + DFT + Analytical frequencies + ESPRIT (PDAEM);
- ESPRIT + DFT + Analytical frequencies + Prony (EDAPM);
- ESPRIT + DFT + Analytical frequencies + ESPRIT method (EDAEM).

The results obtained by the above methods were compared in terms of both accuracy and computational burden. All of the programs are implemented by MATLAB and are not optimized for computational speed, since the aim is only to give a rough and relative comparison of efficiency in different methods. MATLAB programs were developed and tested on a Windows PC with an Intel i7-3770 3.4 GHz and 16 GB of RAM.

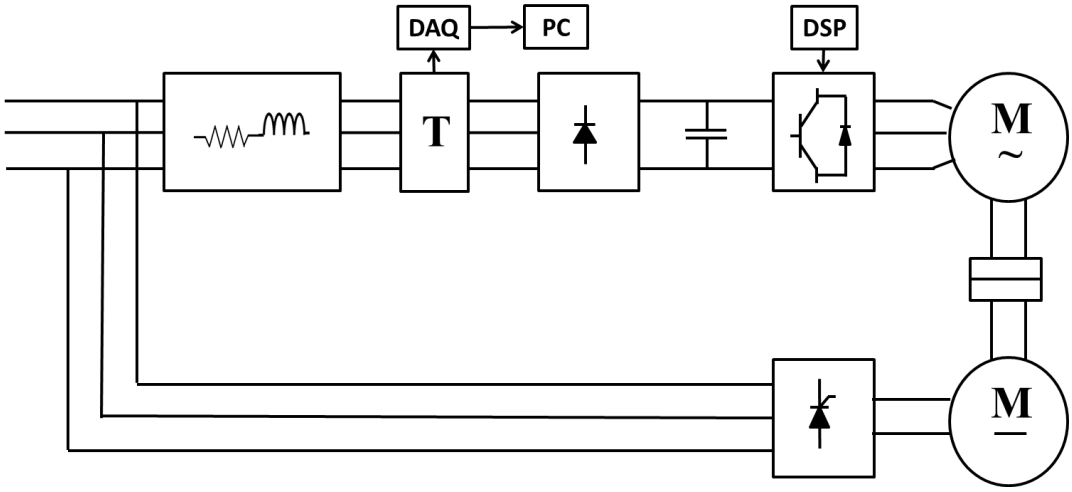

Figure 3.6 *– Test bench scheme*

a) Case study 1

The first synthetic waveform was a 3-s AC supply current of an ASD with a fundamental frequency of the output voltage equal to 32.32 Hz and a fundamental frequency of the supply-side current equal to 50.01 Hz.

A white noise with a standard deviation of 0.001 was added to the signal in order to make the analysis more realistic. The sampling rate was 20 kHz, so the bounds of the parametric methods were broadly satisfied, since the maximum frequency of the test signal was fixed at 1 kHz. For the parametric methods, the selected reconstruction error threshold was $0.5 \cdot 10^{-3}$.

Taking into account that m_f is an integer ($m_f = 21$), the fundamental frequency was 50.01 Hz, and $\hat{f}^{os}$ was not an integer multiple of 5 Hz, so it follows that the interharmonic frequencies obtained by using relationships (3.4) through (3.6) were not integer multiples of the IEC frequency resolution (5 Hz).

Figure 3.7 shows the spectrum of the values of the components of the test signal. Table 3.4 shows, for the considered methods, the average percentage errors for the amplitudes and frequencies of some of the significant spectral components. TSM and TPM generally had the best results for all of the spectral components. All of the sliding-window Parametric-DFT-Analytical-Parametric methods always had acceptable amplitude and frequency errors, so that all of them provided a reliable estimation of every spectral component; however, EDAEM and EDAPM were slightly more accurate than PDAPM and PDAEM. Also, it should be noted that the frequency errors of the sliding-window Parametric-DFT-Analytical-Parametric methods were comparable with the errors of the parametric methods applied to the entire waveform (TEM and TPM) and of TSM.

For the amplitudes, the sliding-window Parametric-DFT-Analytical-Parametric methods had errors that were slightly greater than those of TSM; for harmonics and 232-Hz interharmonic, this was due to use of the DFT in the second step of the proposed scheme (Fig. 3.4). In fact, the presence of the interharmonics in the band from 100 Hz to f_{max} in the analysed waveform $\hat{x}_1$ resulted in spectral leakage that also influenced waveform $\hat{x}_2$. In the case of the fundamental and interharmonics from 0 to 100 Hz, the difference in the amplitude errors between the sliding-window Parametric-DFT-Analytical-Parametric methods and TSM were

due to the different filtering schemes. It is also worth noting that TEM and TPM had different behaviors because TEM had a problem with evaluating the amplitude.

Table 3.4 *- Parametric-DFT-Analytical-Parametric methods - Case study 1: average percentage error in the estimation of amplitude and frequency of: (a) the fundamental, 5th , and 17th harmonics; (b) 32-Hz and 232-Hz interharmonics using STFTM, TEM, TPM, TSM, PDAPM, EDAEM, PDAEM and EDAPM*

	Average error [%]					
	Amplitude			Frequency		
	Fundamental	5th	17th	Fundamental	5th	17th
TEM	0.080	2.0	2.6	0.0010	0.010	0.0030
TPM	0.0040	0.090	0.18	$68\cdot10^{-6}$	$310\cdot10^{-6}$	$250\cdot10^{-6}$
TSM	0.0010	0.0020	0.0090	$30\cdot10^{-6}$	$30\cdot10^{-6}$	$30\cdot10^{-6}$
PDAPM	0.16	0.92	0.70	$720\cdot10^{-6}$	$720\cdot10^{-6}$	$720\cdot10^{-6}$
EDAEM	0.17	0.92	0.70	$27\cdot10^{-6}$	$27\cdot10^{-6}$	$27\cdot10^{-6}$
PDAEM	0.16	0.92	0.70	$720\cdot10^{-6}$	$720\cdot10^{-6}$	$720\cdot10^{-6}$
EDAPM	0.17	0.92	0.70	$27\cdot10^{-6}$	$27\cdot10^{-6}$	$27\cdot10^{-6}$
STFTM	0.70	0.92	0.79	0.020	0.020	0.020

(a)

	Average error [%]			
	Amplitude		Frequency	
	32-Hz interharmonic	232-Hz interharmonic	32-Hz interharmonic	232-Hz interharmonic
TEM	1.9	51	0.090	0.23
TPM	0.080	1.5	0.0030	0.0070
TSM	0.007	0.020	$850\cdot10^{-6}$	0.0030
PDAPM	0.63	1.0	0.020	0.0020
EDAEM	0.14	1.0	$710\cdot10^{-6}$	0.0030
PDAEM	0.63	1.0	0.020	0.0020
EDAPM	0.14	1.0	$710\cdot10^{-6}$	0.0030
STFTM	30	21	6.7	0.80

(b)

Finally, it should be noted that STFTM generally had higher errors. With particular reference to the amplitudes of the interharmonics, the average percentage error was more than 20%. This was consistent with the desynchronization between the spectral components of the test signal and window duration fixed by IEC. It is also interesting to note that PDAPM and PDAEM had the same percentage error in the estimation of same spectral components, and Table 3.4 shows same results for EDAPM and EDAEM. This is because i) spectral analysis depended mainly on the results of the first step and ii) there was a reduced number of variables (only interharmonic amplitudes) in the last step.

Table 3.5 shows the computational time for the waveform spectral analysis by all of the methods per unit of the STFTM computational time. It is important to note that, in this case, all of the sliding-window Parametric-DFT-Analytical-Parametric methods had a computational time significantly lower than TEM and TPM; moreover, the sliding-window Parametric-DFT-Analytical-Parametric methods were about the same order of magnitude as that of STFTM.

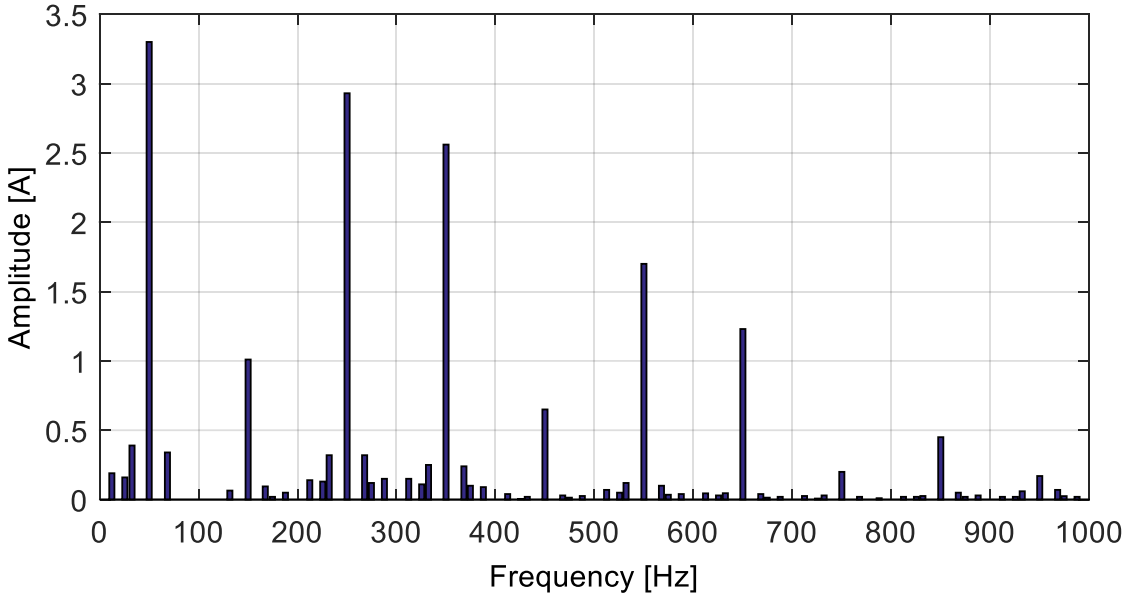

Figure 3.7 *– Case study 1: spectrum of the first test waveform*

Table 3.5 *- Parametric-DFT-Analytical-Parametric methods - Case study 1: computational time by all of the considered methods in p.u. of time required by STFTM*

	Computational time [p.u.]
TEM	$3.8 \cdot 10^4$
TPM	$3.0 \cdot 10^4$
TSM	6.3
PDAPM	4.4
EDAEM	4.1
PDAEM	4.9
EDAPM	3.6
STFTM	1

b) Case study 2

The test signal was a 3-s AC supply current of an ASD with a fundamental frequency of the output voltage equal to 19.99 Hz and a fundamental frequency of the supply-side current equal to 50.01 Hz. Also, in this case study, a white noise with a standard deviation of 0.001 was added. The sampling rate was 20 kHz. For the parametric methods, the selected reconstruction error threshold was $0.5 \cdot 10^{-3}$.

Table 3.6 shows the average percentage errors of amplitudes and frequencies as defined in the previous case study. Specifically, it is interesting to note the behavior of the spectral analysis methods in the estimation of the 10-Hz interharmonic, whose amplitude was about 11% of the fundamental; this interharmonic was near another interharmonic component (at 12 Hz) with halved amplitude.

Note that, for the selected 10-Hz interharmonic, TPM, PDAPM, and PDAEM had percentage errors in the estimation of its amplitude that were greater than that of STFTM, and they had percentage errors in the estimation of the frequency that were the same order of magnitude of that of STFTM.

These phenomena were due to (i) the value of the error threshold ($0.5 \cdot 10^{-3}$) assumed for the parametric methods and (ii) the fact that the Prony model, unlike ESPRIT, did not include noise. In such circumstances, since there were two very close interharmonics, Prony algorithm

identified the aforesaid two components with a single interharmonic having a frequency that was the mean of the actual frequencies and having an amplitude that was the sum of the two actual amplitudes.

Table 3.6 *- Parametric-DFT-Analytical-Parametric methods - Case study 2: average percentage error in the estimation of amplitude and frequency of the fundamental, 10-Hz interharmonic and the 13th harmonic using STFTM, TEM, TPM, TSM, PDAPM, EDAEM, PDAEM and EDAPM*

	Average error [%]					
	Amplitude			Frequency		
	Fundamental	10-Hz interharmonic	13th	Fundamental	10-Hz interharmonic	13th
TEM	0.030	16	0.17	$900 \cdot 10^{-6}$	2.2	$280 \cdot 10^{-6}$
TPM	0.070	32	0.24	0.0020	4.0	$220 \cdot 10^{-6}$
TSM	0.070	0.79	0.090	$55 \cdot 10^{-6}$	0.030	$55 \cdot 10^{-6}$
PDAPM	0.31	29	0.19	0.0050	3.9	0.0050
EDAEM	0.17	0.79	0.13	$46 \cdot 10^{-6}$	0.11	$46 \cdot 10^{-6}$
PDAEM	0.31	29	0.19	0.0050	3.9	0.0050
EDAPM	0.17	0.79	0.13	$46 \cdot 10^{-6}$	0.11	$46 \cdot 10^{-6}$
STFTM	0.14	22	0.22	0.020	5.3	0.020

To analyze the above-mentioned problem in more depth, Table 3.7 shows the PDAPM's errors obtained using a reconstruction error threshold of $0.5 \cdot 10^{-10}$. It is evident that there was a significant improvement in the estimation of the spectral components, especially for the 10-Hz interharmonic. Obviously, this increases in the resolution yielded an increase in the computational burden.

Table 3.7 *- Parametric-DFT-Analytical-Parametric methods - Case study 2: average percentage error in the estimation of amplitude and frequency of the fundamental, 10-Hz interharmonic and the 13th harmonic using PDAPM and setting a reconstruction error threshold equal to $0.5 \cdot 10^{-10}$*

	Average error [%]					
	Amplitude			Frequency		
	Fundamental	10-Hz interharmonic	13th	Fundamental	10-Hz interharmonic	13th
PDAPM	0.17	0.54	0.13	$50 \cdot 10^{-6}$	0.050	$50 \cdot 10^{-6}$

Table 3.8 shows the computational time for the waveform spectral analysis by all of the methods (with threshold for all of the parametric methods equal to $0.5 \cdot 10^{-3}$). Also for this case study, all of the sliding-window Parametric-DFT-Analytical-Parametric methods had computational times that were significantly less than those of TEM and TPM, and the time was about the half of that required by TSM.

Table 3.8 *- Parametric-DFT-Analytical-Parametric methods - Case study 2: computational time by all of the considered methods in p.u. of time required by STFTM*

	Computational time [p.u.]
TEM	$1.3 \cdot 10^{4}$
TPM	$4.9 \cdot 10^{4}$
TSM	5.5
PDAPM	3.4
EDAEM	3.7
PDAEM	3.5
EDAPM	3.5
STFTM	1

Moreover, the sliding-window Parametric-DFT-Analytical-Parametric methods seem to have the same order of magnitude than STFTM. It should be noted that, when the error threshold was equal to $0.5 \cdot 10^{-10}$ (Table 3.7), the computational effort required by PDAPM was about four times greater it was when the error threshold was equal to $0.5 \cdot 10^{-3}$. The same also was true for PDAEM.

c) Case study 3

In this case study, we analysed a 5-s AC supply-side current, measured by the test bench shown in Figure 3.6. For this waveform, the fundamental frequency of the output voltage and the fundamental frequency of the supply side current were about 30 and 50 Hz, respectively. Thus, taking into account that m_f is an integer ($m_f = 21$), $\hat{f}^{os}$ is approximately an integer multiple of 5 Hz, the fundamental frequency, $\hat{f}_{ss}$, is approximately equal to 50 Hz, and the harmonic/interharmonic frequencies, coherently with the relationships (3.4) through (3.6) (Section 3.3.1.c), were all approximately integer multiples of the IEC frequency resolution (5 Hz). Then, STFTM should be able to provide a reliable estimation of all the spectral components, since the spectral leakage should be weak. For the parametric methods, the selected reconstruction error threshold was, once again, $0.5 \cdot 10^{-3}$.

Figure 3.8 shows the time evolution of the first 0.2 s of the considered waveform, and Figure 3.9 shows the spectrum from 0 to 1 kHz obtained by STFTM.

Note that, in the case of actual measured waveforms, TEM and TPM had many spurious components due to the high noise introduced by the measurement instruments; as shown below, they also required very high computational efforts. For TSM and the sliding-window Parametric-DFT-Analytical-Parametric methods, the aforesaid phenomenon was limited since the presence of the two low-pass band filters reduced the influence of noise.

The same predominant spectral components were observed in the spectra provided by all of the methods, with only significant difference being their amplitudes; this is coherent with the results of the two previous case studies in which the percentage errors in the estimations of frequencies were always less than the percentage errors in the amplitudes.

As an example of the results that were obtained, Table 3.9 shows the average values of the amplitudes for some significant spectral components estimated by all of the methods. In particular, note that, for the fundamental component, all of the methods that were used, detected an average amplitude of approximately 3.10 A, and the sliding-window Parametric-DFT-Analytical-Parametric methods had lower values than those of TPM and TEM, but they were very close to that of STFTM.

Also for the average values of the estimated 5^{th} harmonic amplitudes, it can be observed that the sliding-window Parametric-DFT-Analytical-Parametric methods, once again, approached the STFTM values closely, while they had values that were slightly lower than those of TPM and TEM. Finally, for the 70-Hz interharmonic, all of the amplitude values are in a range around 0.40 A. It should be also noted that TSM provided average amplitudes for all the spectral components very close to the values estimated by STFTM.

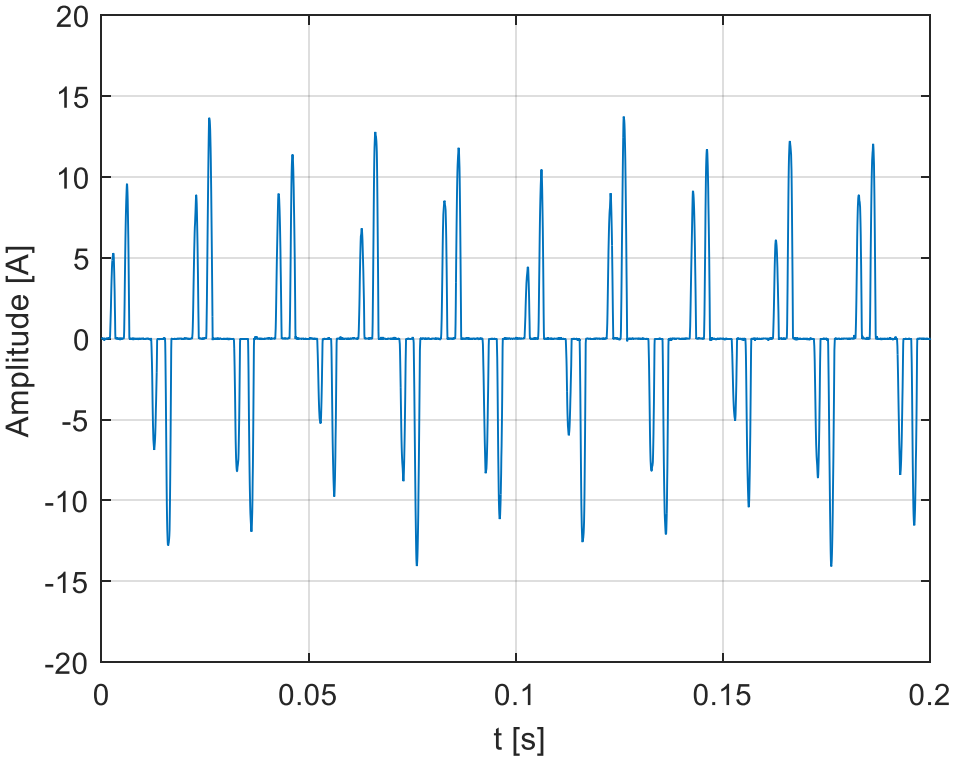

***Figure 3.8** – Parametric-DFT-Analytical-Parametric methods - Case study 3: time evolution of the analyzed waveform*

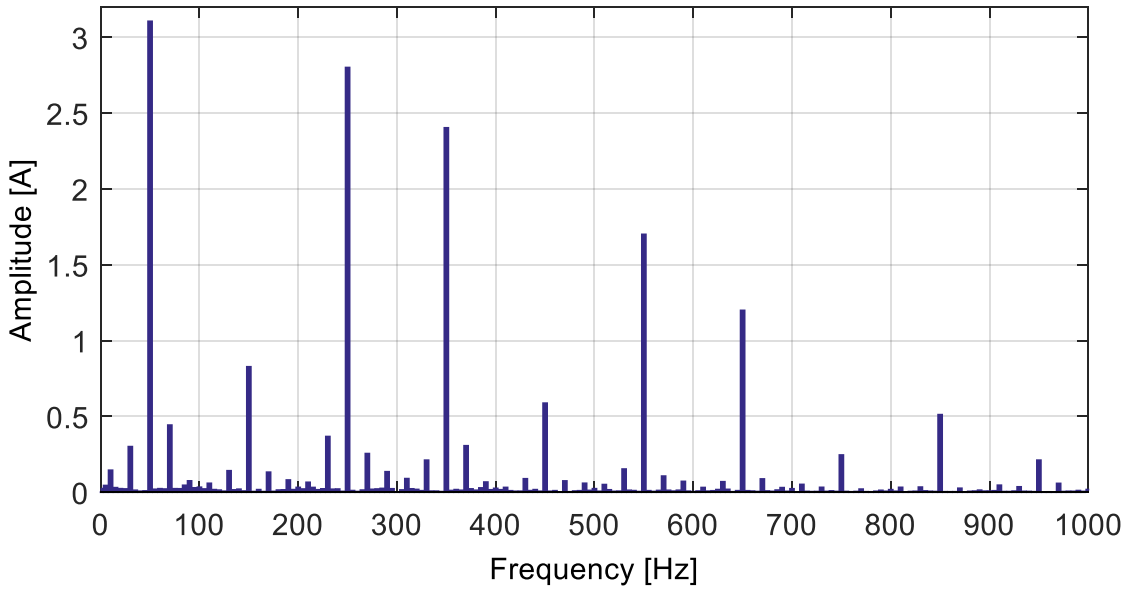

***Figure 3.9** – Parametric-DFT-Analytical-Parametric methods - Case study 3: spectrum obtained by the STFTM*

Table 3.10 shows the computational time for the spectral analysis by all of the methods per unit of the STFTM's computational time. Again, the sliding-window Parametric-DFT-Analytical-Parametric methods had significantly less computational times than TEM and TPM, and, at the same time, the computational effort of the sliding-window Parametric-DFT-Analytical-Parametric methods was about half of that required by TSM. Note that the fastest method for the analysis of this measured waveform was STFTM; however, the sliding-window Parametric-DFT-Analytical-Parametric methods required globally computational

times that had at the most one order of magnitude more than STFTM, with EDAPM having the best computational time among the sliding-window Parametric-DFT-Analytical-Parametric methods.

***Table 3.9** - Parametric-DFT-Analytical-Parametric methods - Case study 3: comparisons of most significant average amplitudes (fundamental, 5th harmonic and 70-Hz interharmonic) using STFTM, TEM, TPM, TSM, PDAPM, EDAEM, PDAEM and EDAPM*

	Average amplitude [A]		
	Fundamental	70-Hz interharmonic	5th
TEM	3.11	0.39	2.80
TPM	3.12	0.40	2.80
TSM	3.08	0.40	2.77
PDAPM	3.06	0.41	2.77
EDAEM	3.07	0.39	2.77
PDAEM	3.06	0.41	2.77
EDAPM	3.07	0.39	2.77
STFTM	3.06	0.41	2.77

***Table 3.10** - Parametric-DFT-Analytical-Parametric methods - Case study 3: computational time by all of the considered methods in p.u. of time required by STFTM*

	Computational time [p.u.]
TEM	$2.9 \cdot 10^5$
TPM	$1.4 \cdot 10^5$
TSM	22
PDAPM	11
EDAEM	9.5
PDAEM	11
EDAPM	8.9
STFTM	1

3.4 Sliding-window Wavelet-Modified ESPRIT method

The problem of the spectral analysis of wide-spectrum waveform is analysed in detail in this Section. In fact, the growing use of devices equipped with static converters determines the injection in the grid of distorted currents with spectral components included in a wide frequency range (up to 150 kHz) [26,39-41]. In order to better underline how the problem of the waveform distortions that involve a wide frequency range is deeply rooted in modern electrical power systems, a detailed list of common supraharmonic emitters is provided in [42]. These are: (i) converters for industrial applications that mainly emit spectral components in the range from 9 kHz to 150 kHz; (ii) oscillation related to the electronic device commutation that mainly emit spectral components up to 10 kHz; (iii) street lamps that mainly emit spectral components up to 20 kHz; (iv) electro-vehicle chargers that mainly emit spectral components in the range from 15 kHz to 100 kHz; (v) photovoltaic and wind turbine inverters that mainly emit spectral components in the range from 4 kHz to 20 kHz; (vi) household devices, e.g., liquid-crystal display televisions or highly-efficient loads, that mainly emit spectral components in the range from 2 kHz to 150 kHz; (vii) PLC that mainly emit spectral components in the range from 9 kHz to 95 kHz.

Since these supraharmonic emitters are very common, the spectral components from 2 kHz to 150 kHz have recently received great interest in the relevant literature [13-14,40-48]. Many research activities have recently focused on the effects of the high-frequency sources on the power systems and their propagation [13-15]. According to these studies, the main difference between the high-frequency emissions and low-frequency emissions is that, while the latter tend to propagate towards the distribution network, the former mainly flow within the installation, towards the other devices that offer a lower impedance than the network at so high frequencies (such as the electromagnetic compatibility (EMC) filter). The presence of EMC filter as interface at the PCC, also provides a low impedance for these high-frequency components coming from the distribution network. Therefore, high-frequency currents from both the installation and the network flow through the capacitor, causing high-frequency voltage distortion at the PCC [15].

Moreover, low-frequency spectral components and high-frequency spectral components are commonly characterized by different behaviours in the frequency and time domain. Specifically, while low-frequency components can be stationary and generally typified by piecewise constant frequencies in time (see also Chapter 2), high-frequency are usually not stationary, with significant time-variability both in frequency and in amplitude. However, these high-frequency spectral components are superimposed to low-frequency spectral components with consequent conflicting needs in term of time window length (and frequency resolution) for their spectral analysis.

These high-frequency disturbances still require not only appropriate analysis tools, but also adequate standardizations, which allow to define proper indices and their maximum thresholds for the evaluation and the limitation of the high-frequency spectral components.

In fact, the IEC standards address the range from 0 kHz to 9 kHz, recommending for signal processing, as previously stated, the use of the STFT with rectangular time windows characterized by a duration fixed as an integer multiple of the fundamental period [24,26]. The problem related to the STFT and to STFT-based methods, i.e. the inaccuracies associated with the inherent fixed frequency resolution and spectral leakage problems, has been proved to became more significant in case of waveforms characterized by wide spectra. This is due to the aforementioned different behaviours of low- and high-frequency spectral components and to the increasing desynchronization of high-frequency components. As attempt to reduce STFT inaccuracies, IEC suggests the use of grouping not only for the low frequency range, but also for the spectral content from 2 kHz to 9 kHz, assuming high-frequency resolution to be unnecessary for this range, in opposition to the modern requirements [18,37]. Recently, in [37], some measurement methods have been also indicated to provide an overview of spectral content in the range from 2 kHz to 150 kHz, as opposed to detailed measurement methods used for low-frequency range. These measurement methods for the high-frequency spectral components are informative and not normative; they include the extension of the grouping from 9 kHz to 150 kHz using a 10 Hz frequency resolution and 200 Hz bands to group this spectral content [37] and, then, they do not allow to obtain acceptable estimations of amplitudes and frequencies of supraharmonic spectral components.

The others measurement methods suggested by IEC standard [37] for the evaluation of the high-frequency spectral content cannot be always applicable. In fact, these measurement methods suffer of complex and expensive implementation; also, they provide an enormous

amount of data to be stored as output. Hence, the IEC standard advises about the possible inclusion of other methods in future editions of the standard.

As seen in Chapter 1, with reference to the low-frequency range, to solve the problems associated with the IEC standard method, many spectral analysis methods have been presented in the relevant literature for the assessment of time varying waveform distortions [23-24,26,37-38,40]. With reference to the high-frequency range, in the relevant literature, only few methods were applied to the spectral analysis of waveforms with wide spectra [38,40]. In particular, the method proposed in [40] was not applied for the simultaneous spectral analysis of the entire range from 0 to 150 kHz. It requires a high computational effort and a priori knowledge of the number of spectral components included in the analysed waveform, as well as the order of the correlation matrix. These two problems were overcome by the method proposed in [38], although it was not proper for the detection of high-frequency time varying spectral component, when large-spectrum waveforms are analysed (see also Chapter 2).

The sliding window Wavelet-Modified ESPRIT method (SWWMEM) proposed in [12] is specifically addressed to analyse electrical waveforms with spectral content up to 150 kHz. In this Section, the SWWMEM is analysed in detail. The method provides accurate estimation of spectral component parameters, while maintaining acceptable computational efforts. Moreover, it is particularly suitable when an accurate contemporary knowledge of low- and high-frequency spectral components and of their time behaviour is required, so SWWMEM is useful for:

a. the evaluation of supraharmonic emission;
b. the definition of adequate power quality indices to introduce standard methods and limits;
c. the study of supraharmonic propagation and impact in power systems;
d. the definition of new models which can emulate supraharmonic injection;
e. the use of proper adaptive active filters to reduce the emission of supraharmonics.

The SWWMEM applies a DWT and a sliding-window modified ESPRIT method (MEM) [38] (see also Chapter 2) in two successive steps. The DWT divides the original signal into low-frequency and high-frequency waveforms. The MEM separately analyzes the two pass bands for a separate estimation of the low-frequency and high-frequency spectral components.

The application of the SWWMEM has the following advantages:

f. it allows a detailed estimation in time of each high-frequency spectral component;
g. it has ability to provide the optimal time and frequency resolutions in each band to obtain an accurate time-frequency representation using the strategy of divide and conquer.

The following Sub-sections first describe the proposed scheme in detail; then, several case studies are analysed with reference to synthetic and actual waveforms.

3.4.1 Model formulation and solving procedure

As stated in the Section 3.4, a waveform in a power system can be characterized by both high-frequency and low-frequency (up to 2 kHz) spectral components involving conflicting needs in term of time window length and frequency resolution for their spectral analysis.

The high-frequency spectrum is generally characterized by spectral components centred around frequencies not directly linked to the power system frequency and that are commonly

defined as “asynchronous” components. The low frequency spectral components are mainly constituted by discrete components at frequencies that are linked to the power system frequency [14-15]. Moreover, as previously evidenced high-frequency and low-frequency spectral components present different time behaviours, being high-frequency components often not stationary with fast dynamics, and consequently with frequencies and amplitudes that can rapidly vary vs. time. Finally, in the absence of resonance effects, the energy content of high-frequency components usually is very small if compared with the characteristic low-frequency spectral components.

Eventually, the spectral analysis of waveforms including both low-frequency and high-frequency spectral components requires an approach different from the traditional approach for the low-frequency components only.

Motivated by above, the main features of the SWWMEM are (i) to isolate the different frequency bands of interest and (ii) to separately analyse each band, taking into account the different behaviour and needs of low-frequency and high-frequency components (Figure 3.10). The SWWMEM involves a two-step procedure as shown in Figure 3.10. In particular, the selected values f_{bs} and f_{max} are the bands’ separation frequency and the maximum frequency of interest, respectively. In the first step, the number of decomposition levels is calculated, the waveform is adequately resampled and then filtered by the decomposition of a DWT, which produces a low-frequency band and a high-frequency band of the original waveform. Then, in the second step, the two parts of the waveform are resampled and analyzed separately by the SW MEM.

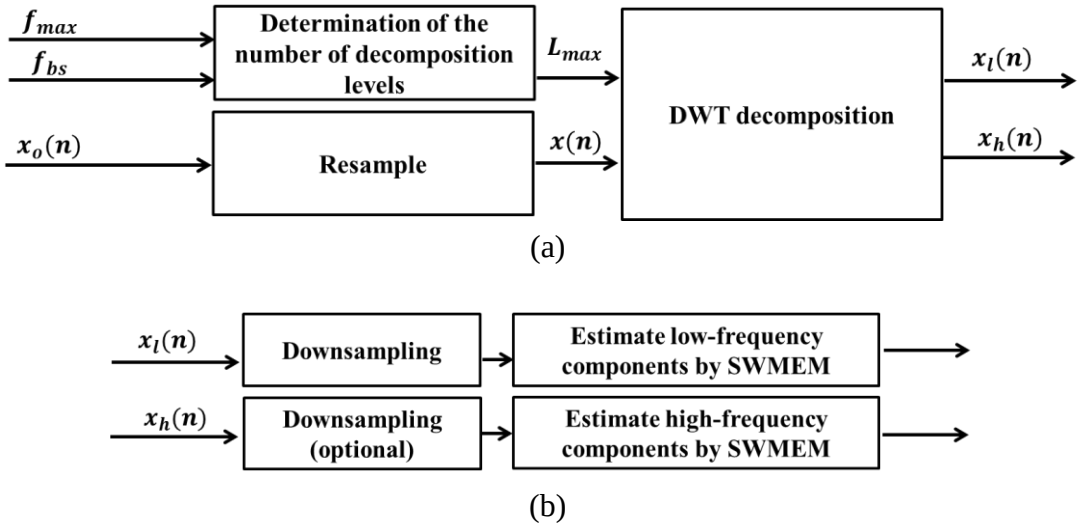

***Figure 3.10** – Scheme of the sliding-window Wavelet-Modified ESPRIT method: (a) first and (b) second step*

In the first step, the advantage of wavelet suitability for studying signals in different frequency bands with different frequency resolution are exploited [26]. Moreover, the DWT, differently to a common low/band-pass filter, performs a waveform decomposition that guarantees no phase-shifting and no signal leakage among the decomposed bands of frequency. This allows that, if all of the reconstructed signals of the different bands of frequency are added up, the original waveform is again obtained. In the second step, the ESPRIT method is used since it is one of the most accurate parametric methods; in particular: (i) ESPRIT method performs better than Prony’s method when the waveform to be analysed

is corrupted by noise; (ii) DWT can be couplet better with ESPRIT method than with other parametric methods; in fact, if f_s is the waveform sampling rate, ESPRIT method, as well as DWT, is able to detect spectral components up to $f_s/2$. In the following subsections, the main features of each of these steps are described in detail.

a) First step

The first step of the proposed hybrid method is based on the application of a DWT obtained by using a sampled mother wavelet with discrete scale and translation parameters, applied to a sampled waveform [24].

Specifically, as shown in Chapter 1 and recalled in this Section for sake of clarity, given a sequence of samples $x(n)$ with $n = 0,1, \dots, L-1$ and the chosen continuous mother wavelet $\psi\left(\frac{t-b}{a}\right)$ with a and b continuous scale and translation parameters respectively, selecting $a = a_0^j$ and $b = ka_0^j b_0$, the sampled discrete mother wavelet $\psi_{j,k}(n)$ is:

$$\psi_{j,k}(n) = \frac{1}{\sqrt{a_0^j}} \psi\left(\frac{n - kb_0 a_0^j}{a_0^j}\right) \forall\, n = 0,1, \dots, L-1, \tag{3.7}$$

where k and j are integers and the values $a_0 > 1$, $b_0 > 0$ are fixed [24]. Hence, the DWT of $x(n)$ is provided by:

$$DWT(j,k) = \frac{1}{\sqrt{a_0^j}} \sum_{n=0}^{L-1} x(n) \check{\psi}\left(\frac{n - kb_0 a_0^j}{a_0^j}\right), \tag{3.8}$$

where the symbol ˇ indicates the complex conjugate [24].

It is well known that the DWT achieves the decomposition of the waveforms on different levels. Two parts are obtained for each level and they represent the approximation a_j and the detail d_j of the waveform in progressively-halved bands of frequency. In particular, by defining the scaling function $\varphi\left(\frac{t-b}{a}\right)$ as the aggregation of wavelets with scale factor $a > 1$, and discretizing it as seen for the mother wavelet, at each level j, the approximation a_j and the detail d_j of the original waveform can be evaluated by the inverse DWT of the approximate $A_j(k)$ and detailed $D_j(k)$ coefficients, computed as follows:

$$D_j(k) = \frac{1}{\sqrt{a_0^j}} \sum_{n=0}^{L-1} x(n) \check{\psi}\left(\frac{n-k}{a_0^j}\right). \tag{3.9}$$

$$A_j(k) = \frac{1}{\sqrt{a_0^j}} \sum_{n=0}^{L-1} x(n) \check{\varphi}\left(\frac{n-k}{a_0^j}\right). \tag{3.10}$$

where k is related to the translation in time and j is related to the selected frequency band [24]. Figure 3.11 shows a representation of the DWT decomposition for a waveform sampled at $2f_{\max}$ Hz, where $f_{\max}$ is the maximum frequency of interest (i.e., 150 kHz).

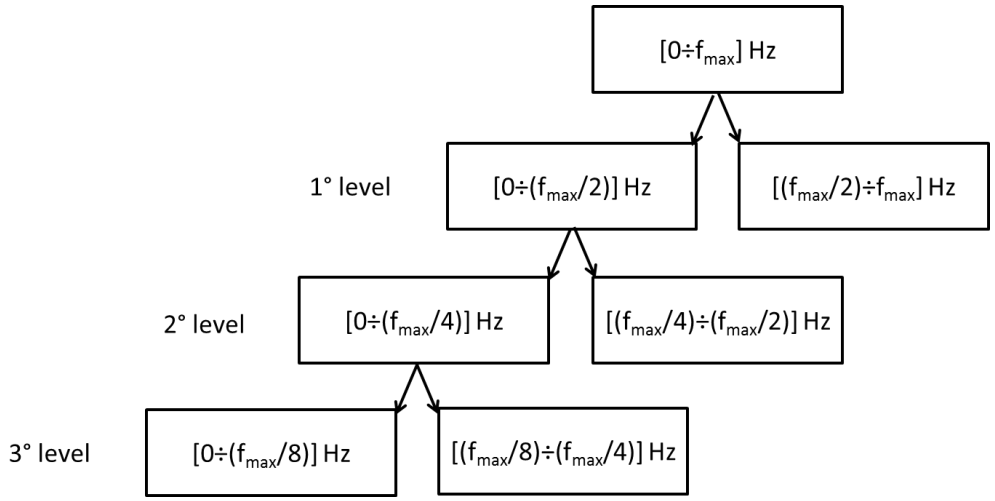

***Figure 3.11** – DWT decomposition scheme*

The DWT decomposition is often used as a filter bank, since it appears a sort of high and low pass band filters in cascade, with two bands of frequency obtained at each level. However, the bands are affected by overlap and attenuation at their edges. In the SWWMEM, by using a Meyer mother wavelet, multi-level DWT decomposition is achieved by assuming, as the number L_{max} of decomposition levels, a value that depends on f_{max} and on the bands' separation frequency f_{bs} (i.e., 2 kHz), i.e., $L_{max} = \left\lceil \log_2 \left(\frac{f_{max}}{f_{bs}} \right) \right\rceil$, where the symbol $\lceil \cdot \rceil$ indicates the rounding up operation.

Note that as shown in Figure 3.10, the original waveform $x_o(n)$ to be analyzed can be pre-processed to adapt the sampling frequency to the maximum frequency of interest f_{max}, obtaining the DWT input waveform $x(n)$. This pre-processing consists in an upsampling of $x_o(n)$, in order to avoid filter bounds to be too close to the frequencies that must be detected.

Once the DWT decomposition is known, two different waveforms, $x_l(n)$ and $x_h(n)$, are obtained. They are the waveform $x_l(n)$ ("low-frequency waveform"), which includes only the approximation $a_{L_{max}-1}$ at the level $L_{max} - 1$ (Figure 3.11) and the waveform $x_h(n)$ ("high-frequency waveform"), which includes the sum of all of the details d_j (Figure 3.11). The level $L_{max} - 1$ instead of L_{max} was chosen to avoid the attenuation effects of the overlap introduced by the canonical DWT in the ranges of frequencies of interest.

Both the low-frequency waveform $x_l(n)$ and the high-frequency waveform $x_h(n)$ are separately analyzed in the second step of the SWWMEM (Figure 3.10).

b) Second step

The second step of the proposed hybrid method is based on the application of the SW MEM described in Chapter 2 [38]. This method is applied for the assessment of the low-frequency and high-frequency components included in $x_l(n)$ and $x_h(n)$, respectively.

Specifically, denoting with $x_i(n)$, of generic size L_i, either the sequence of the L_l-sized sampled data $x_l(n)$ or the sequence of the L_h-sized sampled data $x_h(n)$ (Figure 3.10), the ESPRIT model, shown in Chapter 1, is used to approximate the waveform samples with a linear combination of M_i complex exponentials added to a white noise $r(n)$ [24]:

$$\hat{x}_i(n) = \sum_{k=1}^{M_i} A_k e^{j\phi_k} e^{(\alpha_k + j2\pi f_k)nT_s} + r(n), n = 0,1,\dots,L_i - 1, \quad (3.11)$$

where T_{si} is the sampling period and A_k, ϕ_k, f_k, and α_k are the amplitude, initial phase, frequency and damping factor of the k-th complex exponential, respectively. These are the unknown parameters to be estimated by using the transformation properties of the rotation matrix associated with the waveform samples. However, as demonstrated in Chapter 2, it was shown that a reduction of the unknown parameters in the model (3.11) is possible, considering that the damping factors and the frequencies of spectral components in power system applications generally vary slightly vs. time, especially at low-frequencies [38]. This is the basic principle of the SW MEM, where the estimation of frequencies and damping factors is realized only a reduced number of times along the whole waveform to be analyzed, with a great improvement in terms of computational effort [38]. In particular, the frequencies of the spectral components are initially evaluated in the first sliding window (also called "basis window"). Then the obtained values are assumed to be known quantities in the successive sliding windows (also called "no-basis windows"). The same handling is also performed for the damping factors.

Note that a check is conducted in each no-basis window to evaluate if the frequencies and damping factors obtained in the basis window can be still considered valid. In particular, the reconstruction error of the waveform can be checked; if the reconstruction error is greater than a fixed threshold, a new basis window is generated, the frequencies and the damping factors are updated and these new values are imposed in the following no-basis windows [38]. This check makes the SW MEM also suitable for the high-frequency components assessment, since they might significantly vary vs. time as previously mentioned.

The accuracy of the results and the computational effort of the SW MEM, both for the low-frequency waveform and high-frequency waveform, are influenced significantly by the number of exponentials, M_i, by the selected order L_{1_i} of the correlation matrix and by the sampling frequency f_{s_i} [37].

c) Further details on the presented method performances

It is worthwhile to outline the following considerations:

(1) Thanks to the DWT decomposition in the first step, both $x_l(n)$ and $x_h(n)$ include a reduced number of spectral components than the original sequence $x(n)$, so the analyses of these waveforms require smaller values of M_i than the analysis of the original sequence $x(n)$.

(2) Since $x_h(n)$ include only high-frequency components, the duration of the analysis window for this waveform can be chosen shorter than that for the spectral analysis of $x_l(n)$, consequently reducing the value of L_{1_i}.

(3) Since the maximum frequency that the ESPRIT method and therefore the SW MEM is able to detect is half of the sampling frequency f_{s_i} [37], the low frequency waveform $x_l(n)$ can be downsampled to only $2f_{bs}$ (two times the bands' separation frequency), reducing the number of samples in each window and, once again, the global computational burden.

Note also that to prevent the problem associated with the attenuation introduced by the DWT decomposition, only the spectral components over f_{bs} (i.e., 2 kHz) were stored when analyzing $x_h(n)$, whereas the spectral components up to f_{bs} were stored when analyzing $x_l(n)$.
Finally, it is important to observe that since the duration of window for the spectral analysis of $x_h(n)$ is shorter than that for the spectral analysis of $x_l(n)$, the SWWMEM could provide a number of high-frequency spectra greater than the number of spectra of the low-frequency waveform. This result is in accordance with the need for having a higher time resolution for the detection of the high-frequency components, since these components generally vary vs. time more than the low-frequency components. So, also the SW MEM limits, observed in Chapter 2, in the detection of time-varying supraharmonics are overcome in SWWMEM by analyzing separately the low-frequency and the high-frequency waveform.

3.4.2 Numerical applications

Several numerical analysis of synthetic and measured waveforms in different operating conditions of typical generation systems and loads were performed. For sake of conciseness, only three case studies are shown in this Section. Specifically, the first two case studies analyse synthetic waveforms while the third case study is an actual waveform measured at the PCC of fluorescent lamps installation. In particular, the second synthetic waveform is the same analysed in the case study 5 of Section 2.2.2 in Chapter 2.
In order to test the effectiveness of the proposed hybrid method (SWWMEM) in terms of both computational burden and accuracy, the same waveforms were analyzed also through the STFT method (STFTM), selecting a 5 Hz frequency resolution, and through the traditional sliding-window ESPRIT method (TEM) [24].
Moreover, also the spectrogram presented in [44] is included for all of the considered case studies, in order to underline the different approach of SWWMEM in respect to the currently available high-frequency signal processing technique.
All of the waveform analysis were performed in MATLAB environment. The MATLAB programs were developed and tested on a Windows PC with an Intel i7-3770 3.4 GHz and 16 GB of RAM.

a) Case study 1

A synthetic 3 s waveform that emulates a current at the PCC of a PV system equipped with a full-bridge, unipolar inverter, is analyzed (Figure 3.12). Specifically, the waveform was assembled assuming a fundamental current of 40 A at 50.02 Hz and a frequency modulation index m_f of the inverter PWM technique equal to 200; then, all odd harmonics up to the 27th order (low-frequency components) and a white noise with a standard deviation of 0.001 were added.

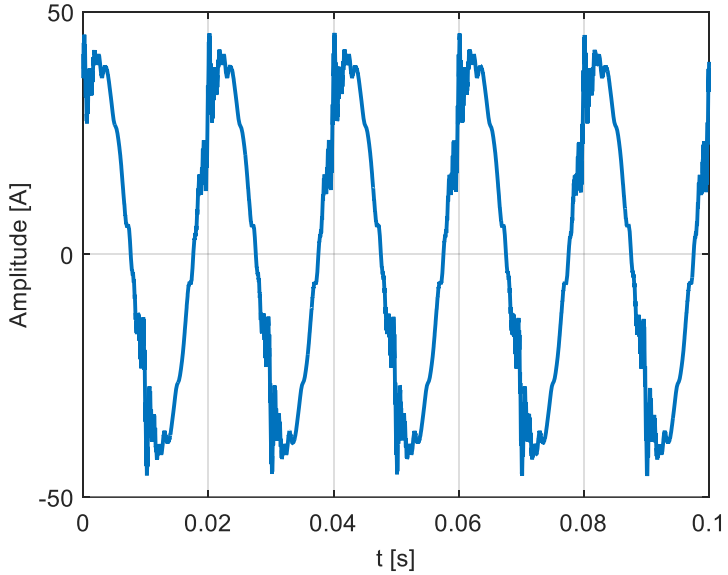

***Figure 3.12** – SWWMEM - Case study 1: synthetic current waveform*

The sampling frequency of the waveform was 50 kHz, in order to provide the most appropriate operating conditions for the parametric methods; this choice allowed the detection of the spectral components around the order $2m_f$, that are the most significant introduced by the inverter PWM and whose amplitudes were fixed up to 2% of the fundamental, in order to emulate the behaviour of the PV system during high-irradiance conditions [49].

A resampling to 100 kHz was required in the first step of the SWWMEM, in order to guarantee an uncorrupted estimation of the spectral components of our interest. Moreover, fixing the bands' separation frequency f_{bs} equal to 2 kHz, the number L_{max} of decomposition levels was 5.

For the TEM, the error threshold was fixed equal to 10^{-5}, and the window of analysis moves by 0.04 s without overlap. The same setting was chosen also for the spectral analysis of the low-frequency waveform (downsampled to 5 kHz) through the SWWMEM. For the analysis of the high-frequency range waveform, instead, the error threshold was fixed equal to 10^{-4}, and the window of analysis moves by 0.018 s without overlap.

Table 3.11 shows the average percentage errors of the frequencies (Table 3.11.a) and of the amplitudes (Table 3.11.b) for five selected spectral components. These spectral components are the fundamental, the 3rd and the 11th harmonic (low-frequency components) and two components ($2m_f + 1$ and $2m_f + 5$) linked to the inverter switching frequency (high-frequency components). The SWWMEM seems to outperform the STFTM, since it provides average percentage errors that are globally very similar to those obtained by the TEM, both for amplitude and frequency estimation.

In particular, for the low-frequency spectral components, the errors of SWWMEM are slightly lower than that of TEM, while SWWMEM provides average percentage errors on frequency and amplitude that are two and three orders of magnitude lower than those obtained through the STFTM.

Table 3.11 *- SWWMEM - Case study 1: (a) average percentage errors of frequency; (b) average percentage errors of amplitude.*

	Average Errors of Frequency [%]				
	Fundamental	3rd harmonic	11th harmonic	$2m_f + 1$	$2m_f + 5$
TEM	$28 \cdot 10^{-6}$	$660 \cdot 10^{-6}$	$41 \cdot 10^{-6}$	$3.4 \cdot 10^{-6}$	$19 \cdot 10^{-6}$
SWWMEM	$8.7 \cdot 10^{-6}$	$260 \cdot 10^{-6}$	$37 \cdot 10^{-6}$	$0.14 \cdot 10^{-6}$	$17 \cdot 10^{-6}$
STFTM	0.040	0.040	0.040	0.040	0.040

(a)

	Average Errors of Amplitude [%]				
	Fundamental	3rd harmonic	11th harmonic	$2m_f + 1$	$2m_f + 5$
TEM	$140 \cdot 10^{-6}$	0.017	0.0031	0.011	0.092
SWWMEM	$460 \cdot 10^{-6}$	0.0029	0.0011	0.010	0.023
STFTM	0.060	0.70	0.25	82	88

(b)

For the high-frequency components, the average percentage errors on the amplitudes obtained by SWWMEM show a significantly improved accuracy compared to the errors obtained through STFTM; in fact, STFTM errors are greater than 82% and are affected by spectral leakage problems that increase as the frequency increases. Also in this range of frequencies, the SWWMEM provides errors very close to the TEM errors, and they do not exceed 0.09% in amplitude and $2.5 \cdot 10^{-5}$% in frequency. Similar mean errors were observed for all the spectral components of the whole waveform using both the SWWMEM and the TEM. However, SWWMEM generally seemed to produce slightly lower amplitude mean errors than TEM.

Note that also the grouping, recommended by the IEC, both for the low-frequency components (using a 200 ms analysis window) and for the high-frequency components (using a 100 ms analysis window) was evaluated. This post-processing provides, for the low-frequency components, percentage errors on the amplitude practically coincident with the values obtained for the STFTM in Table 3.11. Conversely, for the high-frequency components, the grouping provides an aggregation of spectral components centered around fixed frequencies equal to 19.9 kHz and 20.1 kHz, as shown in Figure 3.13. It is clear that at high-frequency, this aggregation allows only to detect approximately the allocation of the energetic content around the fixed frequencies.

In Figure 3.14 the spectrogram with 1 kHz frequency resolution and 1ms time resolution is shown for the considered waveform, in order to underline the different approach of the spectrogram to the spectral analysis of wide-spectra waveforms in respect to SWWMEM.

As shown in Figure 3.14, the spectrogram was able to detect the spectral content both at low- and high-frequency with reduced computational effort, even if a great spread of color intensity around the real spectral components can be observed, cause of the spectral leakage and of the too large frequency resolution. In particular, the high-frequency spectral components related to the switching frequency appear concentrated around 20 kHz, but, unlike SWWMEM, it is impossible to individuate both the correct number of spectral components included in that range and each specific frequency and/or amplitude. Moreover, also a fake periodical variability in time seems to be introduced by this spectral analysis method. Similar behavior can be observed at low-frequency.

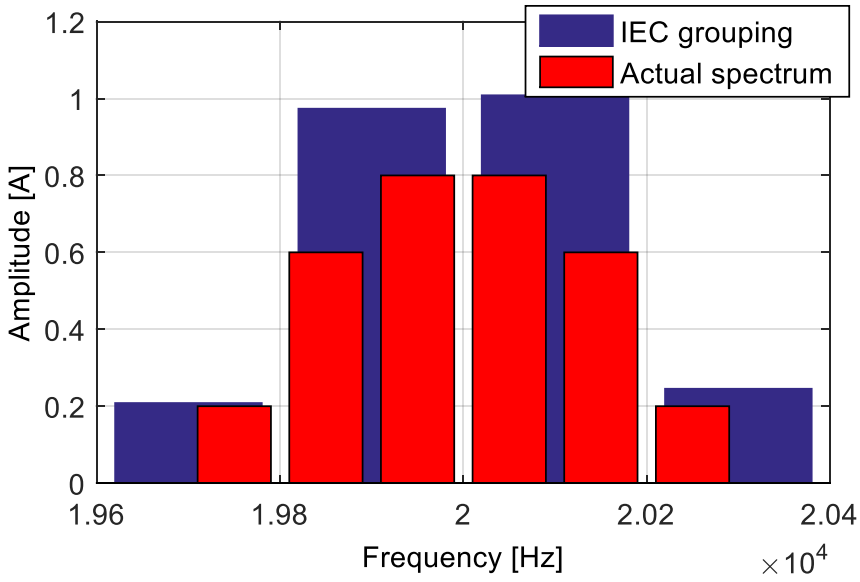

Figure 3.13 *– SWWMEM - Case study 1: comparison between high-frequency International Electrotechnical Commission (IEC) grouping and actual high-frequency spectrum*

Finally, Table 3.12 shows the computational times required by all of the methods to analyze the 3s waveform, per unit of computational time required by STFTM. It is evident that SWWMEM requires a computational time comparable to that required by STFTM and that TEM requires a computational time that is about 22 times greater than SWWMEM, providing however results that are globally affected by similar errors. This is due to the presence of the DWT decomposition and of the resampling in the SWWMEM. In fact, they allow to model both the low-frequency and high-frequency waveforms with a reduced number of exponentials and with a reduced number of samples per analysis window than the TEM. In this way, the computational burden of the SWWMEM is low although the method holds the accuracy of a parametric method.

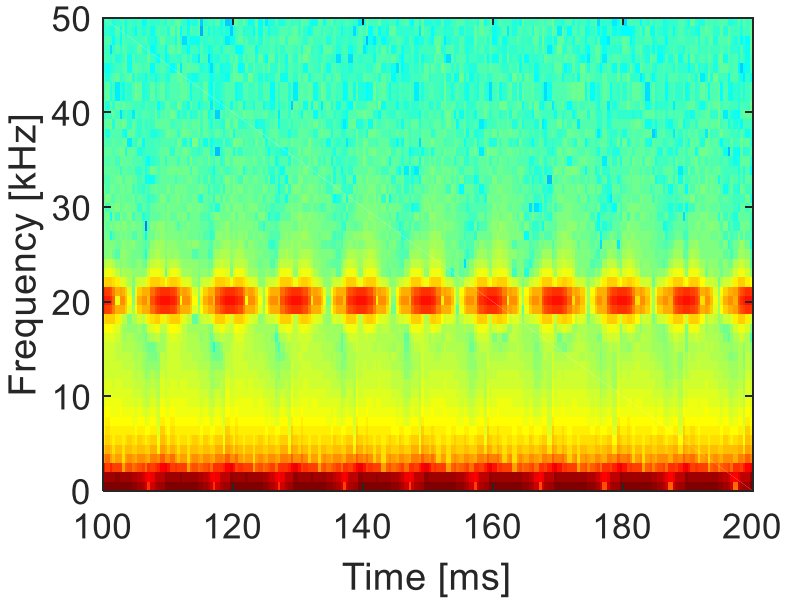

Figure 3.14 *– SWWMEM - Case study 1: time-frequency representation obtained by means the spectrogram with 1 kHz frequency resolution and 1 ms time resolution*

Table 3.12 *- SWWMEM - Case study 1: computational time by all of the considered methods in p.u. of time required by STFTM*

	Computational time [p.u.]
TEM	221
SWWMEM	4.3
STFTM	1

b) Case study 2

In this case study, a frequency-modulated, high-frequency spectral component was added to the synthetic waveform of the previous case study, obtaining the waveform in Figure 3.15. This was made in order to both emulate the presence of secondary emission and to test the performance of the SWWMEM in the detection of time-varying spectral components, that are typical in the high-frequency range. The added spectral component $s_{tv}(t)$ was a tone at $f_{tv} = 17{,}598\ Hz$ with a sinusoidal modulation in frequency, according to Equation (3.12):

$$s_{tv}(t) = A_{tv} \cos(2\pi f_{tv} t + \varphi_{tv}(t)) \tag{3.12}$$

where:

$$\varphi_{tv}(t) = A_{\varphi} \sin(2\pi f_{\varphi} t) \tag{3.13}$$

and A_{tv} was fixed equal to the 0.5% of the fundamental amplitude, A_{φ} was 5 Hz and f_{φ} was 1 Hz. The spectral analyses of this waveform were performed through the same settings of the previous case study.

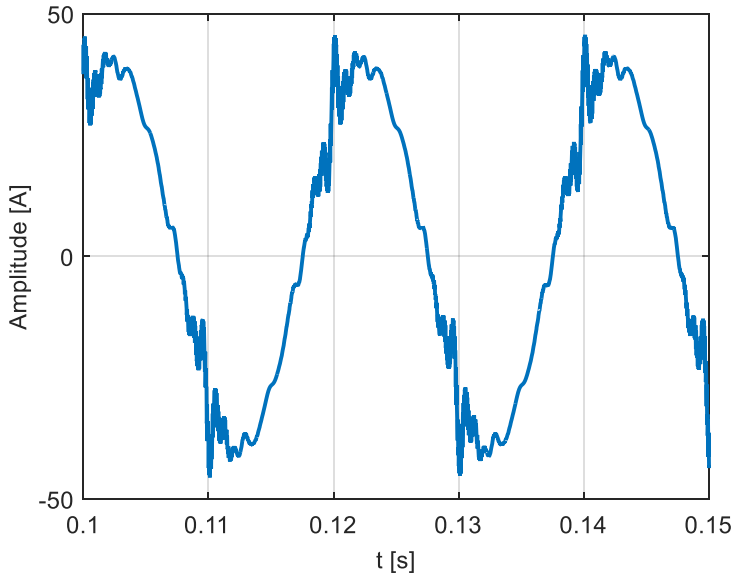

Figure 3.15 *– SWWMEM - Case study 2: synthetic current waveform*

Figure 3.16 shows few ms of the actual modulated frequency and its estimations obtained through STFTM, TEM, SWWMEM and IEC grouping. Specifically, Figure 3.16.a shows that the IEC grouping associates the main part of the energetic content in correspondence of the group at 17.5 kHz. Figure 3.16.b shows a focus on the graphical comparison among the actual

modulated frequency, the STFTM, TEM and SWWMEM estimations. Note that, since in this case the actual value of the spectral component was prior known, for STFTM it is assumed that a single component is around 17,598 Hz and the other components are spectral leakage. So the modulated component in Figure 3.16 is that with the maximum amplitude value in a range of 20 Hz around the actual mean value f_{tv}. Still, it is clear that STFTM fails the detection due to both the spectral leakage problems and the fixed frequency resolution, while TEM and SWWMEM are able to clearly identify the modulation. However, the SWWMEM seemed to provide the best results for this estimation.

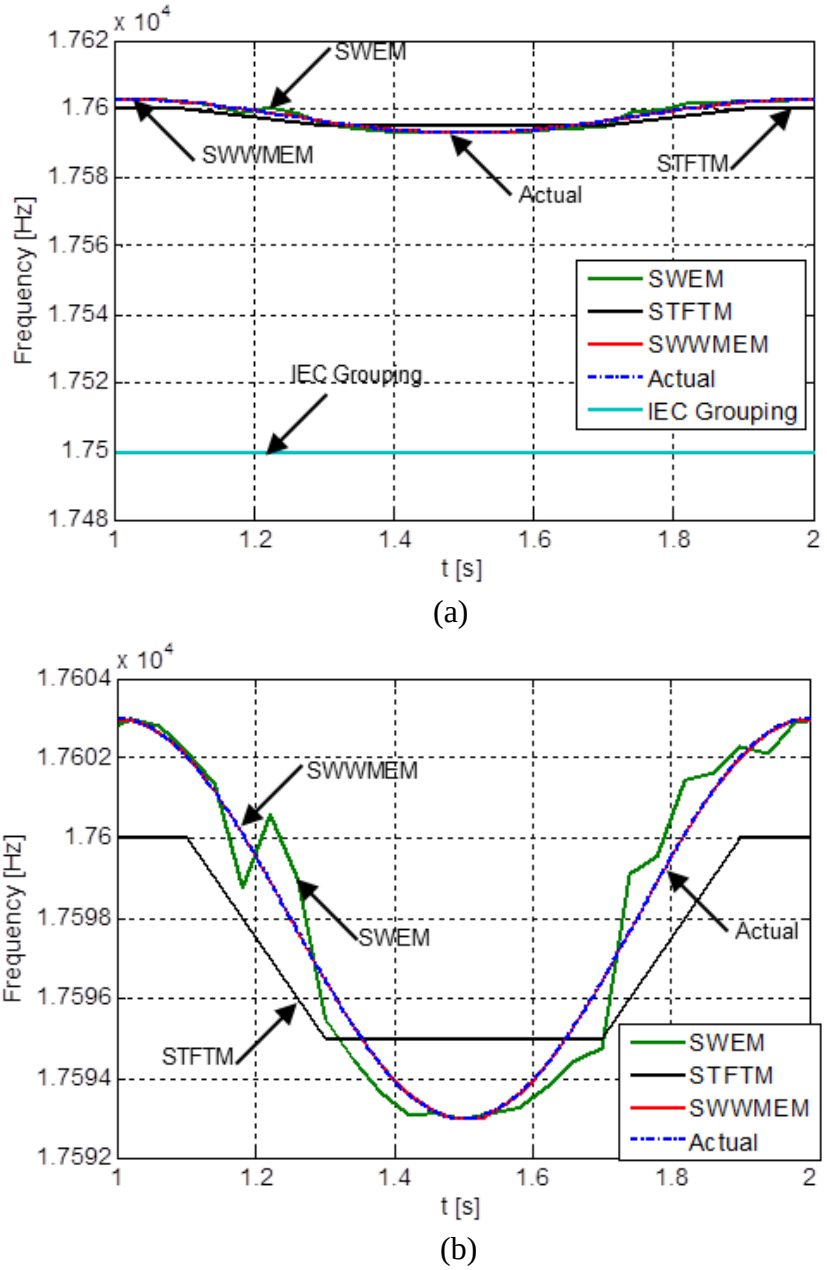

Figure 3.16 *– SWWMEM - Case study 2: comparison among the actual time-varying frequency and its estimations obtained through: (a) IEC grouping, STFTM, TEM and SWWMEM; (b) STFTM, TEM and SWWMEM*

Since the average percentage errors on the estimation of the Table 3.11 spectral components slightly varied with respect to the results in case study 2, Table 3.13 shows only the average

percentage frequency errors and the average percentage amplitude errors for the added spectral component. The results are coherent with the behaviors shown in Figure 3.16, since the lowest amplitude and frequency errors were provided by the SWWMEM. In particular, STFTM and TEM amplitude errors were two order of magnitude higher than SWWMEM amplitude error. Moreover, the average percentage frequency error provided by SWWMEM was two and three orders of magnitude lower than the TEM and STFTM frequency errors, respectively.

In Figure 3.17 the spectrogram with 1 kHz frequency resolution and 1 ms time resolution is shown for the considered waveform, in order to underline once again the different approach of the spectrogram to the spectral analysis of wide-spectra waveforms in respect to SWWMEM.

Table 3.13 *- SWWMEM - Case study 2: average percentage errors of frequency and amplitude for the frequency-modulated spectral component.*

	Average error [%]	
	Amplitude	Frequency
TEM	24	0.0044
SWWMEM	0.060	$27 \cdot 10^{-6}$
STFTM	19	0.010

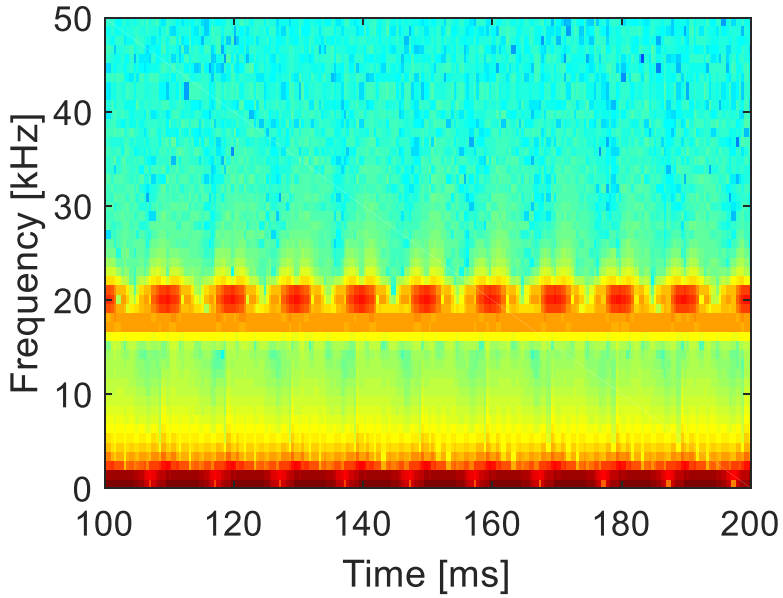

Figure 3.17 *– SWWMEM - Case study 2: time-frequency representation obtained by means the spectrogram with 1 kHz frequency resolution and 1 ms time resolution*

Similarly to the previous case study, in Figure 3.17 the spectrogram was able to detect the presence of spectral content both at low-and high-frequency, but, differently to SWWMEM, only rough and approximated information can be obtained. In particular, also the contribute of the spectral component around 17.958 kHz can be detected, but, in this case the related frequency appears time-invariant, since the real frequency modulation of this spectral component is not individuated, cause of the spectral leakage problems.

Finally, Table 3.14 shows the computational time required by the three methods to analyze the 3-s waveform, per unit of computational time required by STFTM. Note that the SWWMEM required a higher computational time than the previous case study, since the frequency variation of the high-frequency modulated component prevented to keep the

estimated frequencies constant, requiring often an updating of their value (step 2 of SWWMEM). However, the time required by SWWMEM was still one order of magnitude lower than the time required by TEM.

Table 3.14 *- SWWMEM - Case study 2: computational time by all of the considered methods in p.u. of time required by STFTM*

	Computational time [p.u.]
TEM	218
SWWMEM	19
STFTM	1

c) Case study 3

A 0.2 s-current waveform measured at the PCC of a single fluorescent lamp powered by high-frequency ballast was analyzed. The total active power consumption of the lamp was about 0.1 kW. The current waveform was measured with a Pearson current probe, model 411. The probe has its 3 dB cut-off frequencies at 1 Hz and 20 MHz with an amplitude accuracy of −0%, +1% in the frequency range of interest. The phase accuracy is less than 1 degree between 60 Hz to 333 kHz. The current was then sampled with 12 bits resolution and 10 MS/s sampling speed, and a low-pass filter with a cut-off frequency 1 MHz was used for anti-aliasing purpose. More details on the installation structure, instrument specification and error verification of measurement are available in [16].

The analyzed current is shown in Figure 3.18; the high-frequency components on the peak of the waveform are clearly evident, unlike the high-frequency distortion around the zero crossing.

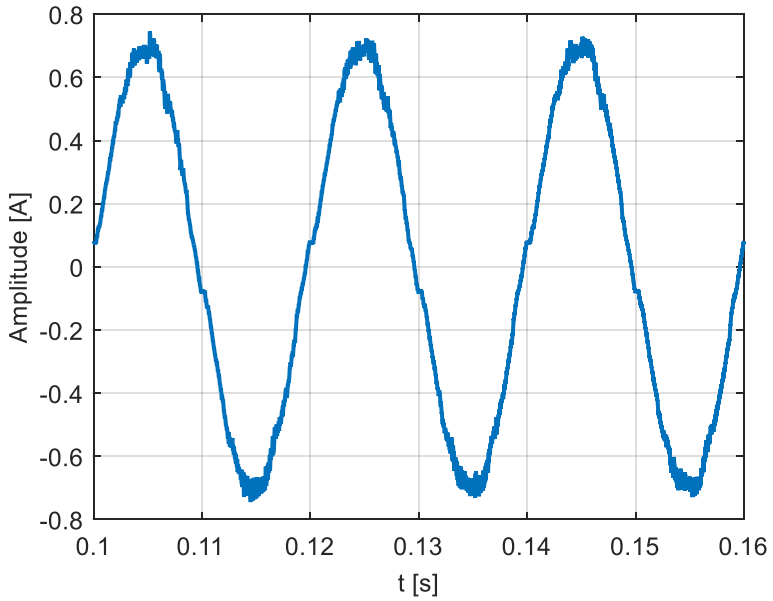

Figure 3.18 *– SWWMEM - Case study 3: actual current waveform*

However, according to the measurement procedure, based on 10 MHz sampling rate, the maximum frequency of interest cannot exceed 5 MHz. In this way, fixing the SWWMEM the bands' separation frequency f_{bs} to 2 kHz, the maximum number L_{max} of decomposition levels was 11. A resample to 10 kHz was performed for the low-frequency waveform while the high-frequency waveform was downsampled to 250 kHz, since our interest was the

detection of the spectral components up to 150 kHz. Then, the two different waveforms, i.e., $x_l(n)$ and $x_h(n)$, were analyzed with a sliding window of 0.04 s and of $5 \cdot 10^{-4}$ s, fixing an error threshold of 10^{-4} and 10^{-3}, respectively. The measured current was downsampled to 250 kHz also for the analyses through TEM and STFTM, in order to guarantee a correct comparison of the methods in terms of computational burden. In particular, for the TEM, the error threshold was fixed equal to 10^{-4}, and the sliding window duration was fixed to 0.04 s.

The spectra obtained through the SWWMEM and STFTM were almost similar at low-frequency. In fact, SWWMEM and STFTM individuated the same significant spectral components, though STFTM provided lower amplitudes than SWWMEM cause of the high spectral leakage. These low-frequency spectra included a fundamental component with a peak amplitude equal to about 0.7 A, and all of the other odd harmonics, whose amplitudes globally decrease as the harmonic order increases. These harmonic components reached a maximum amplitude equal to 3.6% of the fundamental in correspondence of the third harmonic, as shown in Figure 3.19.a. Figure 3.19.a shows the low-frequency spectrum obtained through SWWMEM, in percentage values of the fundamental amplitude. Finally the TEM detected a reduced number of spectral components at low-frequency than the other two methods. Probably, this was due to a too high duration of the analysis window that shifted most of the detected spectral components to high-frequency.

At high-frequency, the STFTM spectral leakage increased, spreading the spectral content and missing the detection of specific tones. In particular, a distributed spectral content from 50 kHz to 90 kHz was observed. The same high-frequency spectrum was also detected by TEM. In both the cases, the amplitudes were decreasing from 50 kHz to 90 kHz, with a maximum equal to the 0.1% and 0.3% of the fundamental amplitude for STFTM and TEM, respectively. Instead, the SWWMEM, due to the shorter analysis window, provided a high-frequency spectrum with defined single tones, as shown in Figure 3.19.b.

The spectrum in Figure 3.19.b is referred to the first $5 \cdot 10^{-4}$ s of the waveform shown in Figure 3.18, but it is very interesting to note that in the following analysis windows the SWWMEM provided a periodic shift of the spectral components around 80 kHz, from 35 kHz to 95 kHz. This means that the SWWMEM is able to detect a time varying high-frequency spectra. Figure 3.20 shows the time trend of the spectral component with maximum amplitude detected in the aforesaid range of frequency. Specifically, Figure 3.20.a shows the frequency variation in time, while Figure 3.20.b shows the amplitude variation in time. This component could be related to the zero-crossing, since, as shown in Figure 3.20, both the frequency and the amplitude variations in time had a periodicity of about 10 ms [16]. Note also that this component reached the maximum amplitude (about 0.03 A) at about 50 kHz, namely when the positive and negative peaks of the current waveform shown in Figure 3.18 occurred.

In Figure 3.21 the spectrogram with 1 kHz frequency resolution and 1 ms time resolution is shown also for the considered measured waveform, always in order to underline the different approach of the spectrogram to the spectral analysis of wide-spectra waveforms in respect to SWWMEM.

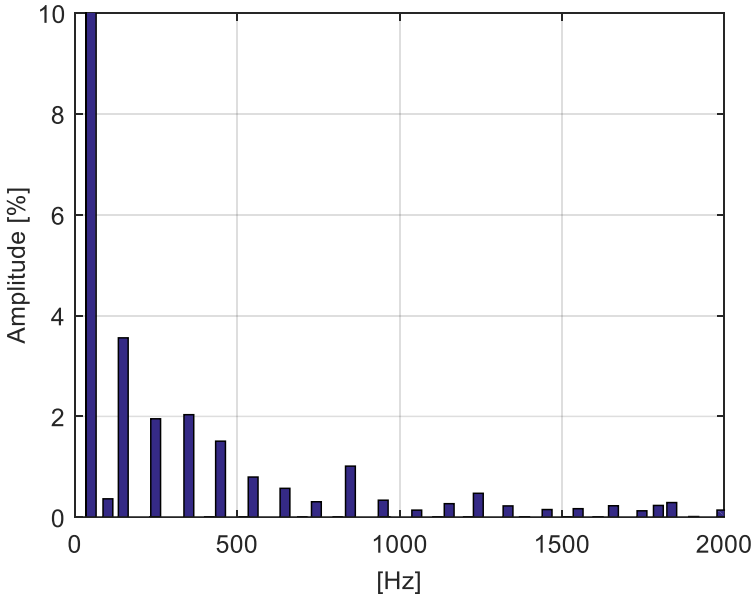

(a)

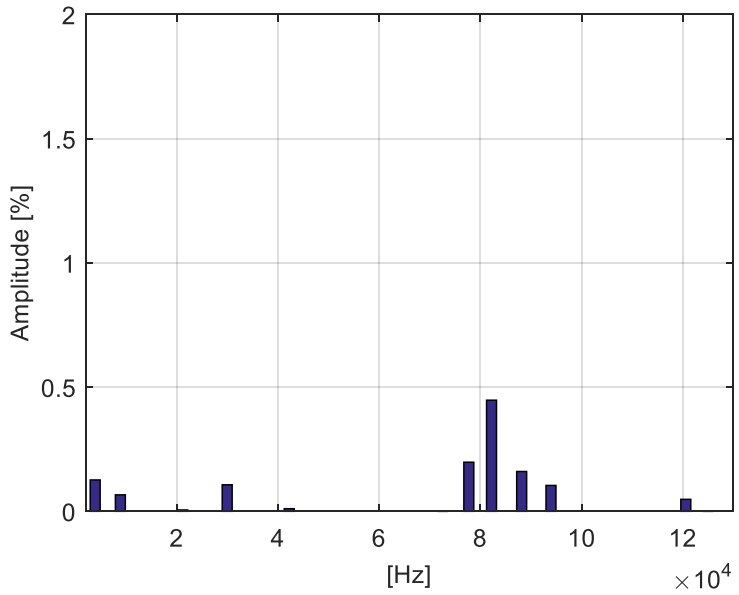

(b)

***Figure 3.19** – SWWMEM - Case study 3: (a) percentage low-frequency spectrum and (b) percentage high-frequency spectrum obtained through SWWMEM*

Figure 3.21 shows the time-varying spectral content in the range from 50 kHz to 100 kHz, so, the spectrogram appeared able to detect significant variations in time of the high-frequency spectral content. However, differently by SWWMEM, once again, only no-detailed information on the specific frequency and amplitude of that spectral component can be obtained.

Finally, Table 3.15 shows the computational times required by all of the methods to analyze the waveform, per unit of computational time required by STFTM: the results are coherent to what was theoretically expected, since the computational time required by SWWMEM is about four time of that required by STFTM, but it is four order of magnitude lower than that required by the TEM.

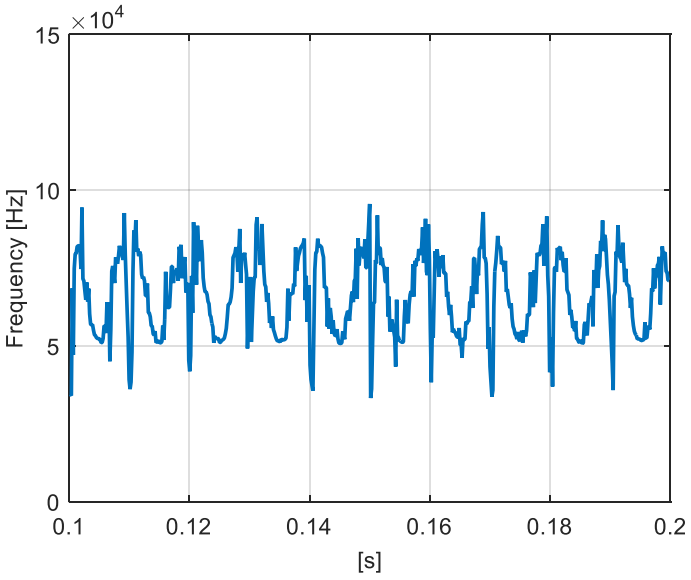

(a)

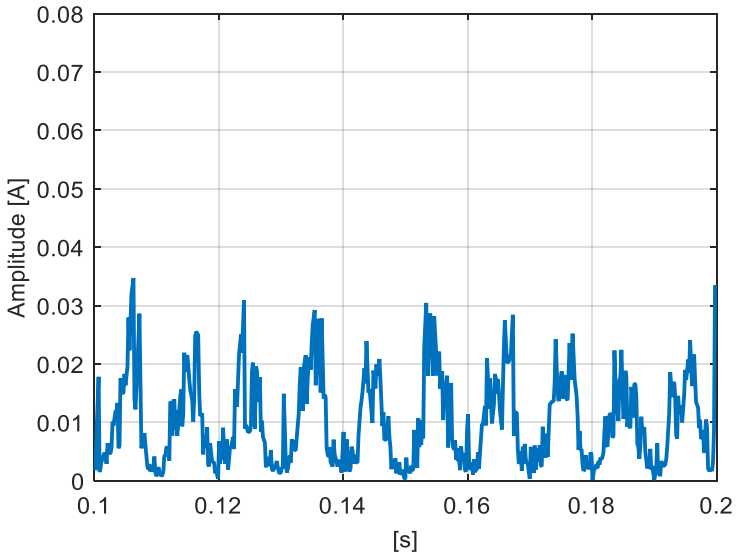

(b)

Figure 3.20 *– SWWMEM - Case study 3: (a) frequency and (b) amplitude of a time varying high-frequency component obtained by SWWMEM*

Table 3.15 *- SWWMEM - Case study 3: computational time by all of the considered methods in p.u. of time required by STFTM*

	Computational time [p.u.]
TEM	$1.2 \cdot 10^5$
SWWMEM	4.4
STFTM	1

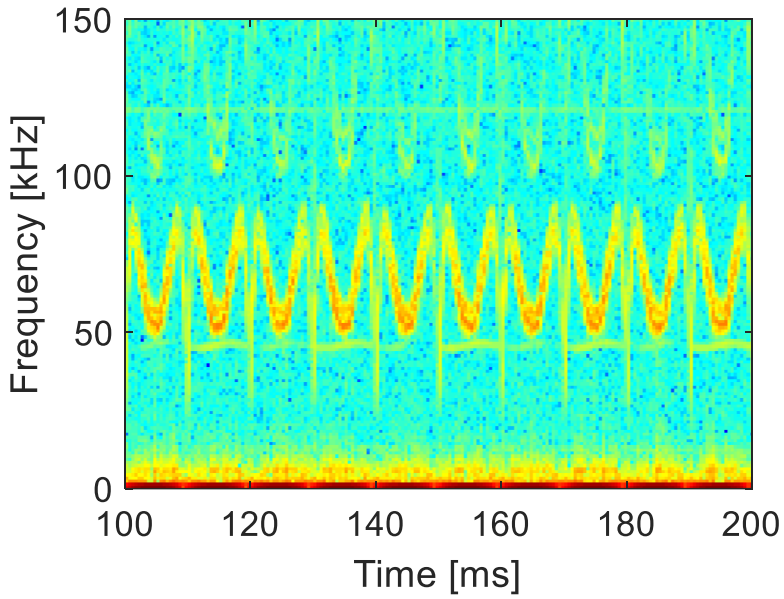

***Figure 3.21** – SWWMEM - Case study 3: time-frequency representation obtained by means the spectrogram with 1 kHz frequency resolution and 1 ms time resolution*

3.5 Conclusions

New hybrid methods based on the joint of non-parametric and parametric methods have been presented in this Chapter, aiming to a fast and accurate estimation of all of the spectral components included in the waveforms to be analysed.

In particular, a new three-step method which alternatively applies DFT and Prony method with sliding windows was described in Section 3.2. This method does not suffer from DFT spectral leakage problems, and it guarantees a significant reduction of computational effort compared with the application of the SW Prony applied for the full-band waveform.

Similarly, new methods for the assessment of the AC supply-side current distortions due to PWM ASDs were explained in Section 3.3. These distortions are critical in power systems, since they include many harmonic/interharmonics components that vary in time and are linked to the double conversion systems that feed asynchronous motors with variable frequency. These methods are based on a four-step procedure, and once again the aim is to combine the accuracy of the parametric (ESPRIT or Prony) methods with the speed of both DFT method and theoretical formulas.

Finally, a new sliding-window Wavelet-modified ESPRIT scheme, suitable for accurate analysis of waveforms that have very wide spectra, was presented in Section 3.4; the scheme also guarantees a relatively low computational cost. This method was based on the DWT decomposition of the original signal into low-frequency and high-frequency waveforms, separately analyzed by the SWWMEM in order to provide optimal time and frequency resolutions in each band and, then, an accurate time-frequency representation.

All of the aforesaid methods have been tested on both synthetic and measured waveforms, and also they have been compared with the STFT, with the traditional Prony's and/or ESPRIT method, and with other advanced methods proposed in relevant literature for the same range of applications.

The numerical experiments confirmed the goodness of the methods presented in this Chapter, for their area of applicability.

3.6 References

[1] A. Bracale, P. Caramia, P. Tricoli, F. Scarpa, L. Piegari, A new advanced method for assessment of waveform distortions caused by adjustable speed drives, IEEE Industry Applications Society Annual Meeting (IAS), 2011, 1-10

[2] A. Bracale, P. Caramia, G. Carpinelli, A. Rapuano, A New, Sliding-Window Prony and DFT Scheme for the Calculation of Power-Quality Indices in the Presence of Non-stationary Waveforms, Int. Journal of Emerging Electric Power Systems, vol. 13, no. 5, 2012

[3] A. Bracale, G. Carpinelli, I.Y.H. Gu, M.H.J. Bollen, A new joint sliding-window ESPRIT and DFT scheme for waveform distortion assessment in power systems, Electric Power Systems Research, vol. 88, 2012, 112-120

[4] T. Tarasiuk, Hybrid wavelet-Fourier spectrum analysis, IEEE Trans. Power Del., vol. 19, 2004, 957–964

[5] C. Chen, T. Xu, Z. Piao, W. Liang, Y. Yuan, The study on FFT harmonic detecting method of rural network based on wavelet denoising, Int. Conf. Energy Environ. Technol., vol. 2, 2009, 365–368

[6] F.F. Costa, A.J.M. Darlan, A. Fernandes, Harmonic analysis based on Kalman filtering and Prony's method, Int. Conf. on Power Engineering, Energy and Electrical Drives, 2007, 696–701

[7] Y.Z. Liu, S. Chen, A wavelet based model for on-line tracking of power system harmonics using Kalman filtering, IEEE Power Eng. Soc. Summer Meet., vol. 2, 2001, 1237–1242

[8] T. Lobos, J. Rezmer, H.-J. Koglin, Analysis of power system transients using wavelets and Prony method, IEEE Power Technol. Proc., vol. 4, 2001

[9] A. Bracale, G. Carpinelli, An ESPRIT and DFT-based new method for the waveform distortion assessment in power systems, 20th Int. Conf. and Exhibition on Electricity Distribution, CIRED, 2009, 1–4

[10] L. Alfieri, G. Carpinelli, A. Bracale, P. Caramia, Waveform distortion assessment in power systems with a new three-step sliding-window method, 12th International Conference on Environment and Electrical Engineering, Wroclaw, 2013, 562-567

[11] L. Alfieri, A Bracale, G Carpinelli, DFT-Parametric Methods for an Accurate and Fast Assessment of Waveform Distortions Caused by Adjustable Speed Drives, Int. Transaction on Electrical Energy Systems, vol. 26, no. 1, 2016, 106–121

[12] L. Alfieri, A. Bracale, G. Carpinelli, A. Larsson, A Wavelet-Modified ESPRIT Hybrid Method for Assessment of Spectral Components from 0 to 150 kHz, Energies, vol. 10, no. 1, 2017

[13] J. Meyer, M. Bollen, H. Amaris, A.M. Blanco, A. Gil de Castro, J. Desmet, M. Klatt, Ł. Kocewiak, S. Rönnberg, K. Yang, Future work on harmonics—Some

expert opinions Part II—Supraharmonics, standards and measurements, Proceedings of the 16th IEEE International Conference on Harmonics and Quality of Power (ICHQP), Bucharest, Romania, 2014

[14] H. Renner, B. Heimbach, J. Desmet, Power quality and electromagnetic compatibility: Special report session 2, Proceedings of the 23rd International Conference and Exhibition on Electricity CIRED, Lyon, France, 2015

[15] A. Moreno-Munoz, A. Gil-de-Castro, E. Romero-Cavadal, S. Rönnberg, M. Bollen, Supraharmonics (2 to 150 kHz) and multi-level converters, Proceedings of the IEEE 5th International Conference on Power Engineering, Energy and Electrical Drives (POWERENG), Riga, Latvia, 2015, 37–41

[16] E.O.A. Larsson, M.H.J. Bollen, Measurement result from 1 to 48 fluorescent lamps in the frequency range 2 to 150 kHz, Proceedings of the 14th International Conference on Harmonics and Quality of Power (ICHQP), Bergamo, Italy, 2010, 1–8

[17] A. Emanuel, A. McEachern, Electric power definitions: A debate, Proceedings of the IEEE Power & Energy Society (PES) General Meeting, Vancouver, Canada, 2013

[18] IEC standard 61000-4-7, General guide on harmonics and interharmonics measurements, for power supply systems and equipment connected thereto, 2010

[19] Y. Shin, E.J. Powers, M. Grady, A. Arapostathis, Power Quality Indices for Transient Disturbances, IEEE Transactions on Power Delivery, vol. 21, no. 1, 2006, 253-261

[20] A. Andreotti, A. Bracale, P. Caramia, G. Carpinelli, Adaptive Prony Method for the Calculation of Power Quality Indices in the Presence of Non-Stationary Disturbance Waveforms, IEEE Transactions on Power Delivery, vol. 24, no. 2, 2009, 874-883

[21] A. Bracale, P. Caramia, G. Carpinelli, Adaptive Prony Method for Waveform Distortion Detection in Power Systems, Int. Journal. of Electrical Power & Energy Systems, vol. 29, no. 5, 2007, 371-379

[22] G.W. Chang, C.I. Chen, Measurement Techniques for Stationary and Time-varying Harmonics, Power & Energy Society General Meeting, 2010, 1-5

[23] L Alfieri, Some advanced parametric methods for assessing waveform distortion in a smart grid with renewable generation, EURASIP J. Adv. Signal Process, vol. 2015, no. 1, 2015, 1–16

[24] P. Caramia, G. Carpinelli, P. Verde, Power Quality Indices in Liberalized Market, John Wiley & Sons, Chichester, West Sussex (UK), 2009

[25] M. Bollen, I. Y. H. Gu, Signal Processing of Power Quality Disturbances, Wiley-IEEE Press, New Jersey, 2006

[26] P. F. Ribeiro, Time-Varying Waveform Distortions in Power Systems, Wiley, 2009

[27] G. Carpinelli, F. Iacovone, A. Russo, P. Varilone, P. Verde, Analytical Modelling for Harmonic Analysis of Three-phase Voltage Source Converters, IEEE Trans. on Power Delivery, vol. 19, no. 3, 2004

[28] F. De Rosa, T. Langella, A. Sollazzo, A. Testa, On the Interharmonic Components Generated by Adjustable Speed Drives, IEEE Trans. on Power Delivery, vol. 20, no. 4, 2005

[29] G.W. Chang, S.K.Chen, An Analytical Approach for Characterizing Harmonic and Interharmonic Currents Generated by VSI-fed Adjustable Speed Drives, IEEE Trans. on Power Delivery, vol. 20, no. 4, 2005

[30] G.W. Chang, S.K. Chen, H.J. Su, P.K.Wang, Accurate Assessment of Harmonic and Interharmonic Currents Generated by VSI-Fed Drives Under Unbalanced Supply Voltages, IEEE Trans. on Power Delivery, 2010

[31] S.K. Chen, H.J. Su, G.W.Chang, Modelling VSI-Fed ASDs by Matlab/Simulink for Harmonic and Interharmonic Assessment, 14th International Conference ICHQP, 2010

[32] D. Gallo, R. Langella, A. Testa, A Self Tuning Harmonics and Interharmonics Processing Technique, European Transaction on Electrical Power, vol. 12, no. 1, 2002

[33] D. Gallo, R. Langella, A. Testa, Desynchronized Processing Technique for Harmonic and Interharmonic Analysis, IEEE Trans. on Power Delivery, vol. 19, no. 3, 2004

[34] G.W. Chang, C.I. Chen, Y.J. Liu, M.C. Wu, Measuring power system harmonics and interharmonics by an improved fast Fourier transform-based algorithm, IET Proc. on Generation, Transmission, and Distribution, vol. 2, no. 2, 2008

[35] G.W. Chang, C.I.Chen, An Accurate Time-Domain Procedure for Harmonics and Interharmonics Detection, IEEE Trans. on Power Delivery, 2010

[36] A. Bracale, G. Carpinelli, Z. Leonowicz, T. Lobos, J. Rezmer, Measurement of IEC Groups and Subgroups using Advanced Spectrum Estimation Methods, IEEE Trans. on Instr. and Meas., vol. 57, no. 4, 2008, 672 – 681

[37] IEC standard 61000-4-30, Testing and measurement techniques – Power quality measurement methods, 2015

[38] L. Alfieri, G. Carpinelli, A. Bracale, New ESPRIT-based method for an efficient assessment of waveform distortions in power systems, Electric Power Systems Research, vol. 122, 2015, 130-139

[39] CIGRE WG 37–23, Impact of increasing contribution of dispersed generation on the power system, 1999

[40] I.Y.H. Gu, M.H.J. Bollen, Estimating interharmonics by using sliding-window ESPRIT, IEEE Tran. Power Deliv., vol. 23, 2008, 13–23

[41] J. Barros, M. de Apráiz, R.I. Diego, Measurement of voltage distortion in the frequency range 2–9 kHz, Proceedings of the IEEE International Workshop on Applied Measurements for Power Systems (AMPS), Aachen, Germany, 2010, 70–73

[42] S. Rönnberg, M. Bollen, Power quality issues in the electric power system of the future, Electr. J., vol. 29, 2016, 49–61

[43] M. Bollen, M. Olofsson, A. Larsson, S. Rönnberg, M. Lundmark, Standards for supraharmonics (2 to 150 kHz), IEEE Electr. Comp. Mag., vol. 3, 2014, 114–119

[44] E.O.A. Larsson, M.H.J. Bollen, M.G. Wahlberg, C.M. Lundmark, S.K. Rönnberg, Measurements of high frequency (2–150 kHz) distortion in low-voltage networks, IEEE Trans. Power Deliv., vol. 25, 2010,1749–1757

[45] M. Bollen, W. Wahlberg, S. Ronnberg, Interaction between narrowband power-line communication and end-user equipments, IEEE Trans. Power Deliv., vol. 26, 2011, 2034–2039

[46] J.M. Carrasco, L.G. Franquelo, J.T. Bialasiewicz, E. Galvan, R.C.P. Guisado, M.A.M. Prats, J.I. Leon, N. Moreno-Alfonso, Power-electronic systems for the grid integration of renewable energy sources: A survey, IEEE Trans. Ind. Electron., vol. 53, 2006,1002–1016

[47] G. F. Bartak, A. Abart, EMI of Emissions in the Frequency Range 2 kHz–150 kHz, Proceedings of the 22nd International Conference and Exhibition on Electricity CIRED, Stockholm, Sweden, 2013

[48] CISPR/1270/INF, International Special Committee on Radio Interference (CISPR) ISPR Guidance document on EMC of equipment connected to the SmartGrid, IEC: Geneva, Switzerland, 2014

[49] D. Gallo, C. Landi, M. Luiso, AC and DC power quality of photovoltaic systems, Proceedings of the IEEE International Instrumentation and Measurement Technology Conference (I2MTC), Graz, Austria, 2012, 576–581

Conclusions

A new advanced modified parametric method (*sliding-window modified ESPRIT method*) and three new advanced hybrid methods (*sliding-window Prony-DFT-Prony method*, *sliding-window Parametric-DFT-analytical-parametric method* and *sliding-window Wavelet-modified ESPRIT method*) have been proposed in this thesis. All of them have firstly been described theoretically, underlining the benefits in terms of accuracy and computational effort. Then, the methods are tested on both synthetic and measured waveforms, in order to evaluate their performances by stressing them in different conditions. The effectiveness of these new methods was also demonstrated by comparing them with the STFT, with the traditional Prony's and/or ESPRIT method and with other advanced methods proposed in relevant literature for the same kind of applications.

Results generally confirmed that:

(i) the state-of-the-art methods, although based on different approaches, offer both pros and cons to the spectral analysis of time-varying waveforms;

(ii) the new advanced methods presented in this thesis proved to be an attractive choice in order to avoid the main shortcomings of both non-parametric and parametric techniques;

(iii) also, they proved to outperform other hybrid methods specifically addressed to the same applications.

In particular, the *sliding-window modified ESPRIT method* was compared with the traditional ESPRIT method, with the hybrid ESPRIT-DFT method and with the DFT method was performed. The main outcomes of the numerical applications are the following:

(i) the proposed method proved to be particularly beneficial for many waveforms; it requires a computational time down to only three times greater than the DFT method, while approaching the accuracy of the ESPRIT method;

(ii) the proposed method can be a good alternative also to the use of the hybrid ESPRIT-DFT method, since it generally provides the same while running the analysis 5÷8 times faster than the hybrid ESPRIT-DFT method;

(iii) the proposed method proved to suffer some inaccuracies and higher computational burden in the analysis of a wide-spectrum waveform with time-varying high-frequencies spectral components. However, also the other methods considered for the comparison failed the same analysis, confirming the need of new methods specifically addressed to this increasingly spreading typology of waveforms.

The *sliding-window Prony-DFT-Prony method* was compared with the traditional Prony's method, with the hybrid ESPRIT-DFT method and with the DFT method. The main outcomes of the numerical application are the following:

(i) the proposed method provideded an accurate estimation of the fundamental period and, then, of the harmonics by using a synchronized analysis window to the fundamental period;

(ii) an accurate estimation of interharmonic components was achieved due to the first and third step based on the Prony's method application;

(iii) the computational time was significantly reduced in comparison to the traditional Prony's method applied for the full-band waveform;

(iv) the proposed method provided performances of estimation that were similar to hybrid ESPRIT-DFT, although little differences in the spectrum have been observed due to the different approach of the ESPRIT and the Prony's methods in the detection of the unknown parameters included in their models.

The *sliding-window Parametric-DFT-analytical-parametric method*, specifically addressed for the assessment of the AC supply-side current distortions due to PWM ASDs, was compared with Prony's method, with ESPRIT method, with DFT method and with the hybrid three-step Prony-ESPRIT-analytical method.

The main outcomes of the numerical application are the following:

(i) the desynchronization problems of DFT method were overcome, limiting the spectral leakage that is due only to the presence of interharmonics above 100 Hz;

(ii) the proposed method usually provided more accurate results than the traditional Prony's and ESPRIT methods, benefitting from the division of spectral content into different frequency bands; the separate analysis partially avoided the difficulty of identifying the proper linear combination of exponentials that fits the analyzed waveforms;

(iii) the accuracy of the proposed method was comparable with the accuracy of the hybrid three-step Prony-ESPRIT-analytical method, although requiring a significantly lower computational time;

(iv) the computational burden of the proposed method is up to four orders of magnitude lower than the computational burden of the traditional Prony's and ESPRIT methods;

(v) the time required by the proposed method is comparable to the time required by DFT;

(vi) the ESPRIT-DFT-analytical-Prony combination required the lowest time.

Eventually, with reference to the *sliding-window Wavelet-modified ESPRIT method*, the problems related to the analysis of wide-spectrum waveforms with time-varying high-frequencies spectral components have been overcome. The proposed method was compared with the traditional ESPRIT method, with the DFT method and with the time-frequency representation obtained with the spectrogram. The main outcomes of the numerical application are the following:

(i) being based on the DWT decomposition of the original signal into low-frequency and high-frequency waveforms that are separately analyzed by the *sliding-window modified ESPRIT method*, the proposed method provided optimal time and

frequency resolutions in each band and, therefore, an accurate time-frequency representation;

(ii) in presence of highly time-varying high-frequency components, the proposed method proved to overcome the limits of both the traditional ESPRIT method and the DFT method for the detection of the high-frequency components, reaching a computational time down to only four times greater than that required by the DFT method;

(iii) the proposed method always outperformed currently available high-frequency signal processing techniques, i.e., the spectrogram, in terms of frequency, amplitude and time-variability of both the spectral components at low- and high-frequency.

List of publications

The research work presented in this thesis has produced the following publications:

[1] L. Alfieri, A. Bracale, P. Caramia, G. Carpinelli, Waveform Distortion Assessment in Power Systems with a New Three-step Sliding-Window Method, 13th IEEE Int. Conf. EEEIC, Wroclaw, Poland, 2013

[2] L. Alfieri, A. Bracale, P. Caramia, G. Carpinelli, Advanced Methods for the Assessment of Time Varying Waveform Distortions Caused by Wind Turbine Systems. Part I: Teoretical Aspects, 13th IEEE International Conference on Environment and Electrical Engineering - Wroclaw, Poland, 2013

[3] L. Alfieri, A. Bracale, P. Caramia, G. Carpinelli, Advanced Methods for the Assessment of Time Varying Waveform Distortions Caused by Wind Turbine Systems. Part II: Experimental Applications" 13th IEEE International Conference on Environment and Electrical Engineering - Wroclaw, Poland, 2013

[4] L. Alfieri, A Bracale, G Carpinelli, New ESPRIT-based method for an efficient assessment of waveform distortions in power systems, Electric Power Systems Research Journal, vol. 122, 2015, 130-139

[5] L. Alfieri, Some advanced parametric methods for assessing waveform distortion in a smart grid with renewable generation, EURASIP Journal on Advances in Signal Processing, vol. 2015, no. 1, 2015, 1-16

[6] L. Alfieri, A Bracale, G Carpinelli, DFT-Parametric Methods for an Accurate and Fast Assessment of Waveform Distortions Caused by Adjustable Speed Drives, Int. Transaction on Electrical Energy Systems, vol. 26, no. 1, 2016, 106–121

[7] L. Alfieri, A. Bracale, Time varying waveform distortions caused by dispersed generators in Smart Grids, Journal of Energy Challenges and Mechanics, vol. 3, 2016

[8] L. Alfieri, A. Bracale, G. Carpinelli, A. Larsson, A Wavelet-Modified ESPRIT Hybrid Method for Assessment of Spectral Components from 0 to 150 kHz, Energies, vol. 10, no. 1, 2017